TOPICS WITHIN THE STRING LANDSCAPE AND METASTABLE SUPERSYMMETRY BREAKING

BY KORNEEL VAN DEN BROEK

A dissertation submitted to the
Graduate School—New Brunswick
Rutgers, The State University of New Jersey
in partial fulfillment of the requirements
for the degree of
Doctor of Philosophy
Graduate Program in Physics and Astronomy
Written under the direction of
Professor Thomas Banks
and approved by

_____

_____

_____

_____

_____

New Brunswick, New Jersey
October, 2008

ABSTRACT OF THE DISSERTATION

Topics within the String Landscape and Metastable Supersymmetry Breaking

by Korneel van den Broek

Dissertation Director: Professor Thomas Banks

In this thesis we focus on different aspects related to the central concept of the string landscape. We will first briefly situate the idea of the landscape within string theory and comment on its appealing and less appealing features. We then proceed to describe three projects which all take a different angle on the landscape. First we focus on a particular string compactification which is part of the landscape and analyze this background in detail. Secondly, we do a survey of the different compactification techniques and investigate which properties of the vacuum might lead to a long lived state. Thirdly, we discuss the idea of metastable dynamical supersymmetry breaking and the computer package `VScape` which was developed to assist in finding metastable states of supersymmetric models.

Acknowledgements

In the first place, I would like to extend a warm thank you to my advisor prof. Tom Banks for his guiding hand during my PhD and for his often direct and fast feedback on my work. I have learned very many things from him. I would also like to thank the professors in my committee and the other professors from the NHETC group and Rutgers Physics, in particular prof. Thomas, prof. Ransome and prof. Dine from SCIPP. Also a special word of thank to Diane.

I was fortunate to meet very many nice people and like to thank my friends in New Brunswick, Santa Cruz and Santa Barbara alike. In particular, though not in any particular order, Gonzalo, Jean-François, Kuver, Rouven, Semyon, Sergio, Sridhar, Levan, José, Haile, Dmitriy and Alberto & Laurie for their warm support and the things I learned from them.

Finally, I would like to thank my parents and siblings who supported we throughout my foreign endeavors.

Dedication

Voor

Mama

&

Papa

Table of Contents

List of Figures

Chapter 1
Introduction

1.1 The String Landscape

1.1.1 String Theory, Flux Compactifications and the Landscape

Perturbative string theory is essentially a conformal field theory (CFT) defined on the two dimensional worldsheets of the string. The fields living on the worldsheet describe how the string is embedded in spacetime. The action of this theory contains background fields that interact with the string. Depending on which kind of string theory one works with, the background consists of e.g. a background metric in spacetime, a scalar field (dilaton) and several antisymmetric tensor fields. The background should be thought of as the net effect from other strings in spacetime.

Essential here is that requiring the two dimensional theory to be consistent leads to two important constraints. First, spacetime should have ten dimensions[1]. As we do not see ten dimensions in Nature, we have to explain why and how the additional six dimensions are small and compactified to obtain our four dimensional world. Secondly, the background fields need to satisfy certain equations of motion, i.e. not all backgrounds are consistent. To leading order, these equations turn out to be the equations of motion of a supergravity theory (type IIA, IIB or I).

An important aim is to compactify the theory down to four dimensions by choosing the background fields appropriately and to get a theory that nicely describes Nature as we see it. It turns out that there are many background configurations that seem to satisfy all the consistency conditions, so there might indeed be a setup that exactly corresponds to our world. This is studied in the field of flux compactifications, where the word flux stands for the various antisymmetric tensor fields being turned on in analogy with Maxwell's theory of electromagnetism where one can turn on magnetic flux. However, there might even too much freedom in choosing the background. String theory does not seem to single out just one background, as

[1] We will not discuss non-critical string theory where this constraint is relaxed.

was originally hoped.

A common approach to flux compactifications is to take a certain ansatz on the form of the background and then to compactify the theory to four dimensions. Usually, one starts with a setup that has no fluxes turned on. A common way to obtain a four dimensional theory with $\mathcal{N} = 1$ supersymmetry, which might be seen at the Large Hadron Collider (LHC) and makes computations tractable, is to assume that the six dimensional manifold, that is compactified, is a Calabi-Yau manifold with an orientifold plane in it. A Calabi-Yau manifold is a manifold with special properties that are well studied. The orientifold is an object which can be compared with half of space being filled with a conductor in electrostatics. The compactified theory still suffers from some problems. There is a large amount of massless scalar fields (they are called 'moduli') which we do not detect in Nature. Turning on the fluxes leads to a potential for (most of) the moduli and stabilizes them.

Flux compactifications and the subsequent stabilization of moduli are often studied using a four dimensional classical effective potential, constructed by integrating out the leading order effects of the compact manifold. The idea that the resulting potential surface might contain a multitude of possible (meta)stable vacua of the theory led to the term 'the string landscape'. To study all the possible flux compactifications we might have to resort to statistical techniques.

1.1.2 Challenges and questions related to the Landscape

As we mentioned in the previous section, the worldsheet action contains contributions from the background fields. That is, we can describe how a string propagates in a certain background, but we do not know how to incorporate strings joining or splitting, we don't have a full string field theory. Thus, the full 1PI effective potential which would contain all low energy information of string (field) theory is unknown. However, the concept of the string landscape is formulated using a four dimensional effective potential. The effective potential that is used is the analog of the Wilsonian effective potential, which by its definition is only valid around a single minima or a set of quasi degenerate vacua[2][10].

An additional problem for specific flux compactifications is that they often combine orientifolds with fluxes that are turned on. We do not have a perturbative string theory definition of such configurations. Instead these backgrounds are commonly constructed in the low energy supergravity approximation.

If, on the other hand, we take the positive point of view with respect to the landscape, then

[2]and has a fixed asymptotic background.

there is a whole new set of interesting questions that one can ask. One of the central questions being, how to characterize the landscape, and find dynamical mechanisms for populating and selecting among the vacua.

1.1.3 Outline of the Thesis

This thesis will describe three related projects which all take a different approach to the central concept that Nature contains a whole set of possible vacua consistent with the idea of the string landscape.

In chapter 2, we will focus on one particular family of flux compactification [7]. This particular setup should be thought of as a specific way of compactifying the ten dimensions from string theory to a four dimensional world. This background itself has a few discrete parameters which are (completely) free and as such it describes a family of backgrounds, all with similar properties. This DeWolfe et al. background is particularly interesting since it seems to address some of the challenges within the field of flux compactifications, as we will discuss extensively below.

In chapter 3, we will take a broader view of the string landscape. Instead of focusing in on the details of a certain compactification as in chapter 2, we will survey all the different known techniques to compactify. In this chapter we assume that the landscape view of string theory is correct, and investigate what the tunneling rate between the different vacua is. The basic idea behind this project is that while the landscape might consist of a multitude of consistent backgrounds, if most of these backgrounds are unstable against decay, only a limited set of specific compactifications will be relevant to our world since our world is clearly (relatively) stable.

In chapter 4, we will address a question which relates more directly to phenomenology. String theory is a supersymmetric theory. However, since supersymmetry is not apparent in our world, we need to find an explanation how supersymmetry is broken. Recently, an interesting new idea[2] was put forward explaining why we might not observe supersymmetry. Instead of trying to construct a theory where the global (i.e. stable) minimum of the effective potential is a supersymmetry breaking vacuum, one could entertain the hypothesis that our world is not global minimum but only a (long lived) local (i.e. metastable) minimum of the potential. Since the computation of the 1PI effective potential is often computationally involved in realistic models, chapter 4 describes the design of a computer program that computes the 1PI effective action of a chiral supersymmetric field theory up to first loop order and searches for the minima

of this potential.

In the following sections we will briefly introduce each of these three projects.

1.2 The DeWolfe et al. background

1.2.1 Interesting features of the background

In 2005, a paper was published discussing a flux compactification with several nice features [7]. First, in this compactification all the moduli are fixed at the classical level in supergravity. Secondly, the solution was formulated in (massive) type IIA theory which has the additional difficulty that turning on the fluxes on the Calabi-Yau basically destroys the Calabi-Yau structure, since it was proven that if one imposes $\mathcal{N} = 1$ supersymmetry with fluxes turned on in type IIA theory, one will generically not get a Calabi-Yau manifold[8]. Usually, one assumes that the fluxes are small so that the manifold only deviates a little from the fluxless Calabi-Yau case. In this paper, this problem was solved by starting from a six dimensional torus, T^6, which has more symmetry than a generic Calabi-Yau. Adding an orientifold and fluxes one can still get a supersymmetric theory. In addition, they arranged their setup so that it resembled the usual Calabi-Yau case by having the same kinds of moduli fields. This allows for the well known Calabi-Yau techniques to be used while we are allowed to turn on a lot of flux.

The third feature of the setup is that some of the fluxes are unconstrained. The net charge of the flux has to be zero in a compact space, since the field lines do not have the option of running off to infinity as in Maxwell's theory in three dimensions. The orientifolds have a negative charge and most fluxes come from positive charges. We cannot choose the number of orientifolds freely since it is linked with the manifold we are working on. Thus, we cannot turn on an arbitrarily high number of fluxes (note that since the supergravity theories are quantum theories the amount of flux is quantized). In this particular setup, though, some fluxes evade this general picture and are unconstrained.

This last feature has interesting implications. The coupling constant between strings depends on the flux background we turn on and as we can turn on as much of certain fluxes as we want, the string coupling constant can come arbitrarily close to zero. Also, the volume of the compact space grows but not faster than the non-compactified spacetime which means that, effectively, this setup remains four dimensional even when a lot of flux is turned on.

In the late nineties, J. Maldacena discovered that a string theory in an Anti de Sitter (AdS) spacetime background (this is a symmetric spacetime with negative cosmological constant) can completely be described by a conformal field theory [1]. We can employ this powerful insight

since the non-compactified spacetime in the DeWolfe et al. solution is a four dimensional AdS space. Just as for (most) flux compactifications, we do not have a perturbative worldsheet description of the DeWolfe et al. background. However, the apparent control we have over this setup with its free parameter that we can crank up arbitrarily, might open the door of finding a conformal field theory which could describe this family of compactifications. The existence of this CFT would then be instrumental in trying to answer the question whether the multitude of landscape vacua can indeed be considered different minima of the same theory, as is presupposed by the idea of the string landscape.

1.2.2 Our aim and methods

In the first place, our aim in chapter 2 will be to shed some more light on the validity of the DeWolfe et al. massive type IIA description of the compactification. In particular, the background contains an orientifold, known to be singular within a supergravity description. In addition, massive type IIA does not have a perturbative worldsheet expansion.

Several aspects of the DeWolfe et al. compactification will guide us to reach our aim. We will discuss them here briefly.

Entropy computation

One can add a black hole to the four dimensional AdS space of our setup. A black hole can be described by thermodynamics and so we can compute its entropy. In the string theory configuration, adding a black hole corresponds to adding a brane of some sort (these are the charged sources for the fluxes we discussed earlier). The entropy scaling of a stack of M2-branes in M-theory was studied. Computing the entropy of a black hole added to the AdS space of the DeWolfe et al. background, we find that this entropy matches the entropy of a stack of M2-branes. This indicates that we should first try to understand the configuration from the M-theory point of view.

Supersymmetry conditions in M-theory

Since we have a number of supersymmetries in the problem, we can study how this restricts the solution in M-theory. It turns out that the M-theory configuration will consist of an eight dimensional part that has to satisfy certain topological conditions, namely it should be a cone over a manifold with G_2-structure. In addition there are other differential restrictions depending on the fluxes in M-theory [30]. Writing down these differential restrictions, one gets that the

M-theory picture should involve a four dimensional AdS space and a seven dimensional space with weak G_2-holonomy. The conditions also indicate that our setup involves M2-branes.

Lift to M-theory

Using a technique similar to the one used by M. Schulz to construct the leading order approximation M-theory setup of a configuration in (non-massive) type IIA [17], we attempt to construct an explicit M-theory lift of the DeWolfe et al. compactification. M. Schulz first applies T-duality transformations before going to M-theory. These duality transformations are symmetries of the string theory (i.e. we are describing exactly the same setup while the actual configuration of the background looks different). We take the same approach and find that we end up after two properly chosen T-dualities with a non-massive type IIA configuration where most fluxes are zero. The effect of the some of the flux shows up as twists in the metric. This is related to 'non-geometrical backgrounds', a branch of string theory that has received a lot of attention lately. This non-massive configuration can then be lifted to M-theory using the standard methods.

1.2.3 Summary of our conclusions

The DeWolfe et al. setup has in particular three different (4-form) fields. The setup studied in the original paper has all those fields turned on and large. We first considered a different regime where we only make one of those fields grow. An entropy computation suggest that the correct approximation scheme to describe this situation is 11 dimensional M-theory. Using the dualities that relate the different approximation schemes of string theory, we succeeded in constructing an (approximate) M-theory setup corresponding to the original compactification. The M-theory picture is a stack of M2-branes at the tip of the cone where the M2-branes are on top of the orientifold. The M-theory configuration is approximate in a sense that we were not able to include the exact geometry which encodes the orientifold. The exact M-theory geometry corresponding to an orientifold is only known for the simple case where one has flat space with an orientifold inserted.

We then proceed to consider the original DeWolfe et al. regime where all fluxes are large. While this regime is harder to describe, an approximate double T-duality relates the massive type IIA compactification to a usual type IIA compactification. This new type IIA point of view, indicates that we have a stack of D2-branes reminiscent of the M2-branes found in the regime discussed above. We argue that there is a region near those D2-branes which grows

as you increase the flux. This region cannot properly be described in the (massive) type IIA approximation scheme, instead one has to use M-theory in this region. We thus believe that the entire configuration cannot be described with (massive) type IIA string theory, instead one has the complex situation where part of the compactification can be studied using one approximation scheme and another part in another approximation.

1.3 Tunneling in the Landscape

1.3.1 The question we aim to address and method used

In chapter 3, we will work under the assumption that the circumstantial evidence for the existence of a vast number of states in the landscape is correct. We thus assume that when we consider the classical effective action and find classically stable stationary points which have a small string coupling and a large internal volume such that supergravity is a valid approximation, that these stationary points are sensible metastable vacua.

The central question we will try to address is whether these states are stable against decay. If it turns out, as we will find, that most generic states are prone to rapid decay to other states, the vast amount of vacua, among which one hopes to find a vacuum describing our world, might not be such a big problem as feared at first. Since the world we observe is fairly stable, we will only need to consider states within the landscape that have the properties that ensure metastability.

In our survey of all known types of compactifications, we distinguish five different classes each with distinct features: weak string coupling, large compactification volume, low energy supersymmetry breaking, light moduli and warping. We will model the tunneling between neighboring states within the landscape using the Coleman-De Luccia decay. This implies several assumptions which will be discussed in detail below. For each of the classes, we will then study how the Coleman-De Luccia decay probability scales as we dial certain characteristic parameters.

1.3.2 Summary of conclusions

We will find that the vast majority of flux vacua with small cosmological constant are unstable to rapid decay to a big crunch. Only compactifications which have a large compactification volume or states which are (approximately) supersymmetric have a suppressed decay. Neither weak string coupling, warping, or the existence of very light particles are, by themselves, enough

to render states reasonably metastable.

With this conclusion a new interesting question emerges: if the world we live in was reached through a decay channel from a highly unstable state, what is a likely decay channel? While our answer with respect to this question is speculative, we propose that a discrete R-symmetry might be a cosmological attractors even though these states are uncommon in the landscape. This since vacua with large compactification volumes seem more difficult to construct and states with low energy supersymmetry breaking without discrete R-symmetry tend to be isolated in the landscape in that they tend to be surrounded by a multitude of AdS states. Such a decay channel is thus less likely since the chance of reaching the isolated state with a positive cosmological constant is smaller.

1.4 Metastable vacua in chiral supersymmetric theories

1.4.1 Supersymmetry breaking

In chapter 4, we will discuss the computer package `VScape` to analyze phenomenological supersymmetric models and their (meta)stable states.

Anticipating new experimental high energy particle data from the LHC by the end of 2008, the theory community has focused more on model building in recent years. Most of the models introduced have supersymmetry built in at high energies. Since our world is definitely not supersymmetric, one has to provide a mechanism by which the supersymmetry is broken at energy scales of our world.

To obtain spontaneous supersymmetry breaking in the minimal supersymmetric extension of the Standard Model (MSSM), one has to add additional fields since both mechanisms to break supersymmetry (D-term and F-term breaking) using only MSSM fields do not lead to acceptable models. Adding another sector that interacts at tree level with the MSSM is also problematic since it generally speaking leads to unacceptable particle spectra. Therefore, the most commonly studied option is that the supersymmetric breaking terms in the MSSM come from an indirect or radiative effect. In many models the supersymmetry breaking happens in a hidden sector. This hidden sector talks to particles which interact with the MSSM fields and as such mediate the breaking to the MSSM by generating soft breaking terms when the effects of the hidden sector are integrated out.

There are two main proposals for what the mediating interactions might be. One, a gravity mediated scenario the mediation happens via new physics at the Planck scale (and includes gravity). Another possibility which is also flavor blind is that the mediating particles interact

through ordinary electroweak or QCD interactions. This is the gauge mediated scenario. A variant of the second scenario is direct gauge mediation where there is no distinction between the mediation sector and the hidden sector.

Below we will discuss a model for metastable supersymmetry breaking that can be used as hidden sector. This model is particularly promising for the construction of direct mediation models where one has a large global symmetry group with a subgroup which is gauged and then identified with the Standard Model gauge group. An example of this setup is given in [66].

1.4.2 Metastability

In [3], spontaneous supersymmetry breaking is tied with the existence of an R-symmetry in the model. Generically, a supersymmetric theory with an exact R-symmetry has a ground state with broken supersymmetry. On the other hand, a theory without (or with a broken) R-symmetry has a supersymmetric ground state. R-symmetry is thus a valuable tool to investigate supersymmetry breaking.

From a phenomenological point of view we want the supersymmetric partners to the gauge bosons, the gauginos, to be rather massive since we have not yet observed these particles in experiments. A gaugino mass term implies that R-symmetry should be broken. This R-symmetry breaking can either be spontaneous in which case you have an R-axion which might cause phenomenological problems since it is a light particle. The breaking can also be explicit. Since a full theory of gravity is not expected to contain any continuous global symmetry, gravity will necessarily break the R-symmetry, though this breaking might not be strong enough to solve the problems with the R-axion.

If we assume that R-symmetry is explicitly broken not just by gravity, then the ground state is supersymmetric unless one constructs a non-generic model. Such models are not as appealing since they tend to be more complex. Models with a supersymmetric ground state, on the other hand, were not considered since most people worked with the assumption that our world should be the ground state of some theory. However, in [2] a paradigm shift was proposed. It was argued that it is possible for our world to be in a metastable state of a model, as long as this metastable state is long-lived.

These metastable states are expected to be common in many models. Indeed, the model studied in the original paper [2] is the simple and well studied supersymmetric extension of quantum chromodynamics (SQCD). Subsequently, many other theories have been studied and were found to exhibit long-lived metastable states too. These models can then be built in as

the hidden sector of a phenomenologically realistic model as was explained earlier.

1.4.3 VScape

The computation of the one-loop effective potential of phenomenologically interesting models are often not tractable analytically due to the complexity of the model and the number of parameters. The computation of the one-loop Coleman-Weinberg potential is calculationally intensive, so we opted to develop `VScape`, a C++ computer program that computes and analyzes the one-loop 1PI effective potential.

The program was tested in a variety of cases. The results of the analytical case presented in [2] where compared to the results of the package and were found to match. By now, the program has been used by other research groups to study different models [4, 5].

Chapter 2
Analysis of the DeWolfe et al. background

2.1 Introduction

In this chapter we will discuss in detail our findings of the work done in collaboration with T. Banks [6].

Flux compactifications [8] provide the arena for most of the discussions of the String Landscape as well as modern approaches to string phenomenology. The discussion of these compactifications is generally carried out in low energy effective field theory [9] [10], despite the fact that they all contain orientifold singularities. Further, there is no perturbative world sheet treatment of these backgrounds. Recently, DeWolfe *et al.*[7] introduced a sequence of models characterized by an integer N. Earlier work on similar type IIA flux compactifications was done in [11]. The DeWolfe *et al.* compactifications are classical solutions of Type IIA SUGRA, with a singular orientifold source and a variety of Ramond-Ramond and Neveu Schwarz fluxes. The parameter N is related to the value of certain quantized fluxes, and may be taken arbitrarily large. This is in marked contrast to typical flux compactifications, where fluxes are bounded [12]. The authors of [7] argue that for large N the moduli can be stabilized at values where all radii are large compared to the string scale, and the string coupling is small. Furthermore, the four non-compact directions are an AdS space with a radius R_{AdS} whose ratio to the compactification scale grows with N. The latter property is in marked contrast to the sequences of models treated in the AdS/CFT correspondence.

Our aim in this paper is to investigate further the models of [7], and to determine whether they admit a systematic low energy field theory expansion (see also [13]) and/or a weakly coupled string expansion. The inevitable orientifold of flux compactifications is one potential barrier to an effective field theory treatment[1]. In addition, these models contain a ten form flux F_0, and correspond to solutions of the massive Type IIA SUGRA Lagrangian. It is well known that quantization of F_0 is a problem for effective field theory, and that the massive Type

[1]G. Moore and S. Ramanujam have emphasized to us the problems with the back reaction of the orientifold, which they have analyzed extensively in the context of the original DeWolfe *et al.* solutions[14].

IIA string theory does not have a perturbative world sheet expansion (the D8-brane solution of this theory has a string coupling which grows at infinity). In addition, the effective field theory treatment has the usual problem of orientifold singularities. Thus despite apparently small parameters, it is far from clear that there is a systematic large N expansion of this system.

We approach this problem indirectly. Ignoring the back reaction of the orientifold, we perform a double T-duality on the DeWolfe *et al.* background[2]. The result is Type IIA string theory on a twisted torus, with flux only in the four AdS directions. Despite the fact that this configuration does not satisfy tadpole cancellation, the T-duality is a legitimate operation on the orbifold CFT. We then restore tadpole cancellation in the T-dual picture (the formal dual of the original orientifold).

Regime with one large 4-flux:

We argue that the resulting model in this regime does not have a weakly coupled Type IIA world sheet expansion. In this limit, from the point of view of DeWolfe *et al.*, the string coupling remains weak, the scales of both AdS_4 and the compact manifold are large, and the Kaluza-Klein radius is parametrically smaller. However, some cycles on the compact manifold shrink to zero size, and this is not a limit in which DeWolfe *et al.* would claim to have a controlled expansion. In the limit where we only turn on one four form flux, the fixed temperature entropy computed from the AdS geometry scales like $N^{3/2}$ as one would expect from a large number of M2-branes. We show that this is explained in the T-dual IIA picture by a large number of D2-branes sitting at the orientifold locus, where the string coupling is large. The D2/M2 world volumes are in the AdS directions. In typical orientifold compactifications that have been studied in string theory, those with a known world sheet expansion, the effect of the orientifold is confined to a region of order string scale. Here we argue that this is not the case, since the parameter N, which apparently tunes the string coupling to be small, in fact counts a large number of branes near the orientifold singularity. We argue that in fact the strong coupling region completely dominates the geometry in the single flux limit. The resulting theory for large N is M-theory on $AdS_4 \times M_7$, where M_7 is a manifold of weak G_2 holonomy. The AdS and compact radii scale the same way with N.

[2]We work in the orbifold limit. The authors of [7] took pains to show that the blow up moduli of the orbifold can be stabilized at large values of the radii of shrinking cycles. We address the analogous question in the T-dual picture.

Regime with all 4-flux large:

For the generic regime of the background, we find that 11D SUGRA is not a valid approximation. This is a consequence of the small string coupling found by DeWolfe et al., combined with the observation that the AdS radius is much larger than that of the compact manifold computed using our naive T-duality rules. Thus, in this region where DeWolfe *et al.* claimed a systematic expansion, many features of their picture are valid. However, our picture also includes large numbers of D-branes sitting at the orientifold locus in the regime where all fluxes are large. We argue that the weak coupling approximation breaks down in a vicinity of the orientifold whose size scales like $N^{1/20} l_s$. This rules out a uniform weak coupling expansion in the large N limit. Furthermore, if we apply 11D SUGRA to the region around the orientifold, it suggests that this region actually blows up to a seven manifold whose radius of curvature is of order the AdS radius. In the conclusions, we also provide a heuristic explanation of the peculiar $N^{9/2}$ entropy scaling of the regime with all fluxes large. This argument also seems to require a compact manifold with volume much larger than that suggested by De Wolfe *et al.*.

Our conclusion is that the generic DeWolfe *et al.* configuration probably exists as a valid model of quantum gravity in AdS_4. However, it is unclear to us whether is has a compactification radius parametrically smaller than the AdS radius. No existing approximation scheme computes its large N expansion. Different approximations, apparently valid in different regions of the compact manifold suggest different values for the ratio of scales. The problem of different approximation schemes for different regions is somewhat analogous to F-theory solutions for fluxless compactifications. However, the large supersymmetry algebra of F-theory compactifications provides reliable computational tools, which are absent for these models.

This chapter is organized as follows. In section 2, we review the DeWolfe *et al.* background. In section 3, we transform the background by a double T-duality, using the approximations noted above. This allows us to eliminate the massive type IIA flux. We also comment on the approximate character of the transformation. Section 4 deals with the Bianchi condition for the dualized background. In section 5, we will argue that the DeWolfe *et al.* solution with one large flux should be considered in an M-theory setting. We will explicitly lift the dualized background to M-theory. Section 6 will detail some of the aspects of the obtained 11D SUGRA solution. We will discuss its interpretation as a stack of M2-branes. We conclude in section 7 where we speculate on the nature of the generic DeWolfe *et al.* compactification. Appendix 2.8 and 2.9 give some more details on the double T-duality transformation of the DeWolfe *et al.*

background, while Appendix 2.10 reviews the formulas to lift the background to M-theory.

2.2 The DeWolfe *et al.* background

2.2.1 The metric, fluxes and discrete symmetries of the solution

In [7], DeWolfe *et al.* describe an infinite set of $\mathcal{N}=1$ solutions of massive type IIA SUGRA [15]. The compact manifold in their solution is $T^2\times T^2\times T^2$, modded out by three discrete symmetries:

- $\Omega_p(-1)^{F_L}\sigma$ with $\sigma: z_i \to -\bar{z}_i$
- $T: (z_1,z_2,z_3)\to(\alpha^2 z_1, \alpha^2 z_2, \alpha^2 z_3)$
- $Q: (z_1,z_2,z_3)\to(\alpha^2 z_1+\frac{1+\alpha}{3}, \alpha^4 z_2+\frac{1+\alpha}{3}, z_3+\frac{1+\alpha}{3})$

with $\alpha = e^{2\pi i/6}$. The resulting space is orientifolded $T^6/\mathbb{Z}_3^2$. The combination of the imposed discrete symmetries and fluxes turned on leads to a background where all moduli are fixed. The metric and the fluxes of the background are given by,

$$
\begin{aligned}
ds^2 &= \gamma_1(dx_1^2+dx_2^2)+\gamma_2(dx_3^2+dx_4^2)+\gamma_3(dx_5^2+dx_6^2)+ds^2_{\mathrm{AdS}_4} && (2.1)\\
H_3 &= -4\pi^2\alpha' h_3\,\beta_0 && (2.2)\\
&= -4\pi^2\alpha' h_3 \sqrt[4]{3}\sqrt{2}\,\big(dx_1\wedge dx_3\wedge dx_5 - dx_1\wedge dx_4\wedge dx_6 \\
&\qquad\qquad - dx_2\wedge dx_3\wedge dx_6 - dx_2\wedge dx_4\wedge dx_5\big) && (2.3)\\
e^{\varphi} &= \frac{1}{4}|h_3|\sqrt[4]{\frac{3^3 5}{|f_0 f_4^1 f_4^2 f_4^3|}} && (2.4)\\
F_4 &= (2\pi\sqrt{\alpha'})^3\sqrt[3]{\kappa} f_4^i \widetilde{w}^i && (2.5)\\
&= 4(2\pi\sqrt{\alpha'})^3\sqrt[3]{3}\Big(f_4^1\, dx_3\wedge dx_4\wedge dx_5\wedge dx_6 \\
&\qquad\qquad + f_4^2\, dx_5\wedge dx_6\wedge dx_1\wedge dx_2 && (2.6)\\
&\qquad\qquad + f_4^3\, dx_1\wedge dx_2\wedge dx_3\wedge dx_4\Big)\\
F_2 &\approx 0 && (2.7)\\
F_0 &= \frac{f_0}{2\pi\sqrt{\alpha'}}\,, && (2.8)
\end{aligned}
$$

where $f_0, h_3, f_4^1, f_4^2, f_4^3 \in \mathbb{Z}$; $z_1 = x_1 + i x_2, \ldots$ and

$$
\gamma_i = 4\pi^2\alpha'\frac{2}{\sqrt[3]{3}}\sqrt{\frac{5|f_4^1 f_4^2 f_4^3|}{|f_0|}}\frac{1}{|f_4^i|}\,. \tag{2.9}
$$

The tadpole cancellation condition for F_2 reduces to $f_0 h_3 = -2$. Notice that we defined the R-R fluxes following the conventions of [16] instead of those in [7] (see footnote 3 in [7] v3). The

non-compact part of the metric, $ds^2_{\mathrm{AdS}_4}$, is a 4-dimensional AdS_4 space with radius (in string frame),

$$R^2_{\mathrm{AdS}} = 4\pi^2\alpha' 16 \sqrt{\frac{5^3|f_4^1 f_4^2 f_4^3|}{3^3|f_0|^3|h_3|^4}}\,. \tag{2.10}$$

The volume of the compact manifold is computed to be

$$\begin{aligned} \mathrm{vol}_6 &= \frac{1}{8\sqrt{3}}\gamma_1\gamma_2\gamma_3 && (2.11)\\ &= (4\pi^2\alpha')^3\sqrt{\frac{5^3|f_4^1 f_4^2 f_4^3|}{3^3|f_0|^3}}\,, && (2.12)\end{aligned}$$

where the factor

$$\frac{1}{8\sqrt{3}} = \left(\frac{1}{9^{1/6}}\right)^3\left(\frac{\sqrt{3}}{9^{1/6}2}\right)^3, \tag{2.13}$$

comes from the discrete identifications in the compact manifold. The four dimensional Planck length then becomes:

$$\begin{aligned} l_{P(4)} &= \frac{1}{\sqrt{16\pi}}\left(\frac{\mathrm{vol}_6}{2\kappa_{10}^2 e^{2\varphi}}\right)^{-1/2} && (2.14)\\ &= |h_3|\sqrt{\frac{3^3\alpha'}{2^7 5}\frac{|f_0|}{|f_4^1 f_4^2 f_4^3|}}\,, && (2.15)\end{aligned}$$

where we used the convention $2\kappa_{10}^2 = (2\pi)^7\alpha'^4$.

2.2.2 The orientifold in the DeWolfe *et al.* background

The orientifold, constructed by modding out by $\Omega_p(-1)^{F_L}\sigma$, lies on

$$x_1 = x_3 = x_5 = 0\,. \tag{2.16}$$

Taking into account the identifications under $\mathbb{Z}_3\times\mathbb{Z}_3$, we get the three dimensional surface along which the orientifold is extended in the compact space. In figure 2.1, this surface is pictured in the fundamental region of one of the tori of $T^2\times T^2\times T^2$. The orientifold also fills the non-compact space.

The 3-cycle that is invariant under $\mathbb{Z}_2\times\mathbb{Z}_3\times\mathbb{Z}_3$, is the cycle on which the orientifold is wrapped. This cycle α_0, is determined by its Poincaré dual 3-form,

$$\begin{aligned} \mathrm{O6} &: \alpha_0-\text{cycle} && (2.17)\\ &: \sqrt[4]{3}\sqrt{2}\left(dx_1\wedge dx_3\wedge dx_5 - dx_2\wedge dx_4\wedge dx_5\right.\\ &\qquad \left. - dx_1\wedge dx_4\wedge dx_6 - dx_2\wedge dx_3\wedge dx_6\right) && (2.18)\\ &= \beta_0\,. && (2.19)\end{aligned}$$

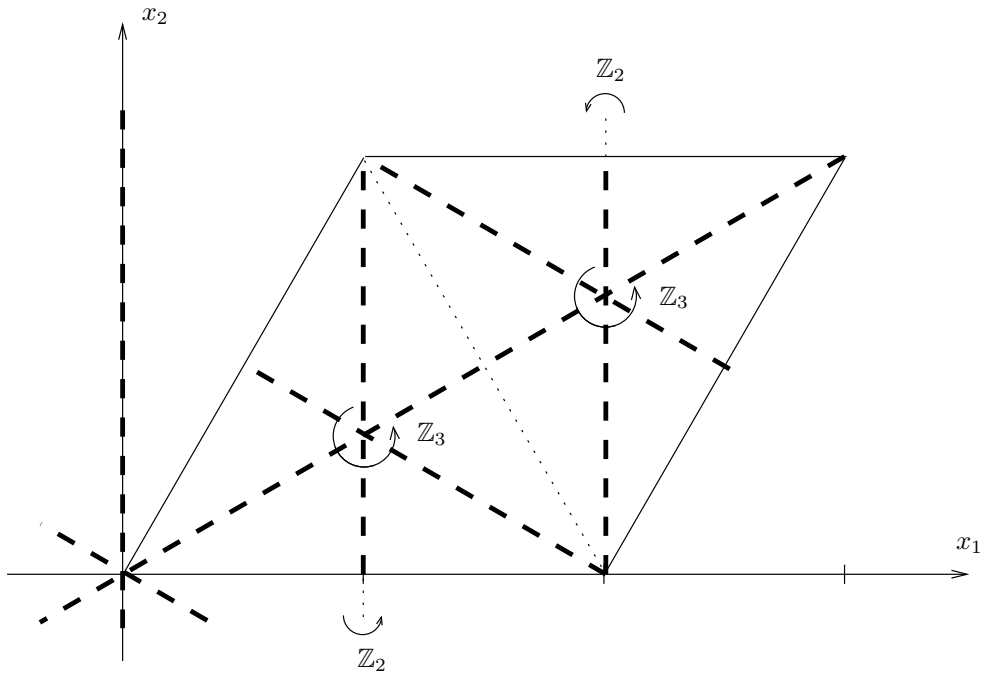

Figure 2.1: The z_1-plane of T^6 with the actions of the non-free $\mathbb{Z}_3$ and the orientifolding $\mathbb{Z}_2$ indicated. The O6-plane is pictured in thicker, dashed lines.

2.2.3 Remark on the F_2-flux

The Bianchi identity for the massive type IIA solution reads:

$$dF_2 = F_0 H_3 + 2\kappa_{10}^2 \mu_p \delta_{\mathrm{O6}} \neq 0\,, \tag{2.20}$$

where $\mu_p = -2\sqrt{\pi}\kappa_{10}^{-1}(4\pi^2\alpha')^{-3/2}$, is the charge of the orientifold. Equation (2.7),

$$F_2 = 0 \tag{2.21}$$

should thus be seen as an approximation to the exact solution.

2.2.4 Scaling behavior

The integer parameters f_4^1, f_4^2 and f_4^3 are not constrained by any tadpole condition, but we need to take each $f_4^i \neq 0$, to have a non-degenerate solution (see (2.9)).

We will be interested in the regime

$$f_4^1 = f_4^2 = f_4^3 = N\,, \tag{2.22}$$

where we take $N \to \infty$. The parameters characterizing the compactification scale as:

$$l_{P(4)} \sim N^{-\frac{3}{2}}\sqrt{\alpha'} \tag{2.23}$$

$$R_{\rm AdS} \sim N^{\frac{9}{4}} l_{P(4)} \tag{2.24}$$

$$R_{\rm KK} \sim N^{\frac{7}{4}} l_{P(4)} \tag{2.25}$$

$$g_s \sim N^{-\frac{3}{4}}\,, \tag{2.26}$$

where $R_{\rm KK} = \sqrt[6]{\rm vol_6}$ is a measure for the size of the compact manifold. We see that the string coupling g_s is small, while the radii characterizing the solution are large. In addition, we notice that the background remains effectively four dimensional since the AdS radius grows faster than the Kaluza Klein radius.

Let us now consider the regime where:

$$f_4^1 = N, \qquad f_4^2 = f_4^3 = O(1)\,, \tag{2.27}$$

which results in,

$$l_{P(4)} \sim N^{-\frac{1}{2}}\sqrt{\alpha'} \tag{2.28}$$

$$R_{\rm AdS} \sim N^{\frac{3}{4}} l_{P(4)} \tag{2.29}$$

$$R_{\rm KK} \sim N^{\frac{7}{12}} l_{P(4)} \tag{2.30}$$

$$g_s \sim N^{-\frac{1}{4}}\,. \tag{2.31}$$

However in this regime, γ_1 (see eq. (2.9)) shrinks to zero, indicating that (massive) type IIA is not the correct description for this case. The above scalings might thus not hold in this scaling limit.

2.3 Approximate double T-duality

The DeWolfe *et al.* model is formulated in massive type IIA SUGRA. This theory does not have a perturbative world sheet expansion and quantization of the F_0 is problematic. The second difficulty is that the model also contains an orientifold which is a singular object when described in type IIA SUGRA [17]. To study the model, we will first apply two T-dualities, ignoring back reaction of the orientifold. These will bring us to non-massive type IIA. We will address the second problem by inserting the orientifold in the dualized configuration. The T-duality transformations have the additional benefit that the H_3 flux vanishes. The original H_3 flux turns into a geometric flux showing up as twists in the metric.

2.3.1 Approximate character of the T-dualities

Let us first point out that applying a double T-duality on a configuration with fluxes results in general in a non-geometric compactification [18]. However, the T-dualities we will perform are chosen such that we do not violate the condition ensuring that we remain in the domain of geometric compactification [19].

We will first perform a T-duality on the x_1-direction, followed by a T-duality in the x_2-direction. The T-duality transformations will only be valid in an approximate sense:

- The loops on the T^6 defined by the x_1 and x_2-directions are contractible on the fixed points of the $\mathbb{Z}_2 \times \mathbb{Z}_3 \times \mathbb{Z}_3$ identifications. We thus do not have an S^1-isometry required for an exact T-duality.

- In addition, we will work in the approximation where $F_2 = 0$. As discussed in section 2.2.3, this flux does not satisfy the Bianchi condition. We thus expect that the Bianchi identity after T-dualities will not be satisfied either. The F_2 flux is sourced by the orientifold and by the flux term $F_0 H_3$. In the T-duality computation we will keep track of the fluxes F_0, H_3 and the cycle on which the orientifold is wrapped. This information will be helpful to correct the T-dualized solution.

- Notice that we can expect the correct F_2 in the original setup to depend on all coordinates x_i, since we expect that close to the orientifold the F_2 flux resembles the F_2 flux of an orientifold in flat space. Because of the identifications the orientifold is extended along all coordinate directions (see figure 2.1). This implies that the F_2 flux breaks the S^1-isometry in the coordinate directions. Thus, if we would include the back reaction of the orientifold, which sources the F_2-flux, we would not be able to T-dualize.

There are two related ways to view our approximate T-dualities. So far we have emphasized the first, which is the interpretation of T-duality mapping solutions of Type IIA supergravity into other solutions. In our case it takes solutions of massive Type IIA into solutions of ordinary Type IIA, because the duality eliminates the F_0 flux. This duality is only approximate and in order to perform it we must ignore the orientifold (or at least its back reaction).

Alternatively, we can start from the orbifold conformal field theory of DeWolfe *et al.* Turning on fluxes corresponds to deformations of the background in the direction of certain vertex operators, and the orientifold corresponds to modding out the CFT by one of its symmetry operations. We can perform an exact T-duality on the CFT (just a change of variables) and

try to understand which vertex operators must be turned on in the T-dual language[3]. Similarly we can mod out by the T-dual symmetry operation. The result of this operation is a CFT just as mysterious as the one, one might have tried to write down in the original picture. However to leading order in the string tension expansion, it leads to a new set of equations of motion, to which we may try to find a solution. The reader may choose whichever interpretation of our procedure (s)he finds most convincing. We do not pretend that we have presented a rigorous argument for either approach.

At any rate, as a consequence of the approximations, we can expect the solution after T-dualities to contain inconsistencies. By imposing the equations of motion, the Bianchi conditions and supersymmetry conditions on the dualized configuration, we hope to find a tractable version of the DeWolfe *et al.* solutions, with a well defined large N expansion.

2.3.2 Orientifold projection in a twisted torus

The H_3-flux in the DeWolfe *et al.* paper leads to twisting in the geometry after T-duality. In this section we study how an orientifold fixed plane behaves under T-duality when a non-trivial H_3-flux background is turned on.

Since the H_3-flux (2.2) and the orientifold (2.17), have several components along different x_i-directions, we get several twisting terms in the metric after T-duality in the x_i coordinate system. The T-duality action allows us to break this problem in several smaller problems by focusing on one term in the orientifold and one term of the H_3-flux. Let us work out the case where we focus on the term

$$H_3 \sim dx_1 \wedge dx_4 \wedge dx_6 + \dots \tag{2.32}$$

and where the orientifold fixed plane is wrapped on the compact 3-cycle

$$\text{O6} : dx_1 \wedge dx_3 \wedge dx_5 + \dots \tag{2.33}$$

in the Calabi-Yau manifold. Let us rename and rescale, x_1, x_4, x_6 as θ, Y, Z. We can now focus on the 3-torus T^3 with H_3-flux [19]:

$$ds_3^2 = d\theta^2 + dY^2 + dZ^2 \tag{2.34}$$

$$H_3 = d\theta \wedge dY \wedge dZ\,, \tag{2.35}$$

where we take θ, Y and Z to have periodicities 2π. The location of the orientifold in this T^3

[3]The real problem here is that since fluxes are discrete, the sought for CFT is not a small perturbation of the original orbifold.

subspace of the compact manifold is determined by the fixed plane of the symmetry,

$$\theta \rightarrow -\theta \tag{2.36}$$

$$Y \rightarrow Y \tag{2.37}$$

$$Z \rightarrow Z\,. \tag{2.38}$$

The bosonic part of the worldsheet action which encodes the dynamics on the T^3 is given by ($d^2z = d\sigma^1 d\sigma^2$):

$$S = \frac{1}{2\pi\alpha'}\int d^2z\{\partial\theta\bar{\partial}\theta + \partial Y\bar{\partial}Y + \partial Z\bar{\partial}Z + Y\partial\theta\bar{\partial}Z - Y\partial Z\bar{\partial}\theta\}\,. \tag{2.39}$$

This action is invariant under the periodic identifications of the target space coordinates since the periodic identification, $Y \rightarrow Y + 2\pi$, only contributes a total derivative. The action is also invariant under the discrete orientifold symmetry $\sigma\Omega_\theta$:

$$\theta(z,\bar{z}) \rightarrow -\theta(\bar{z},z) \tag{2.40}$$

$$Y(z,\bar{z}) \rightarrow Y(\bar{z},z) \tag{2.41}$$

$$Z(z,\bar{z}) \rightarrow Z(\bar{z},z)\,. \tag{2.42}$$

Now we can perform a T-duality in the θ-direction by gauging the $U(1)$-isometry along that direction [20]. The new action reads,

$$S = \frac{1}{2\pi\alpha'}\int d^2z\{(\partial\theta + A)(\bar{\partial}\theta + \bar{A}) + \partial Y\bar{\partial}Y + \partial Z\bar{\partial}Z \tag{2.43}$$

$$+ Y(\partial\theta + A)\bar{\partial}Z - Y\partial Z(\bar{\partial}\theta + \bar{A}) + \widetilde{\theta}F\}\,, \tag{2.44}$$

with $F = \partial\bar{A} - \bar{\partial}A$. The field $\widetilde{\theta}$, is a Lagrange multiplier with period 2π. Integrating out $\widetilde{\theta}$ gives the original action.

The new action is only invariant under the periodicity $Y \rightarrow Y + 2\pi$, if we take $\widetilde{\theta} \rightarrow \widetilde{\theta} - 2\pi Z$, simultaneously. We can also extend the action of the orientifold symmetry by requiring that the new action is invariant under the extended orientifold symmetry. The orientifold symmetry, $\sigma\Omega_\theta$, becomes:

$$\theta(z,\bar{z}) \rightarrow -\theta(\bar{z},z) \qquad Y(z,\bar{z}) \rightarrow Y(\bar{z},z) \tag{2.45}$$

$$A(z,\bar{z}) \rightarrow -A(\bar{z},z) \qquad Z(z,\bar{z}) \rightarrow Z(\bar{z},z) \tag{2.46}$$

$$\bar{A}(z,\bar{z}) \rightarrow -\bar{A}(\bar{z},z) \qquad F(z,\bar{z}) \rightarrow F(\bar{z},z) \tag{2.47}$$

$$\widetilde{\theta}(z,\bar{z}) \rightarrow \widetilde{\theta}(\bar{z},z)\,. \tag{2.48}$$

Fixing the gauge with the condition $\theta = 0$ and integrating out the fields A and $\bar{A}$ gives the dual action:

$$S = \frac{1}{2\pi\alpha'} \int d^2z \{(\partial\widetilde{\theta} + Y\partial Z)(\bar{\partial}\widetilde{\theta} + Y\bar{\partial}Z) + \partial Y\bar{\partial}Y + \partial Z\bar{\partial}Z\} . \tag{2.49}$$

Translating this to the target space gives,

$$ds_3^2 = (d\widetilde{\theta} + YdZ)^2 + dY^2 + dZ^2 \tag{2.50}$$

$$H_3 = 0 , \tag{2.51}$$

with the identifications,

$$\widetilde{\theta} \rightarrow \widetilde{\theta} + 2\pi \tag{2.52}$$

$$Y \rightarrow Y + 2\pi \quad \text{and} \quad \widetilde{\theta} \rightarrow \widetilde{\theta} - 2\pi Z \tag{2.53}$$

$$Z \rightarrow Z + 2\pi . \tag{2.54}$$

The metric is thus a circle bundle over a torus. The non-trivial identifications indicate that the coordinate $\widetilde{\theta}$, along the fibre is not globally well-defined. Let us introduce the one form Θ, which is globally defined by $d\Theta = dY \wedge dZ$ and gives locally $\Theta = d\widetilde{\theta} + YdZ$. The action of the orientifold symmetry now reads:

$$\Theta \rightarrow \Theta \tag{2.55}$$

$$Y \rightarrow Y \tag{2.56}$$

$$Z \rightarrow Z . \tag{2.57}$$

This is, for the example we considered, the orientifold wraps both the fibre and the torus base space after T-duality. The Poincaré dual form of the cycle on which the orientifold is wrapped becomes:

$$\text{O7} : dx_3 \wedge dx_5 + \dots . \tag{2.58}$$

We can repeat this exercise for different combinations of terms in the H_3-flux and orientifold cycle. We find that the orientifold either wraps the fibre of the twisted torus, $\Theta \rightarrow \Theta$, or reflects the fibre $\Theta \rightarrow -\Theta$. In the T-duality computation of the DeWolfe *et al.* solution, we will follow the orientifold by keeping track of the Poincaré dual form of the cycle on which the orientifold is wrapped. The above discussion shows that this is a consistent treatment of the orientifold.

2.3.3 Doubly dualized background

In appendix 2.8, we review the action of T-duality on a background of SUGRA. In appendix 2.9, we work out the double T-duality transformation of the DeWolfe *et al.* model. The result

reads:

$$\begin{aligned} ds^2 &= \frac{4\pi^2\alpha'}{\gamma_1}\left(9^{\frac{2}{3}}\,\Theta_1^2+4^2\,3^{-\frac{2}{3}}\,\Theta_2^2\right)+\gamma_2(dx_3^2+dx_4^2)+\gamma_3(dx_5^2+dx_6^2) \\ &\quad + ds^2_{\mathrm{AdS}_4} \qquad (2.59)\\ H_3 &= 0 \qquad (2.60)\\ e^{\varphi} &= \frac{1}{4}|h_3|\sqrt[4]{\frac{3^3 5}{|f_0 f_4^1 f_4^2 f_4^3|}} \qquad (2.61)\\ F_4 &= 4(2\pi\sqrt{\alpha'})^3\sqrt[3]{3}f_4^1\frac{1}{\gamma_2\gamma_3}\mathrm{vol}_4 \qquad (2.62)\\ F_2 &= -4(2\pi\sqrt{\alpha'})^3\frac{\sqrt[3]{3}}{\gamma_1}(f_4^2\,dx_5\wedge dx_6+f_4^3\,dx_3\wedge dx_4) \\ &\quad + f_0\frac{2\pi\sqrt{\alpha'}}{\gamma_1}\,4\cdot 3^{\frac{1}{3}}\,\Theta_1\wedge\Theta_2 \qquad (2.63)\\ F_0 &= 0 \qquad (2.64)\\ \frac{1}{2\kappa^2_{10\widetilde{A}}} &= \frac{1}{2\kappa^2_{10A}}\frac{\gamma_1^2}{(4\pi^2\alpha')^2\,4\cdot 3^{\frac{1}{3}}} \qquad (2.65)\\ \Theta_1 &= 2\pi\sqrt{\alpha'}dx_1+2\pi\sqrt{\alpha'}h_3\frac{\sqrt[4]{3}\sqrt{2}}{9^{\frac{1}{3}}}(x_3dx_5-x_4dx_6) \qquad (2.66)\\ \Theta_2 &= 2\pi\sqrt{\alpha'}dx_2+2\pi\sqrt{\alpha'}h_3\frac{\sqrt[4]{3}\sqrt{2}}{4\cdot 3^{-\frac{1}{3}}}(-x_3dx_6-x_4dx_5)\,, \qquad (2.67)\end{aligned}$$

where $x_1\in[0,9^{-1/6}]$ and $x_2\in[0,2^{-1}\,3^{1/6}]$.

The original orientifold splits into an O5- and O7-plane after the first T-duality (see appendix 2.9). The second T-duality recombines those two orientifold planes to give an O6-plane wrapped on the Poincaré dual of the $\widetilde{\alpha}_0$-cycle:

$$\begin{aligned} \text{O6} \quad : \quad & \sqrt[4]{3}\sqrt{2}\left(+\frac{2\cdot 3^{-\frac{1}{6}}\Theta_2}{2\pi\sqrt{\alpha'}\,9^{\frac{1}{6}}}\wedge(dx_3\wedge dx_5-dx_4\wedge dx_6)\right. \qquad (2.68)\\ &\qquad \left.+\frac{9^{\frac{1}{6}}\Theta_1}{2\pi\sqrt{\alpha'}\,2\cdot 3^{-\frac{1}{6}}}\wedge(dx_4\wedge dx_5+dx_3\wedge dx_6)\right)\\ = \quad & \widetilde{\beta}_0\,. \qquad (2.69)\end{aligned}$$

2.4 The Bianchi identity after the double T-duality

As mentioned earlier, we expect the dualized solution (2.59)-(2.67) to contain inconsistencies. We will do the full analysis of the consistency conditions later. Here we will focus on the Bianchi condition. Taking the F_2 flux from the dualized solution we compute:

$$\begin{aligned} dF_2 &= f_0\frac{2\pi\sqrt{\alpha'}}{\gamma_1}\,4\cdot 3^{\frac{1}{3}}(d\Theta_1\wedge\Theta_2-\Theta_1\wedge d\Theta_2) \qquad (2.70)\\ &= f_0h_3\frac{(2\pi\sqrt{\alpha'})^3}{\gamma_1}\,2\cdot 3^{\frac{1}{6}}\widetilde{\beta}_0\,. \qquad (2.71)\end{aligned}$$

This 3-form is everywhere non-zero.

On the other hand, since the configuration after T-dualities is a solution of massless type IIA string theory, with the orientifold as only source for F_2, we expect the Bianchi identity to read:

$$\frac{1}{2\kappa^2_{10\widetilde{A}}} dF_2 = \mu_6 \delta_{\mathrm{O6}} = \mu_6 \delta(\widetilde{\beta}_0)\,. \tag{2.72}$$

The distributional 3-form dF_2, is thus localized on the orientifold plane, which lies on the Poincaré dual of the 3-form $\widetilde{\beta}_0$. This is clearly at odds with (2.71). This inconsistency was not unexpected as mentioned earlier.

We will now modify the dualized background such that it satisfies the Bianchi condition. From equation (2.72) we get:

$$dF_2 = -2\,\frac{(2\pi\sqrt{\alpha'})^3}{\gamma_1}\, 2\cdot 3^{\frac{1}{6}}\, \delta(\widetilde{\beta}_0)\,. \tag{2.73}$$

Integration over the $\widetilde{\beta}_0$-cycle gives,

$$\int_{\widetilde{\beta}_0} dF_2 = \int_{\mathrm{vol}_6} dF_2 \wedge *_6 \widetilde{\beta}_0 = -2\,\frac{(2\pi\sqrt{\alpha'})^3}{\gamma_1}\, 2\cdot 3^{\frac{1}{6}}\,, \tag{2.74}$$

or, after partial integration,

$$2\cdot 3^{\frac{1}{6}}\,\frac{\gamma_1}{(2\pi\sqrt{\alpha'})^3}\, h_3 \int_{\mathrm{vol}_6} F_2 \wedge (dx_3 \wedge dx_4 \wedge dx_5 \wedge dx_6) \quad = \quad -2\,. \tag{2.75}$$

In the original DeWolfe *et al.* solution, the flux from the orientifold was absorbed by the $F_0 H_3$ term in the Bianchi identity. This leads to the constraint $f_0 h_3 = -2$. The above derivation shows how the twisted geometry, with the non-closed 3-form $*_6\widetilde{\beta}_0$, absorbs the orientifold flux without the $F_0 H_3$ flux term.

The integrated Bianchi condition also gives us some information on the correct F_2 flux. It should contain a (distributional) term proportional to $f_0 \Theta_1 \wedge \Theta_2$. We also learn that as $N \to \infty$, the F_2 flux has to decrease. From now on we will ignore the term,

$$f_0 \frac{2\pi\sqrt{\alpha'}}{\gamma_1}\, 4\cdot 3^{\frac{1}{3}}\, \Theta_1 \wedge \Theta_2\,, \tag{2.76}$$

in (2.63). Instead we will include a term $F_{2,\,\mathrm{O6}}$ which satisfies (2.73).

2.5 Lift to M-theory

2.5.1 Entropy computation and motivation for an M-theory interpretation

Let us return to the original DeWolfe *et al.* solution. It is supposed to be an AdS_4 space-time, Maldacena dual to a $2+1$ dimensional CFT. Following [21] we can calculate the entropy of this

system,

$$S_{\rm BH} = \frac{A^{\rm Einst}_{\rm horizon}}{4G_N^{\rm 4d}} \tag{2.77}$$

$$= \pi \left(2MR_{\rm AdS}\right)^{\frac{2}{3}} \left(\frac{160\cdot 2^{\frac{7}{8}}3^{\frac{3}{4}}5^{\frac{1}{4}}\pi}{27}\frac{1}{|f_0|^{\frac{5}{4}}|h_3|^2}|f_4^1 f_4^2 f_4^3|^{\frac{3}{4}}\right)^{\frac{2}{3}}, \tag{2.78}$$

where M is the mass of the black hole.

Let us now consider the different scalings of the four form flux as discussed in section 2.2.4. For the regime $f_4^1 = f_4^2 = f_4^3 = N$, we find that

$$S_{\rm BH} \sim N^{\frac{3}{2}}\,. \tag{2.79}$$

This gives us the entropy as a function of the energy of the black hole. Using standard CFT thermodynamics, this implies a scaling

$$S_{\rm BH} \sim N^{\frac{9}{2}}\,. \tag{2.80}$$

as a function of the temperature[4]. We do not know of a conformal field theory with this kind of scaling.

If we take the other scaling regime where $f_4^1 \sim N$, while the other two four form fluxes are held fixed, then we find an entropy scaling like $N^{3/2}$ at fixed temperature, in the large N limit. We know that the entropy of the CFT describing a stack of N M2-branes scales in precisely this manner[23]. This computation thus seems to indicate that we should look for an M-theory interpretation of the special cases of the DeWolfe *et al.* background, with one large four form flux and the others of order one. We note that repeating the entropy computation in the doubly dualized background gives exactly the same answer as (2.78).

Indeed, we found that in our double T-dual solution, there was four form flux in the AdS_4 directions, corresponding to of order N D2-branes at the end of the universe. Note that this flux comes only from f_4^1, the flux we have chosen to be large in order to get M2-branes entropy scaling. Our entropy calculation suggests that these D-branes are behaving like M2-branes. This could be explained, if the IIA string coupling on the compact manifold is strong in the region where the M2-branes are localized.

There is a second reason indicating that we should look for an M-theory setting of the problem. The orientifold is a singular object in 10D SUGRA. The M-theory lift of an orientifold in flat space is the Atiyah-Hitchin manifold [24] [25]. In 11 dimensions, we have thus a non-singular, completely geometric description. The orientifold is singular in the Type IIA limit,

[4]This computation was done independently in [22]

because the string coupling is always large in the core of the Atiyah-Hitchin manifold, no matter what its value is at infinity. Since the orientifold locus includes the AdS_4 directions, the D2-branes in our T-dual configuration are sitting in a strong coupling region. This explains why they behave like M2-branes.

Such a picture is inconsistent with a weak coupling string theory interpretation of the DeWolfe *et al.* configurations, with only one large flux. We note that these observations are valid in the region where f_4^1 is large, and the other two four form fluxes are non-zero, and may be large or small. DeWolfe *et al.* only claimed to have a weakly coupled four dimensional compactification in the region where all fluxes are large. In our T-dual picture, even this regime has a large number of branes sitting near the orientifold. Our next thought was that there might be an M-theory interpretation with N M2-branes embedded in a smooth manifold. We will see that this is possible only for a single large flux with the other fluxes fixed and non-zero. Although the calculations of DeWolfe *et al.* still indicate a weakly coupled four dimensional compactification in this limit, certain cycles of the compact manifold shrink to zero for large N. These authors do not claim to have control over the regime that we claim has a smooth M-theory limit with comparable AdS_4 and M_7 radii.

2.5.2 Lift to M-theory

Given a massive type IIA solution (without H_3 flux), C. M. Hull constructed a procedure to lift the solution to M-theory [26]. This process consists roughly of a T-duality to type IIB and then a lift via F-theory to M-theory[5]. As discussed earlier, if we T-dualize the DeWolfe *et al.* background once, some H_3 flux remains which complicates the lift to M-theory. Therefore, we will follow the slightly different track of T-dualizing twice and then using the strong-weak correspondence between type IIA string theory and M-theory to lift the configuration to 11D[27].

In the 10D theories the orientifold is a singular object which we included by keeping track of the cycle on which it was wrapped and via its source term in the Bianchi identity. As mentioned earlier, in M-theory this singular object translates into a non-singular geometric object. Its explicit form is only known in the case of an orientifold in flat space [29]. Our strategy will be to first construct a naive lift ignoring the orientifold. Appendix 2.10 reviews the formulas to lift a non-singular type IIA SUGRA background to M-theory. However, omitting the orientifold will introduce inconsistencies. In a second step, we will impose the consistency conditions and try to modify the naive lift.

[5]There are complications on the quantum level with this construction [28]. Our analysis has been on the classical level.

Constructing the naive lift to M-theory of the dualized background gives, with $L_M = 2\pi\frac{\kappa_{10\tilde{A}}}{\sqrt{\pi}(2\pi\sqrt{\alpha'})^3}$:

$$
\begin{aligned}
ds^2 &= R_M^2\Theta_M^2 + \widetilde{\gamma}_{11}\Theta_1^2 + \widetilde{\gamma}_{12}\Theta_2^2 + \widetilde{\gamma}_2(dx_3^2+dx_4^2) + \widetilde{\gamma}_3(dx_5^2+dx_6^2) + ds^2_{\mathrm{AdS}_4} && (2.81)\\
G_4 &= 6m\,\mathrm{vol}_4 && (2.82)\\
\Theta_1 &= dx_1 + h_3\frac{\sqrt[4]{3}\sqrt{2}}{9^{\frac{1}{3}}}(x_3dx_5 - x_4dx_6) && (2.83)\\
\Theta_2 &= dx_2 + h_3\frac{\sqrt[4]{3}\sqrt{2}}{4\cdot 3^{-\frac{1}{3}}}(-x_3dx_6 - x_4dx_5) && (2.84)\\
\Theta_M &= dx_M + A_1 && (2.85)\\
dA_1 &= -2\cdot 3^{\frac{1}{6}}(f_4^2dx_5\wedge dx_6 + f_4^3dx_3\wedge dx_4) + \widetilde{F}_{2,\,\mathrm{O6}} && (2.86)\\
\frac{1}{2\kappa_{11M}^2} &= \frac{1}{16\pi l_{P11}^9} = \frac{1}{2\kappa_{10A}^2}\frac{\gamma_1^2}{(4\pi^2\alpha')^2\,4\cdot 3^{\frac{1}{3}}}\frac{1}{L_M}\,. && (2.87)
\end{aligned}
$$

where $\widetilde{F}_{2,\,\mathrm{O6}} = F_{2,\,\mathrm{O6}}/L_M$ and with

$$
\begin{aligned}
R_M &= \frac{3^{\frac{5}{6}}\pi^{\frac{2}{9}}}{2^{\frac{7}{9}}5^{\frac{1}{6}}}|f_0h_3^4|^{\frac{1}{6}}\frac{|f_4^1|^{\frac{1}{6}}}{|f_4^2f_4^3|^{\frac{1}{2}}}l_{P11} && (2.88)\\
\widetilde{\gamma}_{11} &= \frac{2\cdot 2^{\frac{4}{9}}3^{\frac{5}{6}}\pi^{\frac{4}{9}}}{5^{\frac{1}{3}}}\frac{|f_0|^{\frac{1}{3}}}{|h_3|^{\frac{2}{3}}}|f_4^1|^{\frac{1}{3}}l_{P11}^2 && (2.89)\\
\widetilde{\gamma}_{12} &= \frac{32\cdot 2^{\frac{4}{9}}3^{\frac{5}{6}}\pi^{\frac{4}{9}}}{9\cdot 5^{\frac{1}{3}}}\frac{|f_0|^{\frac{1}{3}}}{|h_3|^{\frac{2}{3}}}|f_4^1|^{\frac{1}{3}}l_{P11}^2 && (2.90)\\
\widetilde{\gamma}_2 &= \frac{8\cdot 2^{\frac{4}{9}}3^{\frac{5}{6}}5^{\frac{2}{3}}\pi^{\frac{4}{9}}}{9}\frac{1}{|f_0h_3|^{\frac{2}{3}}}|f_4^1|^{\frac{1}{3}}f_4^3l_{P11}^2 && (2.91)\\
\widetilde{\gamma}_3 &= \frac{8\cdot 2^{\frac{4}{9}}3^{\frac{5}{6}}5^{\frac{2}{3}}\pi^{\frac{4}{9}}}{9}\frac{1}{|f_0h_3|^{\frac{2}{3}}}|f_4^1|^{\frac{1}{3}}f_4^2l_{P11}^2 && (2.92)\\
R_{\mathrm{AdS}} &= \frac{8\cdot 2^{\frac{2}{9}}3^{\frac{5}{6}}5^{\frac{5}{6}}\pi^{\frac{2}{9}}}{9}\frac{1}{|f_0|^{\frac{5}{6}}|h_3|^{\frac{4}{3}}}|f_4^1|^{\frac{1}{6}}|f_4^2f_4^3|^{\frac{1}{2}}l_{P11} && (2.93)\\
m &= \frac{2^{\frac{7}{9}}3^{\frac{7}{6}}5^{\frac{1}{6}}}{160\pi^{\frac{2}{9}}}|f_0|^{\frac{5}{6}}|h_3|^{\frac{4}{3}}\frac{f_4^1}{|f_4^1|^{\frac{7}{6}}|f_4^2f_4^3|^{\frac{1}{2}}}\frac{1}{l_{P11}}\,. && (2.94)
\end{aligned}
$$

Notice that we also rescaled Θ_1, Θ_2 by $1/(2\pi\sqrt{\alpha'})$ as compared to the previous sections.

2.6 Discussion of the naive M-theory lift

2.6.1 Condition on $F_{2,\,\mathrm{O6}}$

The term $L_M\widetilde{F}_{2,\,\mathrm{O6}} = F_{2,\,\mathrm{O6}}$ in (2.86) has to satisfy the Bianchi identity (2.73). Integration as in (2.75) leads to the condition

$$
4\cdot 3^{\frac{1}{3}}h_3\int_{\mathrm{vol}_6}\widetilde{F}_{2,\,06}\wedge(dx_3\wedge dx_4\wedge dx_5\wedge dx_6) = -2\,. \qquad (2.95)
$$

As discussed earlier, this constraint should lead to $f_0h_3 = -2$.

2.6.2 Volume of the compact manifold

The volume of the compact 7 dimensional manifold is

$$\mathrm{vol}_7 = \frac{64 \cdot 2^{\frac{5}{9}} 3^{\frac{5}{6}} 5^{\frac{5}{6}} \pi^{\frac{14}{9}}}{27} \frac{1}{|f_0|^{\frac{5}{6}} |h_3|^{\frac{4}{3}}} |f_4^1|^{\frac{7}{6}} |f_4^2 f_4^3|^{\frac{1}{2}} l_{P11}^7 \,. \tag{2.96}$$

The Kaluza-Klein radius becomes

$$\begin{aligned} R_{\mathrm{KK}} &= \sqrt[7]{\mathrm{vol}_7} && (2.97) \\ &= \frac{2^{\frac{59}{63}} 3^{\frac{29}{42}} 5^{\frac{5}{42}} \pi^{\frac{2}{9}}}{3} \frac{1}{|f_0|^{\frac{5}{42}} |h_3|^{\frac{4}{21}}} |f_4^1|^{\frac{1}{6}} |f_4^2 f_4^3|^{\frac{1}{14}} l_{P11} \,. && (2.98) \end{aligned}$$

2.6.3 The entropy

Let us express the entropy as a function of the energy of the black hole as in (2.78). The scaling part of the entropy of the configuration is given by,

$$\begin{aligned} S_{\mathrm{BH}} &\sim \left(\frac{R_{\mathrm{AdS}}}{l_{P4}} \right)^{\frac{2}{3}} && (2.99) \\ &\sim \left(\frac{160 \cdot 2^{\frac{7}{8}} 3^{\frac{3}{4}} 5^{\frac{1}{4}} \pi}{27} \frac{1}{|f_0|^{\frac{5}{4}} |h_3|^2} |f_4^1 f_4^2 f_4^3|^{\frac{3}{4}} \right)^{\frac{2}{3}} . && (2.100) \end{aligned}$$

Comparing this to the scaling part of the entropy in the original setup (see equation (2.78)), we see that they match perfectly.

2.6.4 Scaling behavior

In the regime $f_4^1 = f_4^2 = f_4^3 = N$, the various parameters of the background scale as,

$$\begin{aligned} R_M &\sim N^{-\frac{5}{6}} l_{P11} && (2.101) \\ R_{\mathrm{AdS}} &\sim N^{\frac{7}{6}} l_{P11} && (2.102) \\ \mathrm{vol}_7 &\sim N^{\frac{13}{6}} l_{P11}^7 && (2.103) \\ R_{\mathrm{KK}} &\sim N^{\frac{13}{42}} l_{P11} && (2.104) \\ m &\sim N^{-\frac{7}{6}} l_{P11}^{-1} && (2.105) \\ S_{\mathrm{BH}} &\sim N^{\frac{3}{2}} \,, && (2.106) \end{aligned}$$

where we express the scaling of the entropy as a function of the energy as in (2.78). We see that just as the original DeWolfe *et al.* solution, the M-theory configuration is effectively 4 dimensional, since R_{AdS} grows faster with N than R_{KK}. Note that the same analysis on the doubly dualized type IIA background teaches us that background is also effectively 4 dimensional in this particular scaling regime. The radii characterizing the solution grow as N increases,

except the M-theory radius R_M, which decreases with growing N. We will discuss this property below.

Taking a look at the other scaling $f_4^1 = N, f_4^2 = f_4^3 = O(1)$, we get,

$$\begin{aligned} R_M &\sim N^{\frac{1}{6}} l_{P11} && (2.107)\\ R_{\text{AdS}} &\sim N^{\frac{1}{6}} l_{P11} && (2.108)\\ \text{vol}_7 &\sim N^{\frac{7}{6}} l_{P11}^7 && (2.109)\\ R_{\text{KK}} &\sim N^{\frac{1}{6}} l_{P11} && (2.110)\\ m &\sim N^{-\frac{1}{6}} l_{P11}^{-1} && (2.111)\\ S_{\text{BH}} &\sim N^{\frac{1}{2}} . && (2.112) \end{aligned}$$

Here we conclude that the AdS and the compact manifold grow at the same rate such that the compactification is not effectively four dimensional. On the other hand, in this case all the radii of the 11 dimensional solution grow with N making 11D SUGRA a valid approximation for large N. As previously mentioned, the scaling of the entropy as function of the temperature in this regime is $N^{3/2}$.

2.6.5 Checking the consistency conditions

M-theory equations of motion

From (2.153), we get the equation of motion for the metric:

$$\text{Ric}_{MN} = \frac{2}{4!}\left(G_{MPQR}\, G_N{}^{PQR} - \frac{1}{12} g_{MN}\, G_{PQRS}\, G^{PQRS} \right) . \tag{2.113}$$

Taking the indices M, N in the AdS space, this condition reduces to:

$$\frac{1}{R_{\text{AdS}}^2} = 4m^2 . \tag{2.114}$$

This condition is satisfied as we can verify from (2.94).

The equation of motion for the compact part of the metric, $g_{mn}^{(7)}$, becomes:

$$\text{Ric}_{mn} = 6m^2 g_{mn}^{(7)} . \tag{2.115}$$

This implies that the compact 7-manifold is an Einstein manifold. As is common in similar cases, this condition will be satisfied if the supersymmetry condition is satisfied.

We can verify that the equation of motion and Bianchi condition on G_4,

$$\begin{aligned} d * G_4 + \frac{1}{2} G_4 \wedge G_4 &= 0 && (2.116)\\ dG_4 &= 0 , && (2.117) \end{aligned}$$

are satisfied.

Supersymmetry conditions

The original background was an $\mathcal{N} = 1$ compactification in four dimensions. From [30], we learn that the supersymmetry requirement on the M-theory lift, $\mathrm{AdS}_4 \times M_7$, is that M_7 has weak G_2 holonomy. Weak G_2 holonomy of a 7-manifold is defined by the condition that there exists a 3-form ϕ_3 and a real number m such that,

$$d\phi_3 = 4m *_7 \phi_3 \,. \tag{2.118}$$

From this condition one can derive the equation of motion (2.115) [31]. We conclude that if the supersymmetry conditions are obeyed then the naive M-theory lift is fully consistent.

When $N \to \infty$, $m \to 0$ and the supersymmetry condition on the compact manifold simplifies to G_2 holonomy:

$$d\phi_3 = 0 \tag{2.119}$$

$$d *_7 \phi_3 = 0 \,. \tag{2.120}$$

The 4 dimensional analysis in [7] led to stricter conditions on the signs of the F_4 flux parameters f_4^1, f_4^2 and f_4^3 [6]:

$$\mathrm{sign}(f_0 f_4^1 f_4^2 f_4^3) < 0 \tag{2.121}$$

$$\mathrm{sign}(f_4^1) = \mathrm{sign}(f_4^2) = \mathrm{sign}(f_4^3) \,. \tag{2.122}$$

Backgrounds violating the above condition are believed to be stable but non-super-symmetric solutions [7]. We can thus expect that the above conditions will follow from the weak G_2 holonomy condition.

If we check the weak G_2 holonomy condition for the naive lift, we find that it does not satisfy the conditions. We included the implicitly determined flux $\widetilde{F}_{2,\,\mathrm{O6}}$ which is sourced by the orientifold, while we did not include the Atiyah-Hitchin like geometry from the orientifold. As the coupling constant flows from type IIA to M-theory, we expect the singular orientifold to get some thickness, modifying the geometry in the region close to the orientifold. We thus expect that the naive lift is only an approximation for the geometry far away from the orientifold.

We did not succeed in finding an explicit solution to (2.118) in the regime where $f_4^1 = N, f_4^2 = f_4^3 = O(1)$, but neither have we found any obstruction to the existence of a metric of

[6] Equation (2.122) follows from the Kähler cone conditions for the background. There are additional Kähler cone conditions for the blow ups of the singularities. We do not consider those conditions here since our strategy was to ignore the singularities in the first step.

weak G_2 holonomy with the scaling properties and behavior near the M2-brane locus that we were led to. We believe that in the limit of a single large flux there is a systematic M-theory expansion. The background is $AdS_4 \times M_7$, with M_7 a manifold of weak G_2 holonomy. The anti de Sitter and M_7 radii are comparable. For other configurations of large flux we believe that the M-theory picture is only valid locally, in the vicinity of the orientifold, but that this region is large and cannot be ignored for large N. The string coupling *does* go to zero over another large region of the manifold.

2.6.6 Interpretation as a stack of M2-branes

The entropy argument of section 2.5.1 indicated that for a certain flux configuration we could expect the DeWolfe *et al.* solution to be the near horizon of a stack of M2-branes. The $\mathrm{AdS}_4 \times M_7$ background with a weak G_2 holonomy condition on M_7, as discussed in the previous section, is in [30] indeed interpreted as the near horizon limit of M2-branes.

The background of a stack of N M2-branes at the tip of a cone, is given by

$$ds^2 = H^{-\frac{2}{3}} ds_3^2 + H^{\frac{1}{3}} ds_8^2 \tag{2.123}$$

$$G_4 = \mathrm{vol}_3 \wedge dH^{-1}\,, \tag{2.124}$$

with ds_3^2 and vol_3 the Minkowski metric and worldvolume of the M2-branes and $ds_8^2 = du^2 + u^2 ds_7^2$ the metric of the cone in the directions transverse to the M2-branes. The function H is given by

$$H = 1 + \frac{a^6}{u^6}\,, \tag{2.125}$$

and a is determined by the number of M2-branes [32]:

$$a^6 = N \frac{\kappa_{11M}^2 T_3}{3\Omega_7} = N \frac{\kappa_{11M}^2}{3a^{-7}\mathrm{vol}_7} \left(\frac{4\pi^2}{2\kappa_{11M}^2}\right)^{\frac{1}{3}}\,, \tag{2.126}$$

with vol_7 the volume form on ds_7^2. The near horizon limit of this background becomes (after a coordinate transformation $r = 2u^2/a$):

$$ds^2 = \frac{r^2}{4a^2}(-dt^2 + dy_1^2 + dy_2^2) + \frac{a^2}{4r^2} dr^2 + a^2 ds_7^2 \tag{2.127}$$

$$G_4 = \frac{6}{a}\mathrm{vol}_4\,, \tag{2.128}$$

where vol_4 is the volume form on the AdS_4 space which has $R_{\mathrm{AdS}} = a/2$. Comparing this to the M-theory lift of the DeWolfe *et al.* solution (2.81), we find that $m = 1/a$ and using (2.126), we compute that the number of M2-branes is given by:

$$N = |f_4^1|\,. \tag{2.129}$$

We know that the entropy (as a function of energy) of the CFT corresponding to a stack of M2-branes scales as $N^{1/2} = |f_4^1|^{1/2}$. We can compare this to the scaling of the entropy of the M-theory lift (2.100), $|f_4^1 f_4^2 f_4^3|^{\frac{1}{2}}$. In the regime where $f_4^1 = N$, $f_4^2 = f_4^3 = O(1)$, the scaling of the entropy is exactly the same. We can thus interpret the M-theory lift of the DeWolfe *et al.* solution in that regime as a stack of N M2-branes at the tip of a cone. We do not have a deep understanding of the more generic regime, where all four form fluxes are large, nor the regime where two are large and one is small. We note again that De Wolfe *et al.* only claimed to have a systematic weak coupling and low energy expansion when all fluxes are large.

2.6.7 Validity of 11 dimensional supergravity in the generic regime

Let us consider the regime $f_4^1 = f_4^2 = f_4^3 = N$. The M-theory radius of the naive lift (2.101) decreases as N grows, indicating that the 11 dimensional supergravity approximation cannot be trusted, since the curvature of the background becomes too large and corrections to 11D SUGRA will be important. We find that $N < 3$ for $R_M > l_{P11}$. However, we also see that we need $N > 1$ for $\sqrt{\widetilde{\gamma}_{11}} > l_{P11}$. We see that supergravity is only valid in a certain small range of values for N.

The above reasoning is entirely based on our naive lift. Including the orientifold in the geometry changes the situation close to the orientifold. For an orientifold embedded in flat space, the dilaton increases the closer you get to the orientifold. This corresponds to a larger M-theory radius R_M. We can expect the same behavior in our configuration: including the correct geometry coming from the orientifold will give an M-theory radius which is larger than our naive estimate.

The geometry of the 11D SUGRA solution that incorporates the orientifold, can be thought of as an interpolation between the region close to the orientifold (bolt-geometry)[29] and the region far away from the orientifold (naive lift). The twisted tori in the region away from the orientifold come from the $F_0 H_3$ term in the original Bianchi identity, while (part of) the twist in the M-theory direction corresponds to the F_2 flux sourced by the orientifold.

Let us now focus on large N. The size of the compact manifold is large, so there are points located far away from the orientifold. We expect this region far away from the orientifold to resemble our naive lift. Further yet from the orientifold we enter into a weak coupling region. This is the region where the original argument of DeWolfe *et al.* operates. In the large flux limit there is a large region where it fails. To see this, note that our T-dual Type IIA configuration has a flux in the AdS_4 directions, consistent with N D2-branes lying in the orientifold locus.

The dilaton in such a D2-brane background has the form

$$e^{\varphi} = \left(1 + \frac{c_2 g_s N l_s^5}{r^5}\right)^{1/4}, \tag{2.130}$$

with c_2 a numerical constant. Plugging in the DeWolfe *et al.* value for the coupling at infinity, we find that the coupling gets large at a distance of order $N^{1/20} l_s$ from the stack of D2-branes. Thus, the weak coupling approximation breaks down over a parametrically large region of the manifold as $N \to \infty$.

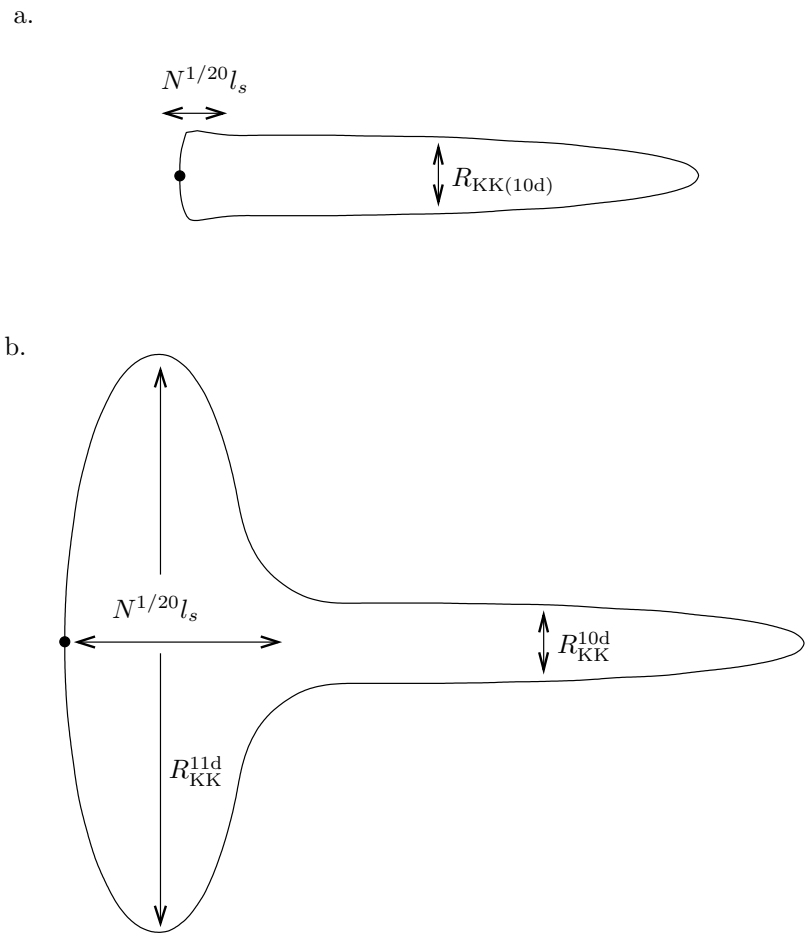

Figure 2.2: Two possible scenarios. The right hand side of each drawing represents the region where (massive) type IIA is the correct description and where the radius of curvature of the compact manifold, $R^{\mathrm{10d}}_{\mathrm{KK}}$, scales with N at a slower rate than R_{AdS}. The left hand side is the region close to the D2/orientifold locus (indicated with the dot). This region has a size that scales as $N^{1/20} l_s$. The compact manifold radii in this region, $R^{\mathrm{11d}}_{\mathrm{KK}}$, scale as fast as R_{AdS} scales with N, resulting in a flat patch (case a) or a mushroom cap (case b).

If we make the plausible assumption that an 11D description is valid near the orientifold, we find that the local radius of curvature in the presence of the branes is of order the AdS radius.

We connect the weak coupling geometry to a seven dimensional patch whose size is of order $N^{1/20} l_s \sim N^{13/60} l_{P11}$ (see figure 2.2), and whose geometry is that of the manifold of weak G_2 holonomy we described above. The radius of curvature of that geometry is of order the AdS radius, and thus, much larger than the size of the patch. There now seem to be two possibilities for a geometrical description of what is going on in the large N limit[7]. In the first, the patch is essentially flat (see figure 2.2a). Alternatively, the whole geometry could mushroom out to a large seven dimensional patch with weak G_2 holonomy and size of order the AdS radius (see figure 2.2b). We believe that neither the methods of DeWolfe *et al.* nor our own, are powerful enough to distinguish between these two alternatives. In the second alternative there would be KK excitations with a mass of order the inverse AdS radius, and the compactification would not be four dimensional.

2.7 Conclusions and speculation

We believe that we have provided ground for suspecting that the massive IIA description of the DeWolfe *et al.* background does not provide a systematic low energy expansion due to the back reaction of the orientifold. The doubly dualized description still has the same problem. However, this low energy effective description has the advantage that the F_0 and H_3 fluxes are absent.

Regime $f_4^1 = N$, $f_4^2 = f_4^3 = O(1)$:

The scaling of the entropy indicates that there might be a correct expansion using 11D SUGRA in this regime. We constructed a naive lift to 11 dimensions. We gave arguments that a 7-manifold of weak G_2 holonomy exists and that N M2-branes at an approximately Atiyah-Hitchin locus on this manifold might give a description of the physics of these compactifications. We reiterate that this is not a regime where DeWolfe *et al.* claimed to have a controlled expansion.

We thus claim that in the regime where f_4^1 is large, and the other four form fluxes are of order 1, there should be a valid 11D SUGRA approximation to the DeWolfe *et al.* models. This would be the near horizon limit of the configuration of f_4^1 M2-branes at the tip of a cone over a seven manifold M_7 of weak G_2 holonomy. The linear size of M_7 scales in the same way as the AdS_4 radius. The exact description of this regime would be a $2+1$ dimensional CFT with fixed

[7]We emphasize that since we have *no* complete approximation scheme for this regime, there is no argument that *any* geometrical picture is valid.

temperature entropy of order $(f_4^1)^{3/2}$. It should be possible to find it as the endpoint of the RG flow along a relevant perturbation of the CFT of M2-branes in flat space, which breaks the symmetry down to minimal $2+1$ dimensional SUSY. The supergravity solution would enable one to compute dimensions of low dimension operators at this fixed point. However, since the SUSY algebra is so small, there might not be any checks of these computations at the UV fixed point.

There is no sense in which this model is well approximated by weakly coupled string theory. In addition, the compactification is not approximately four dimensional. The AdS and M_7 radii are comparable. If our picture is the correct one, the failure of the weak coupling analysis should be attributed to the naive treatment of the orientifold. In M-theory, the center of the orientifold is a locus of strong IIA coupling. In these compactifications, for large f_1^4 (in the T-duality frame we have chosen), a large number of M2 branes sit at this locus, and their back reaction completely changes the weak coupling geometrical picture. Of course, the limit of a single large flux was not controllable in the picture of DeWolfe *et al.*. Nonetheless it is striking that a single shrinking cycle (from their point of view) can actually lead to a completely different picture of the geometry, and of the strength of the coupling.

Generic regime $f_4^1 = f_4^2 = f_4^3 = N$:

This regime is more mysterious. The fixed temperature entropy of the CFT scales like $N^{9/2}$. We would like to propose a heuristic explanation of this scaling law, but we warn the reader that many aspects of this proposal are obscure. Klebanov and Tseytlin proposed an explanation [33] of the N^3 scaling of the $(2,0)$ CFT that describes M5-branes, in terms of partially BPS states of membranes in a pair of pants configuration with boundaries on three different 5-branes. We would like to propose a similar explanation for the generic scaling of the entropy in the models of DeWolfe et al. There are two important differences. First of all, we hypothesize multi-layered pairs of pants (see figure 2.3 for an illustration). That is, each geometrical pair of pants is wrapped by N M2-branes rather than a single one. Secondly, the M2-branes end on Kaluza-Klein monopoles instead of on M5-branes. We claim that the entropy comes from N^3 copies of the M2-brane field theory, each with entropy $N^{3/2}$.

The symmetry of the formulae under interchange of the three four form fluxes, suggests that a picture based on string networks in Type IIB string theory might capture some of the physics. Thus, we would imagine an Argentine bola string junction, with N allowed sites for each of its ends. Each bola would consist of N strings. The M2-brane scaling of the world volume theory of

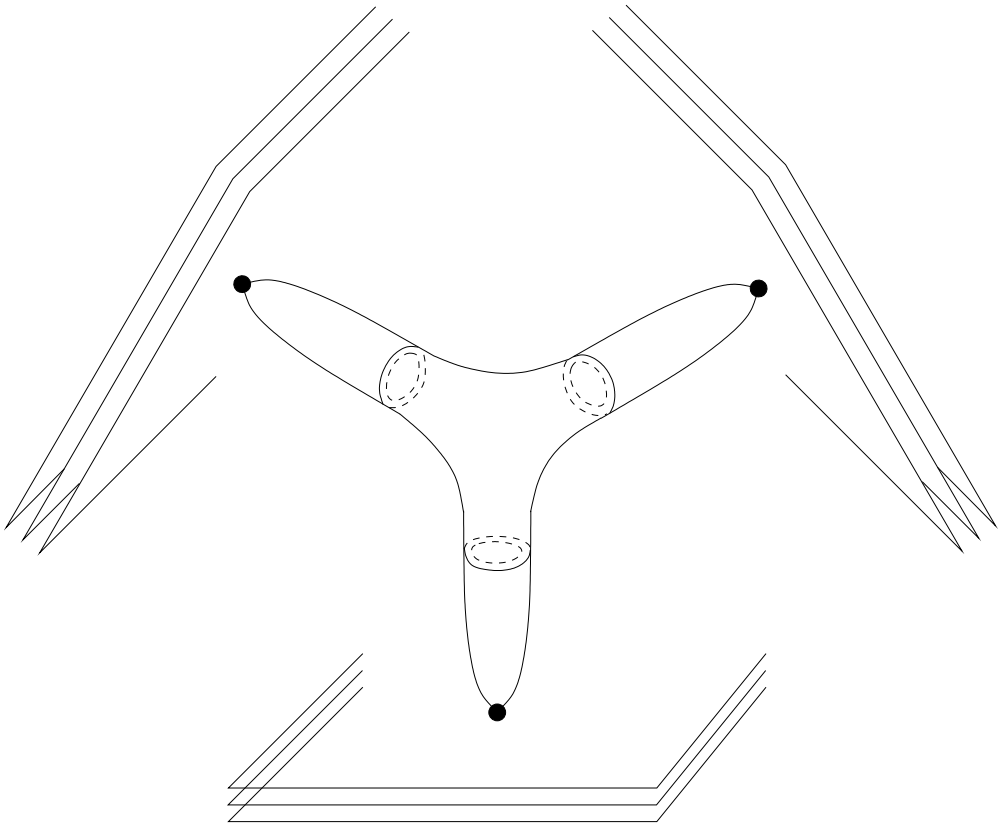

Figure 2.3: N M2-branes ending on 3 stacks of N Kaluza-Klein monopoles. Notice that each end of the trousers is stitched together.

the string junction, could be explained by hypothesizing that it passed through a large volume on the compact manifold, where the M-theory torus had large area. The endpoints of the bola would be better described in terms of weakly coupled Type IIB string theory, though perhaps different ends would be weakly coupled in different S-duality frames.

We have argued that the weak coupling expansion claimed by DeWolfe *et al.* in this regime cannot be uniformly valid, since there is a region of size $N^{1/20} l_s$ where the coupling is not weak in the large N limit. Since there is no single low energy field theory that describes these configurations, and since observables in theories of gravity in Anti-de Sitter space are not local on the compact manifold, we are not sure how one would go about making a systematic computation of these observables for large N.

We presented two heuristic geometrical pictures of how the weak coupling geometry could connect on to a region best described in terms of 11D SUGRA on a manifold of weak G_2 holonomy. The approximate 4 dimensionality of the compactification is valid only in one of them. The weak coupling analysis *might* be missing a large *mushroom cap* region hidden near the strong coupling orientifold singularity. We believe that no extant methods can distinguish between these two pictures, or provide a systematic description of the physics of this system at large N. We have also presented a heuristic model of the entropy of the regime with all fluxes large. This model also depends on the existence of large regions of the compact geometry which are weakly curved eleven manifolds.

Given these arguments, and the success of our 11D picture in the regime of a single large flux where the weakly coupled region completely disappears, we see serious reasons to doubt the validity of the simple weak coupling picture advocated by DeWolfe *et al.*, even when all fluxes are large. The reason for this is the back reaction of a large number of branes near the strongly coupled orientifold locus, which changes the geometry in ways that cannot be understood from the perturbative picture.

In our opinion, the best one could hope for would be some analog of F-theory, in which different string expansions governed local physics in different regions of the compact manifold. It is entirely unclear to us whether the particular duality frame we have emphasized is the best description of this regime. Furthermore, since we are working with a very small amount of supersymmetry, it is unlikely that we can use non-renormalization theorems to glean exact information about these compactifications from their geometrical formulation. This is a pity, because it is the only one in which an approximately 4 dimensional compactification *might* arise.

It would seem that the only way to really investigate the physics of these backgrounds of string theory is to find and solve the dual $2+1$ dimensional conformal field theory. For

the special flux configurations described above, it is plausible that this CFT can be found by perturbing the Yang-Mills theory of D2-branes by an appropriate relevant operator, obtaining the CFT dual to M2-branes at the tip of a cone over a manifold of weak G_2 holonomy. We conjectured that the correct description of more general configurations might be explained in terms of a tensor product of field theories, or some theory which approximately reduced to such a tensor product for purposes of counting the large N asymptotics of the entropy.

2.8 Appendix: Type IIA - Type IIB T-duality dictionary

We take the bosonic type IIA action in the string frame to be (omitting the Chern-Simons terms):

$$\begin{aligned} S_{\rm IIA} &= \frac{1}{2\kappa_{10A}^2}\int \sqrt{-g_{10A}}e^{-2\varphi_A}(R+4\partial\varphi_A\partial\varphi_A) - \frac{1}{4\kappa_{10A}^2}\int e^{-2\varphi_A}H_3\wedge *H_3 \\ &\quad -\frac{1}{4\kappa_{10A}^2}\int F_4\wedge *F_4 + F_2\wedge *F_2 + F_0\wedge *F_0\,, \end{aligned} \tag{2.131}$$

while the bosonic type IIB action is given by:

$$\begin{aligned} S_{\rm IIB} &= \frac{1}{2\kappa_{10B}^2}\int \sqrt{-g_{10B}}e^{-2\varphi_B}(R+4\partial\varphi_B\partial\varphi_B) - \frac{1}{4\kappa_{10B}^2}\int e^{-2\varphi_B}H_3\wedge *H_3 \\ &\quad -\frac{1}{4\kappa_{10B}^2}\int \frac{1}{2}F_5\wedge *F_5 + F_3\wedge *F_3 + F_1\wedge *F_1\,, \end{aligned} \tag{2.132}$$

where we impose the self-duality of F_5 in the equations of motion by hand (see [34] for a consistent treatment of self-dual field theories). The T-duality dictionary between both theories

for a warped metric reads [35],

$$
\begin{array}{rclcrcl}
ds_A^2 &=& L_A^2 e^{2\alpha\phi}\Theta_A^2 + e^{2\beta\phi} ds_9^2 & \leftrightarrow & ds_B^2 &=& L_A^{-2} e^{-2\alpha\phi}\Theta_B^2 + e^{2\beta\phi} ds_9^2 \\
H_3 &=& \widetilde{H}_3 + \widetilde{H}_2 \wedge \Theta_A & \leftrightarrow & H_3 &=& \widetilde{H}_3 - \widetilde{F}^{NS} \wedge \Theta_B \\
\varphi_A & & & \leftrightarrow & \varphi_B &=& \varphi_A - \alpha\phi\,, \\
F_4 &=& \widetilde{F}_4 + \widetilde{F}_3 \wedge L_A \Theta_A & \leftrightarrow & F_5 &=& e^{(\alpha+\beta)\phi} *_9 \widetilde{F}_4 + \widetilde{F}_4 \wedge L_A^{-1}\Theta_B \\
F_2 &=& \widetilde{F}_2 + \widetilde{F}_1 \wedge L_A \Theta_A & \leftrightarrow & F_3 &=& \widetilde{F}_3 + \widetilde{F}_2 \wedge L_A^{-1}\Theta_B \\
F_0 &=& \widetilde{F}_0 & \leftrightarrow & F_1 &=& \widetilde{F}_1 + \widetilde{F}_0 \wedge L_A^{-1}\Theta_B \\
\frac{1}{2\kappa^2_{10A}} & & & \leftrightarrow & \frac{1}{2\kappa^2_{10B}} &=& \frac{L_A^2}{2\kappa^2_{10A}}\,, \\
d\Theta_A &=& \widetilde{F}^{NS} & \leftrightarrow & d\Theta_B &=& -\widetilde{H}_2\,, \\
\Theta_A &=& 2\pi\sqrt{\alpha'}dx + \widetilde{A}^{NS} & \leftrightarrow & \Theta_B &=& 2\pi\sqrt{\alpha'}dx - \widetilde{B}_1\,,
\end{array}
\tag{2.133}
$$

where the last line is valid locally, with $\widetilde{F}^{NS} = d\widetilde{A}^{NS}$, $\widetilde{H}_2 = d\widetilde{B}_1$ and $x \in [0,1]$ parametrizes the $U(1)$ isometry. The Hodge star in F_5 is with respect to the ds_9^2 metric on the type IIB side of the dictionary. In our notation, the forms on the right hand sides of the equations never contain Θ_A or Θ_B explicitly.

2.9 Appendix: Computing the double T-dual of the DeWolfe *et al.* background

We start from the DeWolfe *et al.* solution (2.1)-(2.8). We use the dictionary from Appendix 2.8. To apply a first T-duality in the x_1-direction, $x_1 \in [0,1]$, we take,

$$
\begin{aligned}
L_A^2 &= \frac{\gamma_1}{4\pi^2\alpha'} 9^{-\frac{1}{3}} && (2.134)\\
\Theta_A &= 2\pi\sqrt{\alpha'}\, 9^{\frac{1}{6}}\, dx_1 && (2.135)\\
\Theta_B &= 9^{\frac{1}{6}}\, \Theta_1 && (2.136)\\
\alpha = \beta &= 0\,. && (2.137)
\end{aligned}
$$

The factor $9^{1/6}$ comes from the discrete symmetries $\mathbb{Z}_3 \times \mathbb{Z}_3$ (see (2.13)). This results in:

$$
\begin{aligned}
ds^2 &= \frac{4\pi^2\alpha'}{\gamma_1}\, 9^{\frac{2}{3}}\, \Theta_1^2 + \gamma_1 dx_2^2 + \gamma_2(dx_3^2+dx_4^2) + \gamma_3(dx_5^2+dx_6^2) + ds^2_{\mathrm{AdS}_4} && (2.138)\\
H_3 &= 4\pi^2\alpha' h_3 \sqrt[4]{3}\sqrt{2}\,(dx_2\wedge dx_3\wedge dx_6 + dx_2\wedge dx_4\wedge dx_5) && (2.139)\\
e^{\varphi_B} &= \frac{1}{4}|h_3|\sqrt[4]{\frac{3^3 5}{|f_0 f_4^1 f_4^2 f_4^3|}} && (2.140)\\
F_5 &= 4(2\pi\sqrt{\alpha'})^3\sqrt[3]{3} f_4^1\Big(*_9(dx_3\wedge dx_4\wedge dx_5\wedge dx_6) \\
&\qquad + \sqrt{\frac{4\pi^2\alpha'\, 9^{\frac{2}{3}}}{\gamma_1}} dx_3\wedge dx_4\wedge dx_5\wedge dx_6\wedge\Theta_1\Big) && (2.141)\\
&= \left(4(2\pi\sqrt{\alpha'})^3\sqrt[3]{3} f_4^1 \frac{1}{\gamma_2\gamma_3}\mathrm{vol}_4\right)\sqrt{\frac{\gamma_1}{4\pi^2\alpha'\, 4\cdot 3^{-\frac{1}{3}}}}\wedge(2\pi\sqrt{\alpha'}\, 2\cdot 3^{-\frac{1}{6}} dx_2) \\
&\quad + *_{\tilde{9}}\left(4(2\pi\sqrt{\alpha'})^3\sqrt[3]{3} f_4^1\frac{1}{\gamma_2\gamma_3}\mathrm{vol}_4\right) && (2.142)\\
F_3 &= -4(2\pi\sqrt{\alpha'})^2\sqrt[3]{3}\sqrt{\frac{4\pi^2\alpha'}{\gamma_1}}(f_4^2\, dx_5\wedge dx_6\wedge dx_2 + f_4^3\, dx_2\wedge dx_3\wedge dx_4) && (2.143)\\
F_1 &= \frac{f_0}{\sqrt{\gamma_1}}\, 9^{\frac{1}{3}}\,\Theta_1 && (2.144)\\
\frac{1}{2\kappa^2_{10B}} &= \frac{1}{2\kappa^2_{10A}}\frac{\gamma_1}{4\pi^2\alpha'\, 9^{\frac{1}{3}}} && (2.145)\\
\Theta_1 &= 2\pi\sqrt{\alpha'}dx_1 + 2\pi\sqrt{\alpha'}h_3\frac{\sqrt[4]{3}\sqrt{2}}{9^{\frac{1}{3}}}(x_3 dx_5 - x_4 dx_6)\,. && (2.146)
\end{aligned}
$$

The last line is again only valid locally. We use the notation where, $*_9$, means the Hodge star with respect to the metric after T-duality without the x_1-direction, while, $*_{\tilde{9}}$, means the Hodge star with respect to the metric after T-duality without the x_2-direction. vol_4 is the volume form of AdS_4.

The first T-duality transformation splits the original orientifold (2.17) into an O5- and an O7-plane:

$$
\begin{aligned}
\mathrm{O5} &: \frac{\sqrt[4]{3}\sqrt{2}}{2\pi\sqrt{\alpha'}\, 9^{\frac{1}{6}}}\,(+dx_3\wedge dx_5 - dx_4\wedge dx_6) && (2.147)\\
\mathrm{O7} &: \frac{\sqrt[4]{3}\sqrt{2}\, 9^{\frac{1}{6}}}{2\pi\sqrt{\alpha'}\, 2\cdot 3^{-\frac{1}{6}}}\,(-dx_4\wedge dx_5 - dx_3\wedge dx_6)\wedge(2\pi\sqrt{\alpha'}\, 2\cdot 3^{-\frac{1}{6}} dx_2)\wedge\Theta_1 && (2.148)
\end{aligned}
$$

After this first T-duality the solution still has an (approximate) $U(1)$-isometry in the x_2-direction, $x_2 \in [0, \sqrt{3}/2]$. We take

$$
\begin{aligned}
L_A^2 &= \frac{4\pi^2\alpha'}{\gamma_1}\left(\frac{4}{3}\, 9^{\frac{1}{3}}\right) && (2.149)\\
\Theta_B &= 2\pi\sqrt{\alpha'}\left(\frac{2}{\sqrt{3}}\, 9^{\frac{1}{6}}\right) dx_2 && (2.150)\\
\Theta_A &= 2\cdot 3^{-\frac{1}{6}}\,\Theta_2 && (2.151)\\
\alpha = \beta &= 0\,, && (2.152)
\end{aligned}
$$

this results in the solution (2.59)-(2.67).

2.10 Appendix: Type IIA - M-theory dictionary

For the type IIA theory we start again from the action (2.131), for M-theory we take as definition of our theory,

$$S_{\rm M} = \frac{1}{2\kappa_{11}^2}\int \sqrt{-g_{11}}R - \frac{1}{4\kappa_{11}^2}\int F_4 \wedge *F_4 \tag{2.153}$$

$$-\frac{1}{4\kappa_{11}^2}\int C_3 \wedge F_4 \wedge F_4\,. \tag{2.154}$$

The compactification of M-theory on a circle gives the following type IIA - M-theory correspondence:

$$\begin{aligned}
ds_A^2 &= ds_{10}^2 \quad \leftrightarrow \quad ds_M^2 = L_M^2 e^{\frac{4}{3}\varphi_A}\Theta_M^2 + e^{-\frac{2}{3}\varphi_A} ds_{10}^2 \\
\varphi_A & \\
H_3 & \quad \leftrightarrow \quad G_4 = F_4 + H_3 \wedge L_M \Theta_M \\
F_4 & \\
F_2 & \quad \leftrightarrow \quad d\Theta_M = \tfrac{1}{L_M} F_2\,, \\
& \qquad\qquad \Theta_M = dx_M + \tfrac{1}{L_M} C_1\,, \\
F_0 &= 0 \\
\tfrac{1}{2\kappa_{10A}^2} & \quad \leftrightarrow \quad \tfrac{1}{2\kappa_{11M}^2} = \tfrac{1}{2\kappa_{10A}^2 L_M}\,, \\
& \qquad\qquad L_M = 2\pi \tfrac{\kappa_{10A}}{\sqrt{\pi}(2\pi\sqrt{\alpha'})^3}\,,
\end{aligned} \tag{2.155}$$

with $x_M \in [0,1]$.

Chapter 3
Tunneling in the Landscape

3.1 Introduction: Stability in the Landscape

In this chapter we will discuss in detail our findings of the work done in collaboration with M. Dine, G. Festuccia and A. Morisse [36].

Much of the focus of landscape studies has been on states with some degree of supersymmetry. These are easier to study as supersymmetry provides an added degree of theoretical control. KKLT[37] exhibited states in which it appears that all moduli are fixed in a regime of weak coupling and large compactification radius. They (and subsequently others[38]), argued that a substantial number of such states would exhibit dynamical supersymmetry breaking with positive cosmological constant. More generally, if one considers likely mechanisms for supersymmetry breaking among the known supersymmetric states, it is likely that a finite fraction have hierarchically small breaking scales, as expected from conventional ideas about naturalness [39].

While some degree of calculational control is valuable to theorists, however, it is not clear why this should be important to nature. The assumption of low energy supersymmetry restricts the structure of the effective action and permits inferences about the strong coupling and small radius regimes. Plausible assumptions about the distribution of the lagrangian parameters (e.g. uniform distribution of complex parameters in the superpotential) can be checked in the weak coupling region. For example, one can argue that there should be many metastable and stable states even for small radius, and make arguments for the distribution of supersymmetry breaking scales and cosmological constants.[1] But while supersymmetry provides many simplifications and a greater degree of control, one expects that there should be more non-supersymmetric, metastable states, possibly vastly more. There have been some studies of the statistics of non-supersymmetric states, both with spontaneous breaking[7] and explicit breaking[40]. Most of these studies have involved AdS vacua. Attempts to study broader classes

[1] This point was first made to one of the authors (M.D.) several years ago by Shamit Kachru.

of non-supersymmetric vacua include those of Douglas and Denef in the case of IIB orientifolds on Calabi-Yau spaces[42, 43]. Their counting requires approximate supersymmetry. To obtain finite results, a cutoff must be imposed on the scale of supersymmetry breaking. Without such a cutoff, there is no control over the calculations. The vast majority of states are then located at the cutoff scale. Questions such as stability against tunneling are difficult to address for such states. A more ambitious program is that of Silverstein, who argues that there may be various constructions which yield large numbers of non-supersymmetric, de Sitter vacua[41], and that one may have a high degree of control.

One of the most urgent, and potentially accessible, questions in the landscape is the origin of the gauge hierarchy. Is it due to strong dynamics or warping, to supersymmetry, or perhaps just anthropic selection among a vast array of otherwise undistinguished states. In other words, could it be that the explanation of the hierarchy lies not in symmetries or dynamics, but simply in the existence of an overwhelmingly large number states which accidentally have a small scale of weak interactions[44, 45]?

The analysis of Douglas and Denef illustrates why it is hard to settle this question. In a typical, non-supersymmetric state, there will be no small parameters at all, and the crutch of supersymmetry is not available. Unlike the supersymmetric case, there do not seem to be any simple arguments to give a handle on the most rudimentary statistics, much less overall counting.

In the absence of small parameters, one question looms particularly large: stability. If the landscape picture has any validity, the state in which we find ourselves, with small positive cosmological constant, sits in a large sea of states with negative cosmological constant. Many of these are "close by". Stability of any would-be state requires that the amplitude to decay to any one of these states be very small[46, 47]. Indeed, the very notion of *state* requires this. As we will see, the cutoff of Douglas and Denef can be understood as emerging from the requirement of stability.

The significance of this last point can be understood by supposing that one has a flux landscape of 100 dimensions (i.e. 100 independent fluxes), and typical fluxes are large (say 10). Then there are of order 10^{100} states. Among these states will be states of small cosmological constant. Any one of these will be surrounded by many states with negative cosmological constant. One might expect, for example, that there are of order 3^{100} within three flux units. In order that the state be stable, it is necessary that the tunneling amplitude to any one of these states (more precisely to the corresponding big crunch) be small. In the absence of a small parameter, one might imagine that there is a probability of order $1/2$ that the tunneling

amplitude be zero to any one state[47]. So the chance that any particular state is stable, absent any symmetries or small parameters, is of order

$$P_{stab} = \left(\frac{1}{2}\right)^{3^{100}}. \tag{3.1}$$

One might immediately object that there might be qualitative reasons why a particular state does not decay rapidly – or at all – to any of its neighbors. But this is precisely what makes this question important: long-lived states are likely to be special. Optimistically, they might have features related to phenomena we see – or better, might hope to see, in nature. Within the landscape, a number of classes of states have been isolated with distinguishing features. It is natural to ask which of these features might contribute to stability (In what follows, we use "false" vacuum to describe the candidate metastable state; "true" refers to any prospective decay channel):

1. Weak coupling in the "false" vacuum and/or candidate "true" vacua.
2. Large compactification volume in either or both the "false" and "true" vacua.
3. Low energy supersymmetry
4. Light moduli in the "false" vacuum.
5. Warping in the "false" vacuum.

In this chapter, we investigate these possibilities. To be concrete, we consider mainly Type IIB theories compactified on Calabi-Yau spaces with fluxes and an orientifold projection. In this case, the large number of would-be metastable states is due to a large number of possible flux choices. There is, of course, the risk with such specialization that our results are not sufficiently generic. For example, with our present knowledge of IIB theories, it is difficult to make statements about compactification radii (without supersymmetry), yet as we will see, large radius is a regime (unlike weak coupling) where one might have a realistic hope to find large metastable neighborhoods. The constructions of [41] may yield vast sets of non-supersymmetric, large volume compactifications. We will use these, and AdS models in IIA theory, to give some insight into possible behaviors with volume.

In the end, of the list above, we will argue that only the large volume and supersymmetric states are generically stable. The rest of this paper is organized as follows. We first discuss some general scaling arguments for tunneling amplitudes. Theses arguments make clear why states with large flux are prone to rapid decay. We review the argument that supersymmetric

states are stable. We then consider the (supersymmetric) states discussed by Giddings, Kachru and Polchinski (GKP)[48]. We verify our scaling arguments for domain wall tensions and cosmological constants. Because of supersymmetry, these states are stable; we will see that this is again consistent with simple scaling arguments.

From these exercises, we confirm that our basic scaling arguments for domain wall tensions and energy splittings are robust. We then suppose that one has found a landscape of non-supersymmetric states, and ask what features might account for stability. We find that while weak coupling, by itself, cannot account for metastability, large volume – more precisely volume scaling suitably with flux, N – can. Warping, in the sense discussed by GKP seems not to lead to stability. The existence of approximate moduli, by itself, also does not lead to stability. We consider states with a small breaking of supersymmetry (compared to the fundamental scale), and illustrate in simple models why these are typically metastable or completely stable.

While this sort of reasoning can establish classes of states which are metastable, it does not indicate whether one is likely to make transitions *into* a particular state. This is closely related to the questions of measures for eternal inflation which have been widely studied recently. While we currently have little new to add to this discussion, we point out that the landscape is likely to be more complicated than assumed in many simple models of eternal inflation. For example, a typical KKLT vacuum is likely surrounded by many AdS states, both supersymmetric and not. Whether one can neatly transition into the KKLT minimum seems a serious question. We speculate that states with (discrete) symmetries, though rare, might be attractors in cosmological evolution.

In the conclusions, we indulge in conjecture. Our results, we note, hardly prove that low energy supersymmetry is a feature of the landscape, but they suggest, in ways we explain, that it might be. They suggest, alternatively, what is required to establish the existence of a vast set of non-supersymmetric states in the landscape.

3.2 Scaling Arguments for Non-Supersymmetric States

In this section, we ask how we might expect potentials, domain wall tensions, and tunneling amplitudes to scale in the limit of large fluxes, in non-supersymmetric states. In order that in these hypothetical states there be some validity to a semiclassical analysis in a ten dimensional effective field field theory, we will suppose that the compactification volume, V, is large. We will also assume, when necessary, that couplings are small. We suppose that we have many three-form fluxes (b), with typical values of order N. The potential is quadratic in N/V (in the

Einstein frame, i.e. in four dimensional Planck units).

We are considering a Type IIB landscape, with various RR and NS 3 form fluxes, N_i and K_i. We will think of the fluxes as very large, $N_i \sim N$, and $K_i \sim K$, for some large N and K. We wish to compare neighboring states in the landscape, i.e. states in which one flux, say, N_i, changes by one, or perhaps a few fluxes change by a few. Take the first case. For simplicity, suppose first that $K \sim N$. In this case, there is no particular reason for a semiclassical approximation to be valid, but we will use the classical formulas for the potential in order to get some feeling for how amplitudes might scale with N in a "typical" state. Later, we will adjust the fluxes so that the string coupling is weak.

When all fluxes are comparable, because the potential is homogeneous in N, the changes in the moduli fields are of order $1/N$, and the change in the potential is of order N for small changes ($\Delta N \ll N$) in flux.

In the decays of interest to us, both the four dimensional fields and the fluxes change, and General Relativity plays an important role.. But first it is worthwhile to review some aspects of tunneling in ordinary field theory, without gravity. For our discussion it is important to recognize that even though the barrier may be quite high, if the neighboring well is very deep and the field excursions are not too large, the tunneling amplitude is not necessarily small.

Consider a theory of a scalar field ϕ, in 4 dimensions, with a potential of the form:

$$V(\phi) = \frac{N^2}{V^2} f(\phi). \tag{3.2}$$

Here N is supposed to be large, as in our problem above, and $f(\phi)$ is a function with two minima. Let's first ask about the range of validity of the semiclassical analysis in the two would-be minima. Assuming a canonical kinetic term, corrections to the kinetic term, at one loop, behave as N^2/V^2 (the vertices each give a factor of N^2/V^2, and there is a factor of $1/m_\phi^2$ from the integral). So the perturbative analysis would seem to be valid if $V \gg N$. We will see that stability seems to give a somewhat stronger condition.

Turning to tunneling, ignoring gravity, the bounce action behaves as V^2/N^3. This follows from simple scaling arguments on the terms in the action. But it can be seen by considering the standard thin wall analysis, which will be valid in the case that the two minima of f are nearly degenerate, differing by ΔE. Then the bubble tension is given by ($\Delta\phi \sim 1/N$)

$$T = \int^{\Delta\phi} d\phi \sqrt{2V(\phi)} \sim \frac{1}{V}, \tag{3.3}$$

so the standard thin wall analysis[46] gives

$$S_b = C\frac{T^4}{\Delta E^3} = AV^2/N^3, \tag{3.4}$$

where C and A are numerical constants. So unless the volume is large (of order $N^{3/2}$ in fundamental units), the bounce action is small and the tunneling amplitude is of order one. This same scaling can readily be shown to hold for more general functions f.

Typically, gravitational corrections will be large. From the Coleman-De Luccia analysis, in the case of tunneling, say, from flat or AdS space to AdS space, one learns that gravitational corrections are important when the radius of the would-be bubble is comparable to the AdS radius. In our example above, the radius of the bubble wall is:

$$R_b = \frac{T}{\Delta E} \sim V/N \tag{3.5}$$

while the AdS radius is of order V/N.

On the other hand, for the case of interest to us in the landscape, the initial state, by assumption, has zero or nearly zero cosmological constant. So,

$$R_{AdS} \sim \frac{V}{\sqrt{N}} \tag{3.6}$$

and one does not expect gravitational corrections to be important. More generally, one does not expect a suppression of decays from states with large positive to negative cosmological constant.

Of course, by definition, if the bounce action is not large, the semiclassical calculation is not reliable. We take this result as evidence that suppressing tunneling requires $N^3 \ll V^2$. Note that this constraint is more severe than the naive perturbative condition, $V \gg N$.

When we consider flux vacua, we will be interested in the Coleman or Coleman-De Luccia analysis in cases where the bubble can be thought of as a brane ($M5$ or $D5$) wrapped on some internal manifold. Such branes can be thought of as thin-walled bubbles. To make the comparison, it is useful to reformulate the conventional field theory analysis in terms of a collective coordinate. If the bounce is described by a function $\phi_{cl}(r-R)$ (spherically symmetric), we can introduce a collective coordinate, $R(t)$, and obtain an action for R by writing:

$$\phi(r) = \phi_{cl}(r - R(t)) : \tag{3.7}$$

$$S = \int dt \left(T R^2 \dot{R}^2 - V(R) \right) \tag{3.8}$$

with

$$V(R) = TR^2 - \Delta E R^3. \tag{3.9}$$

The bounce action follows from an ordinary WKB calculation with this action.[2] For the case of wrapped branes, this is the structure of the appropriate Born-Infeld action.

[2] In terms of our earlier remark about quantum tunneling, it is the unusual form of the kinetic term for R and the pressure term which account for the enhanced tunneling rate.

The estimates in this section suggest that the tunneling amplitude quickly becomes of order one as N increases, if V and the couplings are fixed. But one might worry that this field theory analysis is not applicable to the case of interest, where transitions are accompanied by changes of flux and emission of extended objects like branes. In the next section, we will see that precisely these scalings of tensions and cosmological constants occur in well-studied string theory examples.

3.3 A Prototype: GKP

A useful model for stabilized moduli and domain wall tensions is provided by the work of Giddings, Kachru and Polchinski. This is a IIB orientifold model, with compactification on a Calabi-Yau space at a point in the (approximate) moduli space near a conifold singularity. In this model, the moduli are τ, ρ and z, z_i. τ is the IIB string coupling; ρ describes the overall size of the compact manifold,

$$\rho = R^4 M_{10}^4 \tag{3.10}$$

(where M_{10} is the ten-dimensional Planck scale), and z is a complex structure modulus which describes the deformation of the conifold. The z_i represent other complex structure moduli. τ, z_i and z are fixed by fluxes; ρ is undetermined in a semiclassical treatment (the model has a no-scale structure). It will be useful to consider an effective field theory without ρ, as well, in which supersymmetry is unbroken.

For large ρ, the theory turns out to be approximately supersymmetric. Following GKP, we will consider light fields z, τ and ρ. Their dynamics can be described by a superpotential and Kahler potential. The superpotential takes the form:

$$W = M\mathcal{G}(z) - K\tau z - K'\tau h(z) \tag{3.11}$$

where M is the RR three-form flux along the A cycle associated with the conifold; K is the NS-NS three form flux along the corresponding B cycle; and K' is the flux along some other cycle, B'. The function $\mathcal{G}$ has the form:

$$\mathcal{G}(z) = \frac{z}{2\pi i}\ln(z) + \mathcal{G}(0) + f(z) \tag{3.12}$$

where $f(z)$ is a holomorphic function of z which vanishes as $z \to 0$. The Kahler potential

$$K = -3\ln(\rho - \rho^*) - \ln(\tau - \tau^*) + f(z, z^*) \tag{3.13}$$

where $f(z, z^*)$ is a finite function of z which tends to a constant as $z \to 0$.

For suitable choices of flux, the equations for supersymmetric stationary points of z and τ have solutions with z small and τ large:

$$z = \exp(\frac{2\pi K \,\mathrm{Im}\,\tau}{M}) \qquad \mathrm{Im}\tau = -\frac{M\mathcal{G}(0)}{K'h(0)}. \tag{3.14}$$

As noted above, at these points, ρ is undetermined and the potential, classically, vanishes. For large ρ, the gravitino mass is small and one can argue that the computation is self-consistent. The masses of the lightest Kaluza-Klein modes are of order

$$m_{KK}^2 \sim \frac{1}{\rho^2}, \tag{3.15}$$

where this, which is expressed in four dimensional Planck units, applies in the limit of large ρ and moderate z.

The masses of the gravitino, $m_{3/2}$, is of order:

$$m_{3/2}^2 \sim |M\mathcal{G}(0)|^2 \rho^{-3} g_s, \tag{3.16}$$

justifying the use of a the supersymmetric lagrangian, for large ρ (and/or small z). The masses of z and τ are of order:

$$m_\tau^2 \sim |M\mathcal{G}(0)|^2 \frac{g_s}{\rho^3} \qquad m_z^2 \sim M^2 \frac{g_s}{\rho^3 z^2}. \tag{3.17}$$

So the inclusion of τ in the low energy effective lagrangian is sensible; for fixed ρ, however, z becomes massive as $z \to 0$, and a more careful analysis seems required. We will proceed without worrying about this potential subtlety, as we will be generally interested in rough scalings of tunneling amplitudes, in any case.

3.3.1 Tensions and Cosmological Constants

The vacua in this leading approximation are all degenerate (zero cosmological constant), so this model is not useful for discussing tunneling amplitudes. As a toy model, we can consider a theory without ρ, with minima which are supersymmetric and AdS. However, because of supersymmetry, there is still no tunneling between the vacua. The model is useful, however, for studying how domain wall tensions and vacuum energies (cosmological constants) scale with flux, and also how warping effects these quantities. Without ρ (or with ρ fixed), the domain wall tension between vacua of different flux is[49]:

$$T = 2\Delta |e^{K/2} W|. \tag{3.18}$$

We can consider various types of transitions. For transitions with $\Delta M = \pm 1$, the tension is given by

$$T \approx 2 \left| \mathcal{G}(0) e^{K/2} + e^{K/2}(K'h(0) - \frac{1}{2\tau}[M\mathcal{G}(0) + \tau K'(0)])\Delta\tau \right| \tag{3.19}$$

$$\sim 2|\mathcal{G}(0)|\rho^{-3/2}g_s^{1/2}.$$

Where we used that at the minima $\tau = -\bar{\tau}$ and neglected contributions of order z. This is in accord with the general scaling arguments of section 3.2; the tension is of order one, if all fluxes are scaled uniformly. In addition, in the theory absent ρ, the change in the cosmological constant is of order M, again in accord with our general scaling arguments.

For those with $\Delta K' = \pm 1$, the tension is of order:

$$T \sim M/K'\rho^{-3/2}g_s^{1/2}. \tag{3.20}$$

Again, if all scales become uniformly large, this is in accord with our earlier arguments. Interestingly, however, for small string coupling, this is enhanced relative to the $\Delta M = 1$ transitions. The change in the cosmological constant is of order

$$M^2/K'\rho^{-3}g_s. \tag{3.21}$$

Finally, changes in K are associated with domain walls with tension suppressed by z, and with changes in cosmological constant similarly suppressed.

3.3.2 GKP As a Prototype for Non-Supersymmetric Scalings

Because of the supersymmetry of the GKP solution, without ρ, or the degeneracy with ρ, semiclassically there is no tunneling. But we have seen that the domain wall tension and energy splittings behave as expected for theories without supersymmetry, so we can use the GKP solution as a model for transitions among non-supersymmetric states. We would then expect that tunneling amplitudes would behave roughly as e^{-S_b}, where $S_b \sim T^4/\Delta E^3$. So, for example, for the for transitions with $\Delta M = 1$, we would have, for the bounce action:

$$S_b = \frac{e^{-K}}{M^3} \sim \frac{V^2\tau}{M^3} \sim \frac{V^2}{M^2K'}. \tag{3.22}$$

Here we have used the flux dependence of τ, eqn. 3.14 This flux and volume behavior is as we anticipated in section 3.2, in the sense that it involves three powers of flux in the denominator, though one of these factors is the small (NS-NS) flux.

In any case, this model is compatible with our naive estimates: obtaining a large set of metastable non-supersymmetric compactifications would seem to require that the volume scale as a power of the flux. Following our discussion in section 3.2, we would expect that, while in general, gravitational corrections are important and might suppress the decay amplitude in some cases, this is not the case if the initial state has small cosmological constant.

This has a close parallel to the field theory discussion along the lines of [46, 47]. For the case of a change of one unit of RR flux, the expanding bubble can be thought of as a wrapped $D5$ brane. Three of the directions along the brane are wrapped on a three cycle; the remaining two dimensions correspond to the bubble wall. Of the four collective coordinates of the brane, three are located at a point on the internal manifold; the remainder is the coordinate, $R(t)$, describing the wall surface. The tension of the D5 brane is just the tension we identified before:

$$T = \frac{1}{g_s} M_s^6 (R^3 M_{10}^3) M_{10}^{-3} \tag{3.23}$$

$$= \frac{1}{g_s} \rho^{-3/2} M_p^3$$

which is what we found from the heuristic field-theoretic argument.

We need, also, to worry about conservation of $D3$ brane charge. In general, transitions involving changes in flux will involve emission of $D3$ branes, as well. We won't consider this problem in detail. However, for special cases (those for which $\int H \wedge F$ vanishes), there need be no $D3$ brane emission. In cases where there is brane emission, the energetics are the same as suggested by the field theory arguments. For a change in K of order one, one needs a change in the $D3$ brane density of order M. Wrapped $D3$ branes have tension (mass) of order $1/g_s M_p$ (independent of ρ), so the energy density is of the same order as the change in energy due to the change in flux. So we expect that our estimates of tunneling rates above are still correct.

3.4 Tunneling From Approximately Supersymmetric Vacua

From the point of view of stability, supersymmetric vacua are special. According to quite general arguments, they are stable. This is perhaps surprising, since in supergravity it is perfectly possible for a lagrangian to exhibit a supersymmetric state (say with vanishing cosmological constant) and a non-supersymmetric state with large, negative cosmological constant. In such a case, one does not expect, for example, a BPS domain wall.

The essential point was made by Deser and Teitelboim[50], Witten[52], Hull[51] and others long ago. They noted that in a classical supergravity theory in an asymptotically flat space, one can define not only a total energy and momentum, but also global supercharges. These obey the standard supersymmetry algebra, so, just as is familiar in global supersymmetry, the energy of any configuration can be shown to be greater than or equal to zero. (This is a special case of the positive energy theorem.)

The stability of exactly supersymmetric states may or may not be of interest, but clearly the stability of *approximately* supersymmetric states is of great potential importance. Suppose the

scale of supersymmetric breaking, F, is small compared to the Planck scale and other possible scales of interest (string scale, compactification scale). Then the decay probability behaves as

$$\Gamma \sim e^{-1/|F|^2} \tag{3.24}$$

or vanishes. It is only non-vanishing if susy breaking in the AdS state is comparable or smaller than that in the approximately flat space state.

3.4.1 Models

These features of decays of (nearly) supersymmetric states can be illustrated with simple models. Consider, first, a theory of a single scalar field, ϕ, with superpotential:

$$W = \frac{1}{2}M\phi^2 - \frac{1}{3}\gamma\phi^3. \tag{3.25}$$

Before coupling to gravity, this theory has supersymmetric minima at

$$\phi_0 = 0;\ \phi_0 = \frac{M}{\gamma}. \tag{3.26}$$

These can be joined by a domain wall, with tension:

$$T = 2\Delta W. \tag{3.27}$$

Now couple the system to (super)gravity, with $M \ll M_p$. In this case, the domain wall tension is approximately unchanged, but there is a splitting between the states,

$$\Delta E = 3\frac{|\Delta W|^2}{M_p^2} \tag{3.28}$$

ΔE is small compared to the scales in the superpotential, so a thin wall approximation is appropriate. The bubble radius is, again,

$$R_b = \frac{3T}{\Delta E} \tag{3.29}$$

As explained by Coleman and De Luccia, the decay amplitude vanishes if

$$\frac{R_b}{\Lambda} = 2 \tag{3.30}$$

and precisely this condition is satisfied in this model.

Now let's add supersymmetry breaking to the mix. This can be done by adding an additional chiral field, Z, and taking for the superpotential:

$$W = \frac{M}{2}\phi^2 - \frac{\gamma}{3}\phi^3 + Z\mu^2 + W_0. \tag{3.31}$$

The Z field can be stabilized in both vacua by adding a term $Z^\dagger Z Z^\dagger Z$ to the Kahler potential. W_0 is chosen so that the $\phi = 0$ state has zero cosmological constant:

$$3|W_0|^2 = |\mu^4|. \tag{3.32}$$

Note that the phase of W_0 is not fixed by this condition.

For this system, the bubble wall tension is approximately as it was in the previous case, but the energy shift is different. Calling the original shift ΔE_0, the shift is larger or smaller by an amount of order $FM^3/(\gamma^2 M_p)$, depending on the sign of W_0. In the latter case, the amplitude vanishes; in the former, it is of order

$$\Gamma \approx e^{-6\pi^2 M_p^4/|F|^2}. \tag{3.33}$$

Note that even for moderately small F (in whatever are the appropriate units) and in the presence of an exponentially large number of decay channels, the decay rate is extremely small. We might expect that $|F| \sim 10^{-3}\ M_p^2$ would more than adequately suppress the decay rate. The implications of this observation for a possible *prediction* of low energy supersymmetry will be discussed in the conclusions.

3.5 Large volume, Weak Coupling, Light Moduli and Warping

From our studies of the GKP model, we can already see that weak string coupling, by itself, does not insure stability. However, a combination of weak coupling and large volume does. What is required is that there be a large number of states whose volume scales with a power (3/2) of the flux. One suspects, more generally, that whatever is the parameter(s) which account for the exponentially large number of states, the volume must scale with a power of this parameter.

In the IIB constructions which have been studied, the fixing of the volume is not well understood (except in special cases which have exact or approximate low energy supersymmetry). In IIA theories, however, candidate vacua have been identified with all moduli fixed[7, 40]. In these cases, one has an infinite sequence of AdS vacua, with or without supersymmetry, with progressively larger volume and smaller cosmological constant. We can again take these as a model, supposing that there exists a set of dS vacua with similar scalings, and ask how the tunneling amplitudes would behave.

Without reviewing the IIA models in detail, we note that the important large number in these constructions is the four-form flux, which we will refer to generically as N. As in the IIA case, the action scales as N^2. At the minimum, one finds that the the volume, v, and the

dilaton, e^{ϕ}, scale as

$$v \sim N^{3/2} \quad e^{\phi} \sim N^{-3/4} \tag{3.34}$$

and the cosmological constant behaves as $N^{-9/2}$. As a result, the tension of the bubble walls and the energy splittings between states behave as

$$T \sim N^{-13/4} \quad \Delta E \sim N^{-11/2} \tag{3.35}$$

giving a result for the bounce action which grows rapidly with N:

$$S_b \sim N^{3.5}. \tag{3.36}$$

Another model for scaling with volume is provided by the proposal of Silverstein and Saltzman to compactify string theory on products of Riemann surfaces[41]. Again, without reviewing the details of the model, there are various numbers, such as 5-form flux, q_5, which can become large, accounting for the large number of states, many of which are believed to be de Sitter. The volume, in this case, scales as q_5^3, while the vacuum energy scales as $V^{-4/3}$. So again the bounce action grows as a power of the large parameter.

Both of these models suggest that if there do exist large sets of de Sitter vacua with growing volume and decreasing cosmological constant, they are likely to be highly metastable.

Warping, on the other hand, does not seem, by itself, to lead to suppression of tunneling rates, as we see from the GKP model. One might have expected this in any situation where there are large numbers of fluxes. The GKP construction suggests that warping is obtained by tuning some set of fluxes on cycles associated with the warp region; changing far away fluxes, then, may be possible without spoiling this feature. Formulas 3.19-3.21 exhibit no singular dependence on z.

3.6 Tunneling from states with Light Moduli

Supersymmetric vacua with moduli are very familiar. Much of the recent focus on flux vacua is motivated by the observation that these have few or no light moduli. Still, we might speculate that there exist classes of non-supersymmetric vacua with comparatively light pseudomoduli. Those with small cosmological constant would likely have neighbors with negative cosmological constant, and no moduli at all.

One can ask whether the presence of light moduli would somehow suppress tunneling. In the standard treatment (we will ignore the effects of gravity in this section) one needs to study an analog problem, the motion of a particle in a potential, with boundary conditions that in

the far future, the system settle into the false minimum of the potential. One might hope that the light field would only slowly settle into its minimum, giving rise to a large bounce action. This turns out not to be the case, in general.

In the transition, one expects a significant rearrangement of the degrees of freedom. The final state in the transition likely will have no light fields, or at least different numbers of them. High energy string states in one vacuum might be relatively light states in another. To develop some intuition, we consider a field theory with two fields, X and ϕ. ϕ is light in the "false" vacuum but heavy in the "true" vacuum; X is heavy in both. For the potential we take:

$$V = \frac{1}{2}\mu^2\phi^2 + \frac{M^2}{2}X^2 - \frac{1}{4}X^4 + \frac{\Gamma}{6}X^6 + \epsilon X^2(\phi - \phi_0)^2. \tag{3.37}$$

The idea here is that μ is extremely small compared to M, Γ, which define mass scales of the same order. To permit simple calculations, we can take ϵ to be a small number. Γ is chosen so the vacuum with $X \neq 0$ has lower energy than the $X = 0$ vacuum. Again, to allow simple approximations, we can tune Γ so that the energy difference between the $X = 0$ vacuum and the $X \neq 0$ vacuum is, say, of order ϵM^4.

For small ϵ, we can consider first the dynamics of X by itself. We will also ignore gravity at first. This is then a standard thin wall tunneling problem. The bounce has a size of order $r_0 = t_0 = 1/(\epsilon M)$, where r_0 is meant to denote the bubble radius and t_0 denotes the typical time in the analog particle problem. In the particle analogy with inverted potential, X starts extremely close to the top of the hill (the true vacuum),

$$X - X_0 \sim Me^{-Mt_0}. \tag{3.38}$$

It then rolls quickly to the false vacuum. As it approaches the false vacuum ($X = 0$), it behaves, again, as

$$X \sim Me^{-M(t-t_0)}. \tag{3.39}$$

For sufficiently large time ($M(t - t_0) = -\ln(\epsilon)$), $\epsilon X^2 \approx \mu^2$. Until that time, the minimum of the ϕ potential lies at ϕ_0. In the inverted problem, ϕ_0 then rolls away from that point (towards the origin).

Note, however, that this time is much smaller than μ^{-1} (it is also smaller than r_0). So ϕ satisfies the equation:

$$\ddot{\phi} + \frac{3}{t}\dot{\phi} = 0. \tag{3.40}$$

This has solutions $\phi = 1/t^2 + \text{constant}$. By tuning the initial conditions, one can arrange that $\phi < \mu$ in a time much less than μ^{-1}; for such motions, there is no enhancement of the bounce action.

3.7 Implications and Speculations

From this survey, we have concluded that generic, metastable states, are likely to satisfy special conditions. We have identified two possibilities:

1. (Approximate) Supersymmetry at scales well below the fundamental scale.

2. Compactification radii much larger than the string scale

and ruled out several others.

The strongest indication for the existence of large numbers of large volume, dS states comes from the work of [41], but the work of [42, 7] is also suggestive. For many of these constructions, there are good reasons for skepticism (see, e.g., [6], though it should be noted that there are also reasons to be skeptical of supersymmetric constructions). Even if such states exist, it is conceivable that many are in some sense uninteresting, since coupling constants become small in the large volume limit. If, in the end, the explanation of hierarchy is the existence of a vast array of non-supersymmetric states (with large volume or some other feature which accounts for metastability), the question will be: are these states distinguished in some other way? Otherwise, observations of phenomena at accelerator energies will provide us with no information about physics at extremely high energies.

One might speculate that there do not exist such large sequences of large volume compactifications, no some other generic vast class of non-supersymmetric metastable dS states. Stability might favor low energy supersymmetry. It is then interesting to ask whether among these states, there might be further selection effects.

3.7.1 R Symmetric Points as Cosmological Attractors

Having established that some set of states are metastable, it is natural to ask whether the universe might find its way into them. To address this issue, the first task is to survey the neighborhood of some particular state (or class of states) of interest. Let's begin with the KKLT vacua. It seems likely that these are surrounded by AdS vacua, largely non-supersymmetric. From our arguments above, the KKLT vacua are likely stable against decays to these states. Because of these many AdS states, transitions *into* the KKLT vacua might be difficult.

A potentially interesting set of states are those which exhibit discrete R symmetries. Such states are likely rare in the landscape[53], but their neighborhoods may be more interesting. In general, one finds such states by setting to zero all fluxes which transform non-trivially under the candidate symmetry. Typically, this is a substantial fraction of the fluxes – 2/3 or more.

Arguably this is what one expects for symmetric states: they are special and thus rare. But the idea that cosmological considerations (e.g. high temperatures) can favor symmetric states is familiar. For the flux lattice, things cannot be so simple; we are concerned about discrete transitions. But it seems possible that such symmetric states might be cosmological attractors. Consider the neighborhood of the R symmetric states, i.e. states for which the symmetry preserving fluxes, N_i, are large, while those which break the symmetry are much smaller, say n_α. Similarly, there are fields, Z_i, which transform like W at the R symmetric point, and fields, ϕ_a, which transform differently. At the R symmetric point, there is a superpotential:

$$W = Z_i f^i(\phi_a, Z_i) \tag{3.41}$$

The condition for unbroken supersymmetry is:

$$Z_i = 0; \quad f_i(\phi_a, 0) = 0. \tag{3.42}$$

Provided there are more ϕ_a type fields then Z_i fields, these equations, generically, possess a moduli space of solutions.

Now treat N_i and n_α as sufficiently large that they can be thought of as continuous, with $|N_i| \gg |n_\alpha|$, for all i and α. As we turn on small n_α we can study an effective lagrangian for the light moduli of the symmetric vacuum. There is no reason to think that the structure of stationary points of the effective lagrangian for this potential is different than the general (non-R) case. So there will typically be solutions with broken supersymmetry, and positive or negative cosmological constant[42]. Introducing polar coordinates, $\vec{n} = (n, \theta_1, \theta_2, \dots)$. The cosmological constant, as a function of $\vec{n}$, then has the structure:

$$\Lambda(\vec{n}) = n^2 v(\theta_i). \tag{3.43}$$

It is then plausible that there are finite elements of "solid angle" with either sign of the cosmological constant, and in particular finite regions with positive cosmological constant and energy tending to zero as $n \to 0$. For these regions, the symmetric state may function as a *cosmological attractor*. Since most "jumps" will be very rapid, it is perhaps appropriate to think of $\vec{n}$ as a collective coordinate, and the motion in this space as reasonably smooth. Note that in the last few transitions, the continuous approximation for n will break down, and there may be AdS states close to the symmetric point, which may have catastrophic consequences for a particular decay chain. But it is at least plausible that finite domains of the landscape are attracted to R symmetric vacua.

3.7.2 Implications of Stability

Of cosmological issues within the landscape, metastability is the simplest criterion which states must satisfy. Of generic features of landscape states, we have seen that only large volume, or approximate supersymmetry, seem to result in some degree of metastability. It is conceivable that we could settle the question of whether vast arrays of large volume, non-supersymmetric states exist in an underlying theory of gravity. As we have noted, if they do, and they are otherwise undistinguished, it is unclear how one might imagine developing a string phenomenology. Not only would we fail to make predictions, e.g. for LHC physics, but we would not know how to interpret LHC outcomes. If not, however, low energy supersymmetry would seem a prediction of string theory.

We should stress, of course, that stability, by itself, does not imply *weak scale* supersymmetry. A quite high scale of supersymmetry breaking will insure an adequate level of stability. However, within the supersymmetric branches of the landscape, the scale of supersymmetry breaking is likely flat on a log scale[39]. So, just as expected from conventional naturalness arguments, light Higgs should arise with low supersymmetry breaking scale.

We have gone further, examining the neighborhood of the KKLT vacua, as well as sets of vacua with approximate R symmetries, suggesting reasons why cosmology might favor the later. These remarks are on far shakier ground, but are worthy of further study.

Chapter 4
Metastable supersymmetry breaking and Vscape

4.1 Introduction

In this chapter we will discuss in detail our work published in [54].

The requirement that supersymmetry is broken at the global minima in field theories with dynamical supersymmetry breaking[55] puts tight constraints on model building. Recently, dynamical supersymmetry breaking in metastable vacua has attracted attention as a promising phenomenological possibility. This greatly simplifies the model building problems. The metastable states are viable candidates to describe our world, when the tunneling probability to the supersymmetric ground state is highly suppressed. As argued in [2], metastable vacua might be quite generic in supersymmetric theories[56][57]. With some mild assumptions, low energy supersymmetry breaking even requires our world as we know it to be a long lived metastable state[58]. From the string theory point of view, non-supersymmetric flux compactifications might also be rather generic in the landscape of vacua[59].

An important role in studying the moduli space of supersymmetric theories is played by the one-loop effective potential of the field theory. The classical (pseudo)moduli space can contain flat directions. The one-loop corrections often lift those pseudomoduli directions of the classical theory, thus creating isolated (meta)stable vacuum. Generically, several fields will have vacuum expectation values (vevs) at those local minima. The important phenomenological objective is then to create models that communicate this dynamical breaking of supersymmetry to the supersymmetric standard model such that one gets attractive superpartner spectra[60].

The computation of the Coleman-Weinberg potential[61] in realistic models often becomes rather involved as the mass matrices become large and one can expect several fields to gain vevs. Even for symbolic software package, multiple diagonalization of large mass matrices is rather time consuming, while numerical packages usually do not provide the flexibility of working with symbolic formulas. `Vscape` aims to bridge this gap between symbolic and numerical packages. The flexibility of the `Vscape` users interface gives the user the freedom to define the physics of the model symbolically, while the computationally intensive evaluations of the Coleman-Weinberg

potential rely on fast numerical C++ routines.

In addition `Vscape` provides the necessary tools to analyse a metastable vacuum once one is found. Commands are provided to compute the mass spectrum at the local minimum. Those results can then be used as input data for a spectrum generator such as `SOFTSUSY`[62]. Vscape has a command implemented with allows for the creation of files formatted according the Model Input File standard described in the Les Houches Accord 1.0. to supply the high energy input to the spectrum generator.

The code for `Vscape` was written in object-oriented C++ since this language compiles to speed efficient programs, allowing for fast diagonalization of large matrices for the Coleman-Weinberg potential. Using C++ also has the advantage that an extensive collection very powerful, mathematical libraries are freely available. `Vscape` makes use of the recent libraries GSL [63], GiNaC and CLN [64]. `Vscape` also has Tab-completion build in, if one has the readline library installed. The program can freely be downloaded and installed from either:

`http://www.physics.rutgers.edu/~korneel/vscape/vscape.html`

or

`http://projects.hepforge.org/vscape/`

Detailed installation instruction (Linux and Windows) can also be found there. Updates and fixes of possible errors will also appear on those websites.

In section 4.2, we briefly introduce the physics behind the commands of `Vscape`. We then give a short account on how the program is structured in section 4.3. Section 4.4 lists several possibilities for further extensions of the program. Appendix 4.5 and 4.6 contain the detailed syntax and functionality of all the commands understood by `Vscape`. Section 4.6.8 discusses the precision of the numerical computations, while section 4.6.9 lists the commands to change the control parameters of the program to influence the algorithms underlying the program.

4.2 Physics Overview

4.2.1 The supersymmetric model of chiral fields

The current version of `Vscape` allows one to study various $\mathcal{N} = 1$ supersymmetric models with chiral fields[65]. The user defines the model by specifying the parameters and chiral fields ϕ_i of the model. In addition, one has to specify the subset of fields which are a priori allowed to obtain a vev for their scalar component. Let us denote this subset of background fields as

φ_i, while we will use the symbol $\widetilde{\varphi}_n$ for the fields that are not allowed to get a scalar vev. The model is then defined through the superpotential W and the D-term potential V_D. The D-term potential is only taken into account in the tree level potential[1]. The current version of the program does not include terms from vector multiplets in the Coleman-Weinberg potential computation. The program assumes a canonical Kähler potential,

$$K = \mathrm{Tr}\,\phi^\dagger\phi\,. \tag{4.1}$$

When a new model is loaded, the program computes and stores the following information symbolically:

$$\begin{aligned} V_0 &= W_i^*|_{\widetilde{\varphi}_n=0}\, W^i\big|_{\widetilde{\varphi}_n=0} + V_D|_{\widetilde{\varphi}_n=0} && (4.2)\\ (\mathrm{Fterms})_i &= W_i|_{\widetilde{\varphi}_n=0} && (4.3)\\ (\mathrm{mF})_{ij} &= W_{ij}|_{\widetilde{\varphi}_n=0} && (4.4)\\ (\mathrm{mB})_{ij} &= W^*_{ijk}W^k\big|_{\widetilde{\varphi}_n=0} && (4.5) \end{aligned}$$

where an index i to the superpotential W stands for a derivative with respect to field ϕ_i. The $|_{\widetilde{\varphi}_n=0}$ indicates that the fields that are not allowed to get a vev by the user, are set to zero in the expression. The commands detailed in section 4.6.2 give you access to this information.

4.2.2 Coleman-Weinberg computation

To compute the Coleman-Weinberg potential, the numerical values for the vevs and parameters are substituted into the matrices mF and mB. The program then constructs the numerical mass squared matrices

$$\begin{aligned} M_{1/2}^\dagger M_{1/2} &= W^*_{jk}W^{ik} && (4.6)\\ M_0^2 &= \begin{pmatrix} W^*_{jk}W^{ik} & W^*_{ijk}W^k \\ W^{ijk}W^*_k & W^*_{ik}W^{jk} \end{pmatrix} && (4.7) \end{aligned}$$

The mass squared eigenvalues of these matrices, $(m^2_{1/2})_i$ and $(m^2_0)_i$ respectively, are computed and substituted in the Coleman-Weinberg formula[61]

$$V_{\mathrm{cw}} = \frac{1}{64\pi^2}\left(\sum_i (m_0^2)_i^2 \ln(m_0^2)_i - 2\sum_i (m_{1/2}^2)_i^2 \ln(m_{1/2}^2)_i\right). \tag{4.8}$$

[1]We include the D-terms in the tree level potential to accomodate models like [66] where the hidden sector itself does not have a D-term potential but where the Supersymmetric Standard Model (SSM) sector does contribute D-terms to the tree level potential. This also allows us to described the metastable vacua of the models studied in [2] where the theory is gauged, but the effect of the gauge fields drops out of the one-loop correction.

The effective potential is thus a function of the vevs of the background fields φ_i. Notice that the program implicitly fixes the renormalization scale at 1, in whatever units the model is defined.

To check the proper functioning of the Coleman-Weinberg computation, `Vscape` allows to check the supertrace of the tree-level squared mass matrices. The supertrace is computed completely analogous to the Coleman-Weinberg potential, in that the eigenvalues of the matrices (4.6) and (4.7) are computed. The eigenvalues are then substituted in the formula:

$$\mathrm{STr}(M^2) = \sum_i (m_0^2)_i - 2\sum_i (m_{1/2}^2)_i \,. \tag{4.9}$$

4.2.3 Metastable vacua

`Vscape` contains several commands to scan for local minima on the one-loop effective potential surface. Once a local minima of the effective potential is found, one can compute the one-loop corrected masses at the minima from:

$$V_{\mathrm{eff}}|_{\mathrm{min}} = V_{\mathrm{eff}}|_{\mathrm{min}} + \frac{1}{2}\, H_{ij}|_{\mathrm{min}}\, \varphi_i \varphi_j + \ldots \tag{4.10}$$

where H_{ij} is the Hessian matrix. The eigenvalues of the Hessian are the mass squareds of the associated mass eigenstates. The mass squared eigenvalues allow you to verify (within error bounds, see section 4.6.8) whether the minimum is indeed stable. Depending on the setup studied, the actual mass squared eigenvalues can be used as input parameters for SSM spectrum generators.

4.3 Structure of the program

The physics of the supersymmetric model is entirely encoded in the class CModel which is defined in the files `phenomodel.h` and `phenomodel.cc`. CModel has several routines relying on symbolic computations using the GiNaC library while other GSL-based routines are numerical.

The user-interface of `Vscape` was build on `ginsh`, the interactive frontend for the GiNaC symbolic computation framework [64]. This lightweight package for symbolic computations provided the appropriate user-interface to communicate between the phenomenological model and the user. We slightly extended the commands of the original `ginsh` application, to fit our needs.

`Ginsh` is implemented using the tools flex and bison which provide the detailed code for the lexer which reads the input (`ginsh_lexer.ll`) and parser which interprets the input (`ginsh_parser.yy`). `Ginsh` contains several commands, which are not related to the underlying phenomenological model. Those commands are detailed in Appendix 4.5.

The original `ginsh` implementation allowed for additional commands to be added by other programmers in the separate file `ginsh_extensions.h`. The commands that specifically relate to the phenomenological model are defined in `vscape.h` and `vscape_functions.h`. They are included via `ginsh_extensions.h`. The shorter functions are implemented in `vscape.h` while the longer, mathematically involved algorithms such as minimization, are implemented in `vscape_functions.h`. Appendix 4.6 details the specific commands which allow you to interact with the phenomenological model CModel.

4.4 Outlook

This project grew out of a program written to study the Pentagon Model [66] [67]. Originally, the definition of the model was hardwired into the code. The added symbolic interface of `Vscape` gives the user the freedom to define the physics of the model her/himself. The commands available in `Vscape` provide the functionality that we needed to study the Pentagon Model. There are several additional features which might be interesting to include.

- Including vector multiplets in the computation of the Coleman-Weinberg potential.
- Allowing for a more general Kähler potential instead of the currently assumed canonical one.
- Specific commands to study the barrier heights and associated tunneling probabilities.
- Extending the user interface by introducing indexed symbols and control flow statements such as if-then statements and loops.
- Faster symbolic-numeric interface (technical extension). Currently the interface between the symbolic library GiNaC and the numeric library GSL is based on the GiNaC subs() command, which is rather time consuming. One could create a derived class of the GiNaC numeric class, which stores numerical data as actual C++ doubles. The implementation of the automatically invoked eval() command in the class should then take care of numeric evaluation, without having to do explicit subs() command. GSL could then manipulate directly on the doubles of this class.

4.5 General Symbolic Commands

In this section, we detail the general math commands known to the Vscape. It is a slightly extended set of the original ginsh commands. The original manual of ginsh can be found as the

linux ginsh manual.

4.5.1 Running Vscape

You run Vscape by typing

```
./Vscape [file ...]
```

where the list of files is optional. Vscape will first attempt to read and interpret the commands from the file(s). When no files were specified or all the commands in the files have been executed, Vscape displays a prompt (`> `) signifying that it is ready to accept your input. Acceptable input are numeric or symbolic expressions consisting of numbers (e.g. `42`, `2/3` or `0.17`), symbols (e.g. `x` or `result`), mathematical operators like `+` and `*`, and functions (e.g. `sin` or `normal`). Every input expression must be terminated with either a semicolon (`;`) or a colon (`:`). If terminated with a semicolon, Vscape will evaluate the expression and print the result to stdout. If terminated with a colon, Vscape will only evaluate the expression but not print the result. It is possible to enter multiple expressions on one line. Whitespace (spaces, tabs, newlines) can be applied freely between tokens. To quit Vscape, enter `quit` or `exit`, or type an EOF (Ctrl-D) at the prompt.

4.5.2 Comments

Anything following a double slash (`//`) up to the end of the line, and all lines starting with a hash mark (`#`) are treated as a comment and ignored.

4.5.3 Numbers

Vscape accepts numbers in the usual decimal notations. This includes arbitrary precision integers and rationals as well as floating point numbers in standard or scientific notation (e.g. `1.2E6`). The general rule is that if a number contains a decimal point (`.`), it is an (inexact) floating point number, otherwise it is an (exact) integer or rational. Integers can be specified in binary, octal, hexadecimal or arbitrary (2-36) base by prefixing them with `#b`, `#o`, `#x`, or `#nR`, respectively.

4.5.4 Symbols

Symbols are made up of a string of alphanumeric characters and the underscore (`_`), with the first character being non-numeric. E.g. `a` and `mu_1` are acceptable symbol names, while `2pi` is

not. It is possible to use symbols with the same names as functions (e.g. `sin`), Vscape is able to distinguish between the two.

Symbols can be assigned values by entering

symbol `=` *expression*

To unassign the value of an assigned symbol, type

`unassign('`*symbol*`');`

Assigned symbols are automatically replaced by their assigned value when they are used. To refer to the unevaluated symbol, put single quotes (') around the name, as demonstrated for the `unassign` command above.

Symbols are considered to be in the complex or real domain depending on the mode in which they were defined. If the program is in the complex mode, every new symbol that has not been used before during the session is considered to be complex. If the program is in the real mode, every newly encountered symbol is considered to be real. The mode of the program only affects newly defined symbols. Thus when the program is in the real mode, symbols that were defined previously in the complex mode, remain complex. This mode of the program is switch using the keywords `real_symbols` and `complex_symbols`. The program is in the complex mode by default.

The following symbols are pre-defined constants that cannot be assigned a value by the user:

`Pi`	Archimedes' Constant
`Catalan`	Catalan's Constant
`Euler`	Euler-Mascheroni Constant
`I`	imaginary unit i
`FAIL`	an object of the GiNaC 'fail' class

There is also the special

`Digits`

symbol that controls the numeric precision of calculations with inexact numbers. Assigning an integer value to digits will change the precision to the given number of decimal places.

4.5.5 Wildcards

The `has()`, `find()`, `match()` and `subs()` functions accept wildcards as placeholders for expressions. These have the syntax

`$`*number*

for example `$0`, `$1` etc.

4.5.6 Last printed expressions

Vscape provides the three special symbols

`%`, `%%` *and* `%%%`

that refer to the last, second last, and third last printed expression, respectively. These are handy if you want to use the results of previous computations in a new expression.

4.5.7 Operators

Vscape provides the following operators, listed in falling order of precedence:

- `!` postfix factorial
- `^` powering
- `+` unary plus
- `-` unary minus
- `*` multiplication
- `/` division
- `+` addition
- `-` subtraction
- `<` less than
- `>` greater than
- `<=` less or equal
- `>=` greater or equal
- `==` equal
- `!=` not equal
- `=` symbol assignment

All binary operators are left-associative, with the exception of `^` and `=` which are right-associative. The result of the assignment operator (`=`) is its right-hand side, so it's possible to assign multiple symbols in one expression (e.g. `a = b = c = 2;`).

4.5.8 Lists

A list consists of an opening curly brace (`{`), a (possibly empty) comma-separated sequence of expressions, and a closing curly brace (`}`). A list is not a set in that it can contain several times the same element (e.g. `{1,2,3,4,3,3,x^2}`).

4.5.9 Matrices

A matrix consists of an opening square bracket (`[`), a non-empty comma-separated sequence of matrix rows, and a closing square bracket (`]`). Each matrix row consists of an opening square bracket (`[`), a non-empty comma-separated sequence of expressions, and a closing square bracket (`]`). If the rows of a matrix are not of the same length, the width of the matrix becomes that of the longest row and shorter rows are filled up at the end with elements of value zero.

4.5.10 Functions

A function call in Vscape has the form

name`(`*arguments*`)`

where *arguments* is a comma-separated sequence of expressions. Vscape provides a couple of built-in functions and also 'imports' all symbolic functions defined by GiNaC and additional libraries. There is no way to define your own functions other than linking Vscape against a library that defines symbolic GiNaC functions.

Vscape provides Tab-completion on function names: if you type the first part of a function name, hitting Tab will complete the name if possible. If the part you typed is not unique, hitting Tab again will display a list of matching functions. Hitting Tab twice at the prompt will display the list of all available functions.

A list of the built-in functions follows. They nearly all work as the respective GiNaC methods of the same name, so I will not describe them in detail here. Please refer to the GiNaC documentation.

`append(`*list1*`,` *list2*`)`
: appends list2 to list1

`charpoly(`*matrix*`,` *symbol*`)`
: characteristic polynomial of a matrix

`coeff(`*expression*`,` *object*`,` *number*`)`
: extracts coefficient of *object*`^`*number* from a polynomial

`collect(`*expression*`,` *object-or-list*`)`

collects coefficients of like powers (result in recursive form)

`collect_distributed(`*expression*`,` *list*`)`

collects coefficients of like powers (result in distributed form)

`collect_common_factors(`*expression*`)`

collects common factors from the terms of sums

`conjugate(`*expression*`)`

complex conjugation

`content(`*expression*`,` *symbol*`)`

content part of a polynomial

`decomp_rational(`*expression*`,` *symbol*`)`

decompose rational function into polynomial and proper rational function

`degree(`*expression*`,` *object*`)`

degree of a polynomial

`denom(`*expression*`)`

denominator of a rational function

`determinant(`*matrix*`)`

determinant of a matrix

`diag(`*expression...*`)`

constructs diagonal matrix

`diff(`*expression*`,` *symbol* `[,` *number*`])`

partial differentiation

`divide(`*expression*`,` *expression*`)`

exact polynomial division

`eigenherm(`*matrix*`)`

compute the eigenvalues and eigenvectors of an n by n hermitian matrix M of numbers. The function returns a list with a 1 by n matrix of eigenvalues followed by the n by n unitary matrix were each column is an eigenvector. The columns of eigenvector are ordered in the same way the eigenvalues appear in the 1 by n matrix. Note: this is a numerical command, it does not accept expressions that cannot be evaluated numerically. The command works with double precision internally.

`eigensymm(`*matrix*`)`

compute the eigenvalues and eigenvectors of an n by n real symmetric matrix M of numbers. The function returns a list with a 1 by n matrix of eigenvalues followed by the n by n orthogonal matrix were each column is an eigenvector. The columns of eigenvector are ordered in the same way the eigenvalues appear in the 1 by n matrix. Note: this is a numerical command, it does not accept expressions that cannot be evaluated numerically. The command works with double precision internally.

`eval(`*expression* `[,` *level*`])`

evaluates an expression, replacing symbols by their assigned value

`evalf(`*expression* `[,` *level*`])`

evaluates an expression to a floating point number

`evalm(`*expression*`)`

evaluates sums, products and integer powers of matrices

`expand(`*expression*`)`

expands an expression

`find(`*expression*`,` *pattern*`)`

returns a list of all occurrences of a pattern in an expression

`fsolve(`*expression*`,` *symbol*`,` *number*`,` *number*`)`

numerically find rootof a real-valued function within an interval

`gcd(`*expression*`,` *expression*`)`

greatest common divisor

`has(`*expression*`,` *pattern*`)`

returns '1' if the first expression contains the pattern as a subexpression, '0' otherwise

`importfile(`*filename*`)`

read commands from *filename*. Note that this command cannot be nested in files.

`integer_content(`*expression*`)`

integer content f a polynomial

`inverse(`*matrix*`)`

inverse of a matrix

`is(`*relation*`)`

returns '1' if the relation is true, '0' otherwise (false or undecided)

`lcm(`*expression*`,` *expression*`)`

least common multiple

`lcoeff(`*expression*`,` *object*`)`

leading coefficient of a polynomial

`ldegree(`*expression*`,` *object*`)`

low degree of a polynomial

`lsolve(`*equation-list*`,` *symbol-list*`)`

solve system of linear equations

`map(`*expression*`,` *pattern*`)`

apply function to each operand, the function to be applied is specified as a pattern with the '$0' wildcard standing for all the operands

`match(`*expression*`,` *pattern*`)`

check whether expression matches a pattern

returns a list of wildcard substitutions or 'FAIL' if there is no match

`minus(`*list1*`,` *list2*`)`

returns the set-theoretic difference of list1 and list2

`nops(`*expression*`)`

number of operands in expression

`normal(`*expression* `[,` *level*`])`

rational function normalization

`numer(`*expression*`)`

numerator of a rational function

`numer_denom(`*expression*`)`

numerator and denumerator of a rational function as a list

`op(`*expression*`,` *number*`)`

extract operand *number* from *expression*, can also be used to get elements in a matrix

`power(`*expression1*`,` *expression2*`)`

exponentiation (equivalent to writing *expression1*`^`*expression2*)

`prem(`*expression*`,` *expression*`,` *symbol*`)`

pseudo-remainder of polynomials

`primpart(`*expression*`,` *symbol*`)`

primitive part of a polynomial

`quo(`*expression*`,` *expression*`,` *symbol*`)`

quotient of polynomials

`rank(`*matrix*`)`

rank of a matrix

`rem(`*expression*`,` *expression*`,` *symbol*`)`

remainder of polynomials

`resultant(`*expression*`,` *expression*`,` *symbol*`)`

resultant of two polynomials with respect to symbols

`rnd(`*number1*`,` *number2*`)`

generate a random number with double precision with uniform distribution within the interval [number1, number2]

`save(`*filename*`[,` *string*`] [,` *expression*`])`

open *filename* and append *string* and/or *expression*; to file

`series(`*expression*`,` *relation-or-symbol*`,` *order*`)`

series expansion

`sprem(`*expression*`,` *expression*`,` *symbol*`)`

sparse pseudo-remainder of polynomials

`sqrfree(`*expression* `[,` *symbol-list*`])`

square-free factorization of a polynomial

`sqrt(`*expression*`)`

square root

`symbolicmatrix(`*integer1*`,` *integer1*`,` *symbol*`)`

create an *integer1* by *integer2* matrix with entries *symbol_XX*

`subs(`*expression*`,` *relation-or-list*`)`

`subs(`*expression*`,` *look-for-list*`,` *replace-by-list*`)`

substitute subexpressions (you may use wildcards)

`tcoeff(`*expression*`,` *object*`)`

trailing coefficient of a polynomial

`time(`*expression*`)`

returns the time in seconds needed to evaluate the given expression

`trace(`*matrix*`)`

trace of a matrix

`transpose(`*matrix*`)`

transpose of a matrix

`unassign(`*symbol*`)`

unassign an assigned symbol

`unit(`*expression*`,` *symbol*`)`

unit part of a polynomial

`unique(`*list*`)`

removes all multiple occurrences of expressions in the list

4.5.11 Special Commands

To exit Vscape, enter `quit` or `exit`. Vscape can display a (short) help for a given topic (mostly about functions and operators) by entering `?`*topic*. Typing `??` will display a list of available help topics. The command

`print(`*expression*`);`

will print a dump of GiNaC's internal representation for the given *expression*. This is useful for debugging and for learning about GiNaC internals. The command

`print_latex(`*expression*`);`

prints a LaTeX representation of the given *expression*. The command

`print_csrc(`*expression*`);`

prints the given *expression* in a way that can be used in a C or C++ program. The command

`iprint(`*expression*`);`

prints the given *expression* (which must evaluate to an integer) in decimal, octal, and hexadecimal representations. Finally, the shell escape

`![`*command* `[`*arguments*`]]`

passes the given *command* and optionally *arguments* to the shell for execution. With this method, you can execute shell commands from within Vscape without having to quit.

4.5.12 Error messages

When you enter something which Vscape is unable to parse, it will report

`syntax error, unexpected` *foo* `at` *bar*

Please check the syntax of your input and try again. If the computer reports

`argument` *num* `to` *function* `must be a` *type*

it means that the argument number *num* to the given *function* has to be of a certain type (e.g. a symbol, or a list). The first argument has number 0, the second argument number 1, etc.

4.5.13 Examples

```
> a = x^2-x-2;
-2-x+x^2
> b = (x+1)^2;
(x+1)^2
> s = a/b;
(1+x)^(-2)*(-2-x+x^2)
> diff(s, x);
-2*(1+x)^(-3)*(-2-x+x^2)+(-1+2*x)*(1+x)^(-2)
> normal(s);
(1+x)^(-1)*(-2+x)
> x = 3^50;
717897987691852588770249
> s;
717897987691852588770247/717897987691852588770250
> Digits = 40;
40
> evalf(s);
0.99999999999999999999999582113329270438496099067 9
> unassign('x');
x
> s;
(1+x)^(-2)*(-2-x+x^2)
>
> s = x^3 + x^2 + y + 1;
1+y+x^3+x^2
> map(s, $0^2);
1+y^2+x^4+x^6
> match(s, $0+$1^2);
{$1==x,$0==1+y+x^3}
>
> series(sin(x),x==0,6);
1*x+(-1/6)*x^3+1/120*x^5+Order(x^6)
```

```
>
> lsolve({3*x+5*y == 7}, {x, y});
{x==-5/3*y+7/3,y==y}
> lsolve({3*x+5*y == 7, -2*x+10*y == -5}, {x, y});
{x==19/8,y==-1/40}
>
> M = [ [a, b], [c, d] ];
[[-x+x^2-2,(x+1)^2],[c,d]]
> op(M, 0); op(M, 2);
-x+x^2-2
c
> determinant(M);
-2*d-2*x*c-x^2*c-x*d+x^2*d-c
> collect(%, x);
(-d-2*c)*x+(d-c)*x^2-2*d-c
>
> save("test.txt", "# test saving M to file");
Wrote to file <test.txt>: "# test saving M to file"
> save("test.txt", "M = ", M);
Wrote to file <test.txt>: "M = [[-2-x+x^2,(1+x)^2],[c,d]];"
> save("test.txt", M);
Wrote to file <test.txt>: "[[-2-x+x^2,(1+x)^2],[c,d]];"
>
> solve quantum field theory;
syntax error, unexpected T_SYMBOL at quantum
> quit
```

In this example, three lines where added to the end of the file `"test.txt"`:

```
# test saving M to file
M =[[-2-x+x^2,(1+x)^2],[c,d]];
[[-2-x+x^2,(1+x)^2],[c,d]];
```

If the file did not exist originally, it was created the first time the command `save()` was executed.

4.6 Commands to find and analyse metastable vacua

In this section, we introduce the Vscape commands that allow you to interact with the build in supersymmetric model in Vscape.

4.6.1 Defining the model

First you need to define the supersymmetric model that you want to study. The command

`ModelConstruct(`*Params*`,` *Fields*`,` *Vevs*`,` *W*`,` *V_D*`)`

allows you to specify the model. *Params* is a list of parameters that appear in the model (e.g. coupling constants). *Fields* is a list of expressions, every symbol in the list will be considered a field in your model. *Vevs* is a subset of *Fields*, it contains the fields which you allow to acquire a non-zero vacuum expectation value. The order in which the symbols appear in *Fields* determines the ordering of fields in the mass matrices and in the list of F-terms (see example later on). The expression *W*, specifies the superpotential and *V_D* is the expression for the D-term potential which is added to the tree level potential. Both expressions may only contain symbols that are listed either in *Fields* or *Params*. The command `ModelConstruct()` will return `0` if it successfully defined the model, otherwise it will show an error message. Once the model is successfully loaded, you can use all the other commands described below to study the model.

The command `ModelConstruct()` computes the F-terms and mass-matrices symbolically. Depending on the number of fields in the model and calculational speed this command might take some time. Once the model is computed with `ModelConstruct()`, you can use the command

`ModelSave(`*filename*`)`

to save the computed model to *filename*. This command saves all the information about the model including F-terms and mass matrices such that, later on, when you want to load that specific model again, the computer does not have to redo the lengthy computation of the F-terms and mass matrices. `ModelSave()` will return `0` if it successfully saved the model otherwise it will show an error message.

Reloading a specific model, is done by simply invoking `importfile(`*filename*`)`. `Vscape` will execute the commands in *filename*. *filename* was created by `ModelSave()` such that it will first define the fields, parameters, vevs, superpotential, D-term potential, F-terms and mass

matrices. The last line of *filename* will call the command `ModelLoad()` (discussed below) which does the actually loading of the model into `Vscape`. So after invoking `importfile(`*filename*`)`, where *filename* is a file that was created with `ModelSave()`, the model is loaded into `Vscape` and you can use all the commands described below to study the model.

I would advise against manually editing files created by `ModelSave()`, since they contain all the information of the model you defined with `ModelConstruct()` in a consistent way. It contains the exact mass matrices and F-terms corresponding to the superpotential with the correct ordering. E.g. the order in which the F-terms appear in *filename* is determined by the order in which the fields are listed in *filename*.

The command

`ModelLoad(`*Params*`,` *Fields*`,` *Vevs*`,` *W*`,` *V_D*`,` *Fterms*`,` *mF*`,` *mB*`)`

is called implicitly as the last line of any file which was created with `ModelSave()`, so you will rarely need to use it explicitly. Like `ModelConstruct()`, this command loads a specific model into `Vscape` such that it can be studied with subsequent commands. However, in this case the F-terms and mass matrices need to be specified as an argument, so this command avoids the sometimes time-consuming computation of the F-terms and mass matrices. *Fterms* should be a list of expressions for the different F-terms. mF and mB are the fermion and scalar mass matrices respectively. The entries in *Fterms*, mF and mB should be ordered as the fields are ordered in *Fields*. Thus e.g. the second entry in the list *Fterms* is the F-term with respect to the second field appearing in the list *Fields*. Warning: the program does not check whether the given F-terms and mass matrices actually correspond to the superpotential given!

If you invoke `ModelConstruct()` (or implicitly `ModelLoad()` via `importfile()`), when a model was already loaded, the internal model of Vscape will be changed to the new model. Thus, all the subsequent commands will involve that new model.

Example

This example and the subsequent examples use the model discussed in [2] with $N = 1$ and $N_f = 6$. A slightly modified version of this example is included in the distribution of Vscape and can be loaded with `importfile("`*path*`/examples/iss.txt")` where *path* is the correct path to the file. Note: the file `iss.txt` was not created with `ModelSave()`, the file does not contain F-terms nor mass matrices, so you safely modify it.

```
> ## Switch to real mode, to introduce two real parameters
> real_symbols;
```

```
  All new symbols introduced from now on are assumed to be real.
> Lambda:
> m_ISS:
>
> ## Switch to complex mode, to introduce all the other symbols
> complex_symbols;
  All new symbols introduced from now on are assumed to be complex.
>
> ## Define the model
> Params = {Lambda, m_ISS}:
> B  = symbolicmatrix(6,1,B_);
[[B_0],[B_1],[B_2],[B_3],[B_4],[B_5]]
> Bt = symbolicmatrix(1,6,Bt_):
> M  = symbolicmatrix(6,6,M_):
> Fields = {B,Bt,M}:
> Vevs   = {B_5,Bt_5,M_00,M_11,M_22,M_33,M_44,M_55}:
> W   = evalm(Bt*M*B)                //
>       - determinant(M)*Lambda^(-3) //
>       + Lambda*m_ISS*trace(M):
> V_D = 0:
>
> ## Construct the model
> ModelConstruct(Params, Fields, Vevs, W, V_D);
Loading Model...
  Computing F-terms and mass matrices...
  F-terms:       i = 047;
  Mass matrices: i = 047; j = 047; k = 047;
  Done.
Model successfully loaded...
0
>
> ## Now we save the model to a file
> ModelSave("examples/isscomputed.txt");
The internal model was successfully saved to <examples/isscomputed.txt>.
```

```
0
```

From now on this specific model can quickly be loaded using the command

```
importfile("examples/isscomputed.txt");
```

Note that the file `isscomputed.txt` was created using `ModelSave()` and thus contains the correctly ordered F-terms and mass matrices of this specific model, so this file should not be modified by hand. Whenever you want to define a new model different from the above one (e.g. with one more term in the superpotential) you will have to use the command `ModelConstruct()` again)

4.6.2 Symbolic commands for the model

There are several commands which give you symbolic information on the model that is loaded.

`ModelParams()`

Returns the parameters of the model in a list

`ModelFields()`

Returns the fields of the model in a list

`ModelVevs()`

Returns the fields with non-zero expectation value in a list

`ModelW()`

Returns the superpotential

`ModelVD()`

Returns the D-term potential

`ModelV0()`

Returns the tree level potential symbolically

`ModelFtermsi(`*integer*`)`

Returns the F-terms related to field *integer*

`ModelFterms()`

Returns the F-terms in a list

`ModelmFij(`a`, `b`)`

Returns entry a, b of the fermion mass matrix: W_ab

`ModelmBij(`a`, `b`)`

Returns entry a, b of the upper right block of the scalar mass matrix: $W * \_abc\ W\_c$

`ModelmF()`

Returns the fermion mass matrix: W_ab

`ModelmB()`

Returns the upper right (off diagonal) block of the scalar mass matrix: $W * \_abc\ W\_c$

The list of F-terms and the entries in the mass matrices are ordered according to the occurrence of the fields in `ModelFields()`. The *integer* values in the above command also refer to the occurrence of the field in `ModelFields()`, the first field has integer `0`.

Example

To try the example below, you will need the file `examples/isscomputed.txt` which was created in the example above.

```
> importfile("examples/isscomputed.txt");
> ModelFields();
{B_0,B_1,B_2,B_3,B_4,B_5,
 Bt_0,Bt_1,Bt_2,Bt_3,Bt_4,Bt_5,
 M_00,M_01,M_02,M_03,M_04,M_05,
 M_10,M_11,M_12,M_13,M_14,M_15,
 M_20,M_21,M_22,M_23,M_24,M_25,
 M_30,M_31,M_32,M_33,M_34,M_35,
 M_40,M_41,M_42,M_43,M_44,M_45,
 M_50,M_51,M_52,M_53,M_54,M_55}
> ModelFterms();
{0,0,0,0,0,Bt_5*M_55,
 0,0,0,0,0,M_55*B_5,
 m_ISS*Lambda-M_33*Lambda^(-3)*M_44*M_11*M_55*M_22,0,0,0,0,0,
 0,m_ISS*Lambda-M_33*M_00*Lambda^(-3)*M_44*M_55*M_22,0,0,0,0,
 0,0,-M_33*M_00*Lambda^(-3)*M_44*M_11*M_55+m_ISS*Lambda,0,0,0,
 0,0,0,-M_00*Lambda^(-3)*M_44*M_11*M_55*M_22+m_ISS*Lambda,0,0,
 0,0,0,0,m_ISS*Lambda-M_33*M_00*Lambda^(-3)*M_11*M_55*M_22,0,
 0,0,0,0,0,-M_33*M_00*Lambda^(-3)*M_44*M_11*M_22+Bt_5*B_5+m_ISS*Lambda}
>
> ## F-term wrt B_5;
> myFterm = ModelFtermsi(5);
Bt_5*M_55
```

```
>
> ## entry associated with B_0, Bt_0 in mass matrices;
> ModelmFij(0,6);
M_00
> ModelmBij(0,6);
m_ISS*Lambda-M_33*Lambda^(-3)*M_44*M_11*M_55*M_22
```

4.6.3 Numerical commands for the model: the effective potential

All commands that involve numeric computations work with double precision, independent from the `Digits` setting for the symbolic computations. The commands to evaluate the potential numerically are,

`ModelnumV0(`*SubsList*`)`

Evaluates the tree level potential numerically

`ModelnumVcw(`*SubsList*`)`

Evaluates the Coleman-Weinberg potential numerically

`ModelnumVeff(`*SubsList*`)`

Evaluates the one loop effective potential numerically

`ModelnumSTrM2(`*SubsList*`)`

Evaluates the supertrace over scalar and fermion mass matrices

`ModelnummF2(`*SubsList*`)`

Returns the numerical (tree level) mass squared eigenvalues of the fermion mass matrix

`ModelnummB2(`*SubsList*`)`

Returns the numerical (tree level) mass squared eigenvalues of the scalar mass matrix

The *SubsList* is a list of equations which specify the value of the parameters and fields which were allowed to have non-zero expectation value.

Example

The example below uses the file `examples/isscomputed.txt` which was created in an example above.

```
> importfile("examples/isscomputed.txt");
> Subs = {Lambda == 1000.0, m_ISS == 10.0,  //
>         B_5  == 0.00 + 100.0*I,           //
```

```
>         Bt_5 == 0.01 + 100.0*I,          //
>         M_00 == 0.0,                     //
>         M_11 == 0.0,                     //
>         M_22 == 0.0,                     //
>         M_33 == 0.0,                     //
>         M_44 == 0.0,                     //
>         M_55 == 0.0}:
> ModelnumVcw(Subs);
3.3551986738766286522E7
> ModelnumSTrM2(Subs);
3.456079866737127304E-11
```

4.6.4 Minima of the effective potential

You can find local minima of tree level and the one loop effective potential by using the commands:

`ModelMinV0(`*SubsPattern*`,` *Variables*`,` *StartPoint*`)`

`ModelMinVeff(`*SubsPattern*`,` *Variables*`,` *StartPoint*`)`

SubsPattern is a list of equations which specifies the values of the parameters and fields with non-zero vev as function of the variables. The variables are specified in the field *Variables* as a list of real symbols. The minimization algorithm will minimize the potential as a function of those variables. The field *StartPoint* is a list of initial value for each of the variables. The command returns a list with values for the variables at the minima. The value for simplex size shown while the command is running is discussed in section 4.6.9

This command is calculationally intensive for the effective potential, the calculation time depends on the number of fields in the model. While the calculation progresses the computer will display the current iteration of the algorithm and the minimum value of the potential that has been reached so far. The algorithm used to minimize the function is the simplex algorithm of Nelder and Mead [68]. This algorithm has the advantage that it does not rely on computational intensive gradients to iterate towards the minimum. Some more details and parameters that influence the simplex algorithm are given in section 4.6.9.

Another command that analyzes the effective potential is

`ModelStatBox(`*SubsPattern*`,` *Variables*`,` *StartPoint*`,` *Point1*`,` *Point2*`)`

where the fields *SubsPattern* and *Variables* have the same function described above. The command starts from the value of the effective potential where the variables have the value specified in *StartPoint*. The algorithm then picks several random points in the box defined by *Point1* and *Point2* and checks whether the value of the effective potential at that point is lower than the minimum value found so far. The command returns a list of values for the variables at the random point with lowest effective potential.

Example

The example below uses the file `examples/isscomputed.txt` which was created in an example above.

```
> importfile("examples/isscomputed.txt");
> Subs = {Lambda == 1000.0, m_ISS == 10.0, //
>         B_5  == 0 + b*I,                 //
>         Bt_5 == c + d*I,                 //
>         M_00 == 0.0,                     //
>         M_11 == 0.0,                     //
>         M_22 == 0.0,                     //
>         M_33 == 0.0,                     //
>         M_44 == 0.0,                     //
>         M_55 == e}:
> ModelMinSimpl(Subs, {b,c,d,e}, {100,0,100,0});
       250:  Veff = +5.334976441748862266 54e+08
             Simplex size = +1.569691689254765876 82e-05
{98.755419109029958236, 8.6554575838203248834E-7,
 98.755388956674764245, 7.920961955373477163 3E-7}
> ModelMinSimpl(Subs, {b,c,d,e}, {0,900,900,900});
       680:  Veff = +5.334976441748861074 45e+08
             Simplex size = +3.023429275407894359 54e-06
{98.7554136717079416,  -3.5353383568610648586E-8,
 98.755391871241812396, 5.7324975688985215976E-8}
>
>
> Subs = {Lambda == 1000.0, m_ISS == 10.0, //
```

```
>         B_5  == 0 + b*I,                  //
>         Bt_5 == c + d*I,                  //
>         M_00 == a,                        //
>         M_11 == a,                        //
>         M_22 == a,                        //
>         M_33 == a,                        //
>         M_44 == a,                        //
>         M_55 == e}:
> ModelMinSimpl(Subs,{a,b,c,d,e},{900,0,0,0,900});
       660:  Veff = -1.0350943237817344 7649e-05
             Simplex size = +1.69541545589374184433e-13
{398.10717886889341344,
   5.7428257024330178013E-7,
   1.7617897585483444842E-6,
  -8.3947951601006729255E-7,
 398.107133987191105}
>
> ModelStatBox(Subs,{a,b,c,d,e},{0,98,0,98,0}, //
>              {200,0,0,0,200},{500,0,0,0,500});
   Checking random point no.    90; (so far     6 lower points found)
{381.46924413740634918, 0.0, 0.0, 0.0, 467.38906654063612223}
```

The first two minimizations started at different points but led to the same metastable minimum discussed in [2]. Both results are equal up to numerical precision as discussed in section 4.6.8. The $U(1)_B$ symmetry is spontaneously broken giving rise to a Goldstone direction. We fixed this freedom by choosing $\mathrm{Re}B_5 = 0$.

The third minimization led to the supersymmetric vacua of the model. Notice that the rank-condition mechanism for supersymmetry breaking for models with $N = 1$ only holds around the origin in fieldspace. Away from the origin there is a point where all the F-terms become zero due to the additional determinant term in the superpotential. The numerical value for the effective potential at the supersymmetric point is slightly negative but zero within error bounds as discussed in section 4.6.8.

The fourth operation was a statistical search. We started from a point close to the metastable vacuum and search randomly in the interval $M_{00} = \cdots = M_{44} \in [200, 500], M_{55} \in [200, 500]$.

The algorithm returned a point in fieldspace relatively close to the supersymmetric minima with a lower value for the effective potential.

4.6.5 Analyzing the vacua

The commands to analyse a minimum all use the same structure of arguments as described above: *SubsPattern* is a list of equations linking the parameters and fields with non-zero vev to the variables which are specified in the list *Variables*. The values for the variables are given in the list of numbers *Point*.

`ModelGradient(`*SubsPattern*`,` *Variables*`,` *Point*`)`

Evaluates the gradient of the effective potential at *Point*. The command returns a list with the gradient followed by error flags on the gradient each formatted as a 1 by n matrix. The computer will show the estimated time to complete the algorithm since this computation is calculationally intensive.

`ModelHessian(`*SubsPattern*`,` *Variables*`,` *Point*`)`

Evaluates the Hessian matrix at *Point*. The command returns a list with the hessian matrix followed by the matrix of error flags. The computer will show the estimated time to complete the algorithm since this computation is calculationally intensive.

`Modeldiff2(`*SubsPattern*`,` *Variables*`,` *Point*`,` *i*`,` *j*`,` *dx_i*`,` *dx_j*`)`

Evaluates the second order derivative with respect to fields *i* and *j*. *dx_i* and *dx_j* are suggested stepsize to compute the derivative (see section 4.6.9 for more information). The command returns a list with the second order derivative followed by the error flag.

`ModelNegEig(`*SubsPattern*`,` *Variables*`,` *Point*`,` *Hessian*`,` *HessianError*`)`

Checks whether there are negative eigenvalues of the Hessian matrix of the effective potential at *Point*. You need to make sure that *Hessian* (and *HessianError*) are indeed the Hessian matrix (and error flags) of the effective potential at *Point*. The function will return the original *Point* or, if there are negative eigenvalues that are larger than the average error flag, another *Point* where the effective potential has a lower value. Used as cross check for the other minimization commands.

Example

The example below uses the file `examples/isscomputed.txt` which was created in an example above.

```
> importfile("examples/isscomputed.txt");
> Subs = {Lambda == 1000.0, m_ISS == 10.0, //
```

```
>         B_5  == 0.0 + b*I,                //
>         Bt_5 == 0.0 + d*I,                //
>         M_00 == 0.0,                      //
>         M_11 == 0.0,                      //
>         M_22 == 0.0,                      //
>         M_33 == 0.0,                      //
>         M_44 == 0.0,                      //
>         M_55 == 0.0}:
> Min = ModelMinSimpl(Subs, {b,d}, {100,100});
       160:  Veff = +5.3349764417488604784e+08
             Simplex size = +3.2924409229629811924e-06
{98.7553948250289579,98.7554093102966277}
>
>
> ModelGradient(Subs, {b,d}, {100,100});
      2/2:  00:01s to go...
{[[44055.476986700297857, 44055.476986670022598]],
 [[6.273248519121328748,      6.27324852896071139]]}
> ModelGradient(Subs, {b,d}, Min);
      2/2:  00:01s to go...
{[[-5.261715075073619019,    -5.2542854259666373906]],
 [[ 3.8105577427291033032,    3.81055711846567835]]}
>
> ModelHessian(Subs, {b,d}, Min);
      3/3:  00:19s to go...
{[[17652.30720837064655,     17140.548392404118204],
  [17140.548392404118204,    17652.301781115671474]],
 [[   10.064568391628851529,    10.455072325682765566],
  [   10.455072325682765566,    10.064565316884026558]]}
> Hessian = op(%, 0): HessianErr = op(%%, 1):
> eigensymm(Hessian);
{[[34792.852887147491856,      511.75610233882599687]],
 [[    0.70710683715979527,   -0.70710672521329531737],
  [    0.70710672521329531737,   0.70710683715979527]]}
```

The second column in the last matrix in the example is the eigenvector corresponding to the pseudo-moduli direction in [2]. The corresponding mass squared eigenvalue indeed corresponds to the theoretical value computed in [2]: $511.756\,\mathrm{GeV}^2$ versus $489.248\,\mathrm{GeV}^2$.

4.6.6 Plots

There are three commands in Vscape to plot:

`ModelPlotV0(`*filename*`,` *SubsPattern*`,` *Variables*`,` *xmin*`,` *xmax*`,` *ymin*`,` *ymax*`)`
`ModelPlotVcw(`*filename*`,` *SubsPattern*`,` *Variables*`,` *xmin*`,` *xmax*`,` *ymin*`,` *ymax*`)`
`ModelPlotVeff(`*filename*`,` *SubsPattern*`,` *Variables*`,` *xmin*`,` *xmax*`,` *ymin*`,` *ymax*`)`

Each commands writes 3d plotting data of respectively V_0, V_{cw} or V_{eff} to the file *filename*. *SubsPattern* again indicates how the parameters and fields with non-zero vev depend on the *Variables*. *Variables* should be a list of 2 variables which will be on the x and y axis of the 3d plot. The variables will be evaluated between *xmin* and *xmax* (*ymin*, *ymax* resp.) with a stepsize of 1. The computer will show the progress for all plotting commands since it is calculationally intensive. The command returns 0 when it was successful. The file is formatted such that it can then easily be imported in other math packages. A maple file (`Plotting.mw`) which can import the data is included in the distribution of Vscape in the directory `examples/`. The file format is

```
xmin xmax
ymin ymax
f(xmin,ymin)   f(xmin+1,ymin)   ... f(xmax,ymin)
f(xmin,ymin+1) f(xmin+1,ymin+1) ... f(xmax,ymin+1)
...
f(xmin,ymax)   f(xmin+1,ymax)   ... f(xmax,ymax)
```

where the first two lines contain integer values, while all other data consists of doubles.

Example

The example below uses the file `examples/isscomputed.txt` which was created in an example above.

```
> importfile("examples/isscomputed.txt");
> pi = evalf(Pi):
```

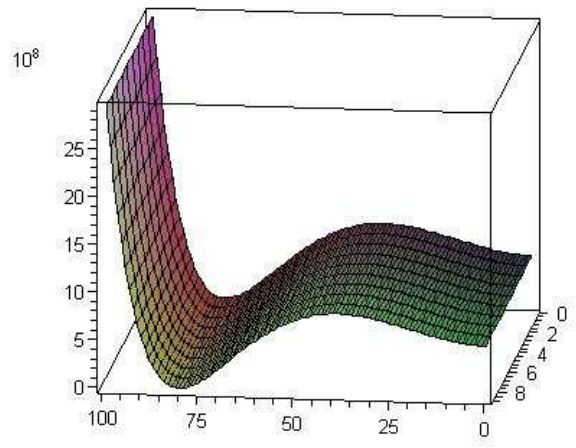

Figure 4.1: The effective potential from the metastable vacuum to the supersymmetry vacuum. The axis into the paper is the flat Goldstone direction of the $U(1)_B$. The axis along the paper cuts through the one-loop effective potential from the metastable minima on the left to the supersymmetric vacuum on the right side.

```
> M  = 398.1*b/80:
> B  = 98.755*(1 - b/80):
> Subs = {Lambda == 1000.0, m_ISS == 10.0,  //
>        B_5  == exp( 2*pi*a*I/10)*(B*I),   //
>        Bt_5 == exp(-2*pi*a*I/10)*(B*I),   //
>        M_00 == M,                         //
>        M_11 == M,                         //
>        M_22 == M,                         //
>        M_33 == M,                         //
>        M_44 == M,                         //
>        M_55 == M}:
> ModelPlotVeff("BarrierPlot.txt", Subs, {a,b}, 0, 9, 0,99);
The 3d plotting data was successfully saved to <BarrierPlot.txt>.
0
```

The plot obtained from the example using `examples/plotting.mw` in Maple 10 is shown in figure 4.1.

4.6.7 Interface with spectrum generators

The command

`ModelSpectr(`*Filename*`,` *SubsList*`)`

allows interaction with spectrum generators. The command takes the file *filename* as input file. This file should be formatted according to the Les Houches Accord [69], except that numbers can be replaced by formulas. `ModelSpectr()` will substitute the values specified in *SubsList* and the current values of all other variables used up to that point in Vscape and generate an output file `<filename.out>`. This file can then be used as input file for spectrum generators. Whenever an unknown symbol is encountered, the entire line is copied verbatim without substitution and a message is printed on the screen. Vscape will add a Block containing version information to the output file, to indicate that the file was generated with Vscape.

Example

The example below uses the file `examples/isscomputed.txt` which was created in an example above. As input file in this example, we use `LesHoucheSymbolic.txt`

```
# SUSY Les Houches Accord 1.0 - example input file
#
Block MODSEL                # Select Model
     1    2                 #   (m)GMSB
Block SMINPUTS              # Standard Model inputs
     3    0.1172            #   alpha_s(MZ) SM MSbar
Block MINPAR                # Susy breaking input parameters
     1  sqrt(Lambda*m_ISS)  #   scale of soft susy breaking
     3  ReHu0/ReHd0         #   tanb
     4    1.0               #   sign(mu)
Block EXPAR                 # Non-minimal susy breaking input parameters
     23   g_S*S             #   mu-term
```

The commands sequence of the example is

```
> importfile("examples/isscomputed.txt");
> Subs = {Lambda == 1000.0, m_ISS == 10.0, //
>         B_5  == 0 + b*I,                 //
```

```
>         Bt_5 == c + d*I,                  //
>         M_00 == 0.0,                      //
>         M_11 == 0.0,                      //
>         M_22 == 0.0,                      //
>         M_33 == 0.0,                      //
>         M_44 == 0.0,                      //
>         M_55 == e}:
> ModelMinSimpl(Subs, {b,c,d,e}, {100,0,100,0});
       250:  Veff = +5.334976441748862266 54e+08
             Simplex size = +1.56969168925476587682e-05
{98.755419109029958236, 8.6554575838203248834E-7,
 98.755388956674764245, 7.920961955373477163 3E-7}
> MinSubs = subs(Subs, {b,c,d,e}, %);
{Lambda==1000.0, m_ISS==10.0,
 B_5==98.755419109029958236*I,
 Bt_5==8.6554575838203248834E-7+98.755388956674764245*I,
 M_00==0.0, M_11==0.0, M_22==0.0, M_33==0.0, M_44==0.0,
 M_55==7.920961955373477163 3E-7}
> g_S = 0.6:
> S   = 0.001:
> ModelSpectr("LesHouchesSymbolic.txt", MinSubs);
unknown symbol 'ReHu0'
 => just copied this data line from inputfile to output file...
Unable to match all symbols in <LesHouchesSymbolic.txt>
with currently defined symbols...
2
```

This example produces the output file <LesHouchesSymbolic.txt.out>

```
# SUSY Les Houches Accord 1.0 - example input file
#
Block VSCAPE          # program info
     1     Vscape     # program
     2     1.0.0      # version number
Block MODSEL                # Select Model
```

```
     1   2                    #   (m)GMSB
Block SMINPUTS              # Standard Model inputs
     3   0.1172                 #   alpha_s(MZ) SM MSbar
Block MINPAR                # Susy breaking input parameters
     1   100.0       #   scale of soft susy breaking
     3  ReHu0/ReHd0         #   tanb
     4   1.0                    #   sign(mu)
Block EXPAR                 # Non-minimal susy breaking input parameters
     23   6.0E-4                  #   mu-term
```

Notice that the line specifying $\tan\beta$ was not replaced by a number, since our simple example did not specify a value for $\mathrm{Re}H_u^0$.

4.6.8 Numerical precision and error flags

The numerical format used for all the numerical computations in Vscape is double precision, which has 52 significant bits or approximately 16 decimal digits.

Precision of the Coleman-Weinberg potential

In one of the examples above, we found that the effective potential at the supersymmetric minima had a negative numerical value of order -10^{-5}. The value for the vevs of some of the fields at that point was around 400. This implies that some of the squares of the mass squared eigenvalues of the mass matrices will be of the order $m^4 \approx 400^4 \approx 10^{11}$. Those squares of mass squared eigenvalues appear in the Coleman-Weinberg potential. As the internal numerical algorithm uses double precision, we can expect the absolute error on the potential to be estimated by

$$|\phi_{\max}|^4 10^{-16}\,. \tag{4.11}$$

Or, in our example of the order of 10^{-5}, which implies that the value for the effective potential at the supersymmetric minimum is zero within error bounds.

Precision of the vevs after minimization

In another example, we found two slightly different sets of vevs for the fields at the metastable minima, since we started the minimization process from a different point. The relative difference between the vevs was of order 10^{-7}. The vevs of some of the fields at the metastable minima was of order 10^2. Following the reasoning from the previous paragraph, we estimate that the

absolute error on the effective potential is of order 10^{-8} and since the actual value of the effective potential at the minimum was of order 10^8, the relative error is of order 10^{-16}. Minimizing the potential then holds,

$$\begin{aligned} V_{\text{eff}}(\phi_i) &\approx V_{\text{eff}}(\phi_i) \pm |\phi_{\max}|^4 10^{-16} && (4.12)\\ &= V_{\text{eff}}(\phi_i)(1 \pm 10^{-16}) && (4.13)\\ &= V_{\text{eff}}(\phi_i + \epsilon_i) && (4.14)\\ &= V_{\text{eff}}(\phi_i) + \frac{1}{2}\frac{\partial^2 V_{\text{eff}}}{\partial\phi_i \partial\phi_j}\epsilon_i\epsilon_j && (4.15) \end{aligned}$$

where ϵ_i is the error on the vev of the field ϕ_i at the minimum coming from the limited precision on V_{eff}. In the example above, V_{eff} was of order 10^8 at the metastable minima, while the second order derivative can be at most of order the cutoff squared, which was 10^6. We find that the highest precision on the fields at the metastable minimum is of order 10^{-7}, which corresponds to the results found in the example. A lower value for the second order derivative gives less precision.

4.6.9 Parameters controlling the internal algorithms

Simplex minimization

The algorithm that is used for the command `ModelMinSimpl()` is the Simplex algorithm by Nelder and Mead [68]. An n-simplex is chosen around the start point in variable space. By changing the vertices of the simplex, the algorithm minimizes the size of the simplex step by step. When the size of the simplex is smaller than *MinimizerSizeTest*, the algorithm considers the minimum to be found. When the command `ModelMinSimpl()` is running, the current size of the simplex is shown on the screen. The parameter *MinimizerInitialStep* determines the size of the initial simplex with which the algorithm starts. *MinimizerMaxIterations* sets the maximal number of iterations, the algorithm will quit even if the algorithm has not found a minimum. Sometimes the size of the simplex never becomes small enough to get a successful end of the algorithm, while the simplex is already at its most optimal position. The parameter *MinimizerMaxDeadIterations* determines the maximal number of iterations that the algorithm can proceed without finding a point with a lower functional value.

Statistical minimization

The number of random points the command `ModelStatBox()` test for a lower value of the effective potential, is determined by the parameter *StatBoxMaxIterations*.

Derivatives

The numerical derivatives are computed using the 11-point rule:

$$\begin{aligned}\frac{df(x_0)}{dx} \approx \frac{1}{2520\Delta x}\Big(&-2f(x_0-5\Delta x)+25f(x_0-4\Delta x)-150f(x_0-3\Delta x)\\ &+600f(x_0-2\Delta x)-2100f(x_0-1\Delta x)\\ &+2100f(x_0+1\Delta x)-600f(x_0+2\Delta x)\\ &+150f(x_0+3\Delta x)-25f(x_0+4\Delta x)+2f(x_0+5\Delta x)\Big) \qquad (4.16)\end{aligned}$$

where Δx is the stepsize of the algorithm. The algorithm estimates the error flags coming from rounding errors where the relative error on the effective potential is set by *diffErrorOnf*. In addition, the truncation error which is estimated by comparing the 9-point rule with the 11-point rule result is also determined. The rounding error scales as Δx^{-1} while the truncation error goes like Δx^8. Using those two competing errors, the algorithm estimates a new optimal Δx and repeats the process until the relative error is smaller than *diffTolerance* [70]. It will iterate at most *diffMaxCycle* times. One more parameter determines the behavior of the algorithm, if the new guess for an optimal Δx is bigger than *diffMaxdx* then the algorithm quits. The command `Modeldiff2()` allows you to suggest the initial step sizes of the derivatives in the i and j direction with the arguments *dx_i*, *dx_j*. The other commands make an automatic initial estimate.

Changing the control parameters

You can get the values of all the parameters discussed above with the command

`GetPrecision()`

You can set the parameters with the command

`SetPrecision(`*StatBoxMaxIterations*`,` *MinimizerSizeTest*`,` *MinimizerInitialStep*`,` *MinimizerMaxIterations*`,` *MinimizerMaxDeadIterations*`,` *diffMaxCycle*`,` *diffTolerance*`,` *diffMaxdx*`,` *diffErrorOnf*`)`

If you set an argument in `SetPrecision()` to zero, the parameter will maintain its old value.

The default parameters of the program have been optimized for models of the kind used in the examples, with a cutoff of the order of 1000 where we think in units of GeV. Different models might require different parameters. For example, if one has a very shallow metastable minima, *MinimizerInitialStep* should not be chosen too large, since this would result in the

algorithm jumping out of the metastable minima in favor of another minima with a lower effective potential.

References

[1] J. M. Maldacena, *The large N limit of superconformal field theories and supergravity*, Adv. Theor. Math. Phys. **2**, 231 (1998) [Int. J. Theor. Phys. **38**, 1113 (1999)] [arXiv:hep-th/9711200].

[2] K. Intriligator, N. Seiberg, D. Shih, *Dynamical SUSY breaking in meta-stable vacua*, JHEP **0604**, 021 (2006) [arXiv:hep-th/0602239].

[3] A. E. Nelson and N. Seiberg, *R symmetry breaking versus supersymmetry breaking*, Nucl. Phys. B **416**, 46 (1994) [arXiv:hep-ph/9309299].

[4] R. Essig, K. Sinha and G. Torroba, *Meta-Stable Dynamical Supersymmetry Breaking Near Points of Enhanced Symmetry*, JHEP **0709**, 032 (2007) [arXiv:0707.0007 [hep-th]].

[5] S. Abel, C. Durnford, J. Jaeckel and V. V. Khoze, *Dynamical breaking of* $\mathrm{U(1)_R}$ *and supersymmetry in a metastable vacuum*, Phys. Lett. B **661**, 201 (2008) [arXiv:0707.2958 [hep-ph]].
S. A. Abel, C. Durnford, J. Jaeckel and V. V. Khoze, *Patterns of Gauge Mediation in Metastable SUSY Breaking*, JHEP **0802**, 074 (2008) [arXiv:0712.1812 [hep-ph]].

[6] T. Banks, K. van den Broek, *Massive IIA flux compactifications and U-dualities*, JHEP **0703**, 068 (2007) [arXiv:hep-th/0611185].

[7] O. DeWolfe, A. Giryavets, S. Kachru, W. Taylor, *Type IIA Moduli Stabilization*, JHEP **0507**, 066 (2005) [arXiv:hep-th/0505160].

[8] M. Graña, *Flux compactifications in string theory: A Comprehensive review*, Phys. Rept. **423**, 91 (2006) [arXiv:hep-th/0509003].
M. R. Douglas, S. Kachru, *Flux Compactification*, Rev. Mod. Phys. **79**, 733 (2007) [arXiv:hep-th/0610102].

[9] T. Grimm, J. Louis, *The Effective action of type IIA Calabi-Yau orientifolds*, Nucl. Phys. B **718**, 153 (2005) [arXiv:hep-th/0412277].
P. G. Camara, A. Font, L. E. Ibanez, *Fluxes, moduli fixing and MSSM-like vacua in a simple IIA orientifold*, JHEP **0509**, 013 (2005) [arXiv:hep-th/0506066].

[10] T. Banks, *Landskepticism or why effective potentials don't count string models*, [arXiv:hep-th/0412129].

[11] J.-P. Derendinger, C. Kounnas, P.M. Petropoulos, F. Zwirner, *Superpotentials in IIA compactifications with general fluxes*, Nucl. Phys. B **715**, 211 (2005) [arXiv:hep-th/0411276].
G. Villadoro, F. Zwirner, *N=1 effective potential from dual type-IIA D6/O6 orientifolds with general fluxes*, JHEP **0505**, 047 (2005) [arXiv:hep-th/0503169].
J.-P. Derendinger, C. Kounnas, P.M. Petropoulos, F. Zwirner, *Fluxes and gaugings: N=1 effective superpotentials*, Fortsch. Phys. **53**, 926 (2005) [arXiv:hep-th/0503229].

[12] M. R. Douglas, Z. Lu, *Finiteness of volume of moduli spaces*, [arXiv:hep-th/0509224].
B. S. Acharya, M. R. Douglas, *A Finite landscape?*, [arXiv:hep-th/0606212].
G. Torroba, *Finiteness of Flux Vacua from Geometric Transitions*, JHEP **0702**, 061 (2007) [arXiv:hep-th/0611002].

[13] B. S. Acharya, F. Benini, R. Valandro, *Fixing Moduli in Exact Type IIA Flux Vacua*, JHEP **0702**, 018 (2007) [arXiv:hep-th/0607223].

[14] G. Moore, S. Ramanujam, unpublished.

[15] L. J. Romans, *Massive N=2A Supergravity in Ten-Dimensions*, Phys. Lett. B **169**, 374 (1986).

[16] J. Polchinski, *String theory. Vol. 1-2*, Cambridge University Press, 1998.

[17] M. B. Schulz, *Calabi-Yau duals of torus orientifolds*, JHEP **0605**, 023 (2006) [arXiv:hep-th/0412270].

[18] C. M. Hull, *A Geometry for Non-Geometric String Backgrounds*, JHEP **0510**, 065 (2005) [arXiv:hep-th/0406102].
J. Shelton, W. Taylor, B. Wecht, *Nongeometric flux compactifications*, JHEP **0510**, 085 (2005) [arXiv:hep-th/0508133].

[19] S. Kachru, M. B. Schulz, P. K. Tripathy, S. P. Trivedi, *New Supersymmetric String Compactifications*, JHEP **0303**, 061 (2003) [arXiv:hep-th/0211182].

[20] A. Giveon, M. Roček, *Generalized Duality in Curved String-Backgrounds*, Nucl. Phys. B **380**, 128 (1992) [arXiv:hep-th/9112070].
A. Giveon, M. Porrati, E. Rabinovici, *Target Space Duality and String Theory*, Phys. Rept. **244**, 77 (1994) [arXiv:hep-th/9401139].

[21] E. Witten, *Anti-de Sitter Space, Thermal Phase Transition, And Confinement in Gauge Theories*, Adv. Theor. Math. Phys. **2**, 505 (1998) [arXiv:hep-th/9803131].

[22] O. Aharony, Y. E. Antebi and M. Berkooz, *On the Conformal Field Theory Duals of type IIA AdS4 Flux Compactifications*, JHEP **0802**, 093 (2008) [arXiv:0801.3326 [hep-th]].

[23] I. Klebanov, A. Tseytlin, *Entropy of near extremal black p-branes*, Nucl. Phys. B **475**, 164 (1996) [arXiv:hep-th/9604089].

[24] N. Seiberg, *IR dynamics on branes and space-time geometry*, Phys. Lett. B **384**, 81 (1996) [arXiv:hep-th/9606017].

[25] N. Seiberg, E. Witten, *Gauge dynamics and compactification to three-dimensions*, [arXiv:hep-th/9607163].

[26] C. M. Hull, *Massive String Theories from M-theory and F-theory*, JHEP **9811**, 027 (1998) [arXiv:hep-th/9811021].

[27] M. Haack, J. Louis, H. Singh, *Massive type IIA theory on K3*, JHEP **0104**, 040 (2001) [arXiv:hep-th/0102110].
H. Singh, *Duality symmetric massive type II theories in D = 8 and D = 6*, JHEP **0204**, 017, (2002) [arXiv:hep-th/0109147].
H. Singh, *Romans type IIA theory and the heterotic strings*, Phys. Lett. B **545**, 403 (2002) [arXiv:hep-th/0201206].

[28] G. Moore, N. Saulina, *T-Duality, and the K-Theoretic Partition Function of Type IIA Superstring Theory*, Nucl. Phys. B **670**, 27 (2003) [arXiv:hep-th/0206092].

[29] G. W. Gibbons, N. S. Manton, *Classical And Quantum Dynamics Of Bps Monopoles*, Nucl. Phys. B **274**, 183 (1986).
A. Sen, *A Note on Enhanced Gauge Symmetries in M- and String Theory*, JHEP **9709**, 001 (1997) [arXiv:hep-th/9707123].

[30] D. Martelli, J. Sparks, *G Structures, Fluxes and Calibrations in M Theory*, Phys. Rev. D **68**, 085014 (2003) [arXiv:hep-th/0306225].

[31] A. Bilal, J.P. Derendinger, K. Sfetsos, *(Weak) G_2 holonomy from self-duality, flux and supersymmetry*, Nucl. Phys. B **628**, 112 (2002) [arXiv:hep-th/0111274].

[32] M. J. Duff, *TASI lectures on branes, black holes and Anti-de Sitter space*, Boulder 1999, Strings, branes and gravity, [arXiv:hep-th/9912164].

[33] I. Klebanov, A. Tseytlin, *Intersecting M-branes as four-dimensional black holes*, Nucl. Phys. B **475**, 179 (1996) [arXiv:hep-th/9604166].

[34] D. Belov, G. Moore, *Holographic Action for the Self-Dual Field*, [arXiv:hep-th/0605038].

[35] T. H. Buscher, *A Symmetry Of The String Background Field Equations*, Phys. Lett. B **194**, 59 (1987).

[36] M. Dine, G. Festuccia, A. Morisse and K. van den Broek, *Metastable Domains of the Landscape*, JHEP **0806**, 014 (2008) [arXiv:0712.1397 [hep-th]].

[37] S. Kachru, R. Kallosh, A. Linde, S. P. Trivedi, *De Sitter vacua in string theory*, Phys. Rev. D **68**, 046005 (2003) [arXiv:hep-th/0301240].

[38] T. Banks, M. Dine, E. Gorbatov, *Is there a string theory landscape?*, JHEP **0408**, 058 (2004) [arXiv:hep-th/0309170].

[39] M. Dine, E. Gorbatov, S. D. Thomas, *Low energy supersymmetry from the landscape*, [arXiv:hep-th/0407043].

[40] M. Dine, A. Morisse, A. Shomer, Z. Sun, *IIA moduli stabilization with badly broken supersymmetry*, JHEP **0807**, 070 (2008) [arXiv:hep-th/0612189].

[41] A. Saltman, E. Silverstein, *A new handle on de Sitter compactifications*, JHEP **0601**, 139 (2006) [arXiv:hep-th/0411271].

[42] F. Denef, M. R. Douglas, *Distributions of nonsupersymmetric flux vacua*, JHEP **0503**, 061 (2005) [arXiv:hep-th/0411183].

[43] M. Dine, D. O'Neil, Z. Sun, *Branches of the landscape*, JHEP **0507**, 014 (2005) [arXiv:hep-th/0501214].

[44] L. Susskind, *Supersymmetry breaking in the anthropic landscape*, [arXiv:hep-th/0405189].

[45] M. R. Douglas, *Statistical analysis of the supersymmetry breaking scale*, [arXiv:hep-th/0405279].

[46] S. R. Coleman, *The Fate Of The False Vacuum. 1. Semiclassical Theory*, Phys. Rev. D **15**, 2929 (1977) [Erratum-ibid. D **16**, 1248 (1977)].

[47] S. R. Coleman, F. De Luccia, *Gravitational Effects On And Of Vacuum Decay*, Phys. Rev. D **21**, 3305 (1980).

[48] S. B. Giddings, S. Kachru, J. Polchinski, *Hierarchies from fluxes in string compactifications*, Phys. Rev. D **66**, 106006 (2002) [arXiv:hep-th/0105097].

[49] M. Cvetic, S. Griffies, S. J. Rey, *Static domain walls in N=1 supergravity*, Nucl. Phys. B **381**, 301 (1992) [arXiv:hep-th/9201007].

[50] S. Deser, C. Teitelboim, *Supergravity Has Positive Energy*, Phys. Rev. Lett. **39**, 249 (1977).

[51] C. M. Hull, *The Positivity Of Gravitational Energy And Global Supersymmetry*, Commun. Math. Phys. **90**, 545 (1983).

[52] E. Witten, *A Simple Proof Of The Positive Energy Theorem*, Commun. Math. Phys. **80**, 381 (1981).

[53] M. Dine, Z. Sun, *R symmetries in the landscape*, JHEP **0601**, 129 (2006) [arXiv:hep-th/0506246].

[54] K. van den Broek, *Vscape V1.1.0: An interactive tool for metastable vacua*, Comput. Phys. Commun. **178**, 52 (2008) [arXiv:0705.2019 [hep-ph]].

[55] E. Witten, *Dynamical Breaking of Supersymmetry*, Nucl. Phys. B **188**, 513 (1981).
K. Intriligator, N. Seiberg, *Lectures on Supersymmetry Breaking*, Class. Quant. Grav. **24**, S741 (2007) [arXiv:hep-ph/0702069].

[56] M. Dine, J. L. Feng, E. Silverstein, *Retrofitting O'Raifeartaigh models with dynamical scales*, Phys. Rev. D **74**, 095012 (2006) [arXiv:hep-th/0608159].

[57] M. Dine, J. Mason, *Gauge mediation in metastable vacua*, Phys. Rev. D **77**, 016005 (2008) [arXiv:hep-ph/0611312].

[58] D. Shih, *Spontaneous R-symmetry breaking in O'Raifeartaigh models*, JHEP **0802**, 091 (2008) [arXiv:hep-th/0703196].
K. Intriligator, N. Seiberg, D. Shih, *Supersymmetry breaking, R-symmetry breaking and metastable vacua*, JHEP **0707**, 017 (2007) [arXiv:hep-th/0703281].

[59] F. Denef, M. R. Douglas, *Distributions of flux vacua*, JHEP **0405**, 072 (2004) [arXiv:hep-th/0404116].
M. R. Douglas, J. Shelton, G. Torroba, *Warping and Supersymmetry Breaking*, [arXiv:0704.4001 [hep-th]].

[60] G. F. Giudice, R. Rattazzi, *Theories with gauge mediated supersymmetry breaking*, Phys. Rept. **322**, 419 (1999) [arXiv:hep-ph/9801271].
Y. Shadmi, Y. Shirman, *Dynamical supersymmetry breaking*, Rev. Mod. Phys. **72**, 25 (2000) [arXiv:hep-th/9907225].
M. A. Luty, *2004 TASI lectures on supersymmetry breaking*, [arXiv:hep-th/0509029].

[61] S. Coleman, E. Weinberg, *Radiative Corrections as the Origin of Spontaneous Symmetry Breaking*, Phys. Rev. D **7**, 1888 (1973).

[62] B. C. Allanach, *SOFTSUSY: A C++ program for calculating supersymmetric spectra*, Comput. Phys. Commun. **143**, 305 (2002) [arXiv:hep-ph/0104145].

[63] M. Galassi, J. Davies, J. Theiler, B. Gough, G. Jungman, M. Booth, F. Rossi, *GNU Scientific Library Reference Manual - Revised Second Edition*, ISBN 0954161734.

[64] C. Bauer, A. Frink, R. Kreckel, *Introduction to the GiNaC Framework for Symbolic Computation within the C++ Programming Language*, J. Symbolic Computation **33** (2002) 1.
J. Vollinga, *GiNaC: Symbolic computation with C++*, Nucl. Instrum. Meth. A **559**, 282 (2006), [arXiv:hep-ph/0510057].

[65] S. Martin, *A Supersymmetry Primer*, [arXiv:hep-ph/9709356].

[66] T. Banks, *Remodeling the Pentagon After the Events of 2/23/06*, [arXiv:hep-ph/0606313].

[67] T. Banks, K. van den Broek, to appear.

[68] J. A. Nelder, R. Mead, *A Simplex Method for Function Minimization*, Comput. J. **7** (1965) 308.

[69] P. Skands, B. C. Allanach, H. Baer, C. Balázs, G. Bélanger, F. Boudjema, A. Djouadi, R. Godbole, J. Guasch, S. Heinemeyer, W. Kilian, J-L. Kneur, S. Kraml, F. Moortgat, S. Moretti, M. Mühlleitner, W. Porod, A. Pukhov, P. Richardson, S. Schumann, P. Slavich, M. Spira, G. Weiglein, *SUSY Les Houches Accord: Interfacing SUSY Spectrum Calculators, Decay Packages, and Event Generators*, JHEP **0407**, 036 (2004) [arXiv:hep-ph/0311123].

[70] W. H. Press, B. P. Flannery, S. A. Teukolsky, W. T. Vetterling, *Numerical Recipes in C*, 2nd edition, Cambridge University Press, 1997.

Curriculum Vita
Korneel van den Broek

Degrees

	Rutgers University, New Brunswick, New Jersey USA
September 2003 – present	Enrolled in Physics Ph.D. program
	Ghent University, Ghent, Belgium
September 2003	B.S., Mathematics (additional enrollment)
June 2003	M.S., Physics Engineering
September 2001	B.S., Physics (additional enrollment)
June 2000	B.S., Engineering

Positions Held

January 2008 – June 2008	Kavli Institute for Theoretical Physics Graduate Fellow
January 2007 – July 2007	Visiting student at the Santa Cruz Institute for Particle Physics
September 2004 – June 2006	Teaching Assistant
September 2003 – June 2004	Francqui Fellow through the Belgian American Educational Foundation

Publications

- M. Dine, G. Festuccia, A. Morisse, K. van den Broek, *Metastable Domains of the Landscape*, JHEP 0806:014, 2008, arXiv:0712.1397 [hep-th].
- K. van den Broek, *An Interactive tool for metastable vacua*, Comput. Phys. Commun. 178:52-72, 2008, arXiv:0705.2019 [hep-ph].
- T. Banks, K. van den Broek, *Massive IIA flux compactifications and U-dualities*, JHEP 0703:068, 2007, [hep-th/0611185].